Doctoral Program in Chemical and Biological Engineering

Thesis

Autonomous biosensor for screening cancer biomarkers using passive Fuel Cells

Nádia Silva Ferreira

This thesis is supervised by Doctor Maria Goreti Ferreira Sales, Departamento de Engenharia Química, Faculdade de Ciências e Tecnologia da Universidade de Coimbra and Co-supervised by Doctor Alexandra Maria Pinheiro da Silva Rodrigues Pinto, Departamento de Engenharia Química, Faculdade de Engenharia da Universidade do Porto

If we knew what it was we were doing, it would not be called research, would it?

Albert Einstein

This work was financially supported by “Fundação para a Ciência e Tecnologia” with a scholarship grant (reference SFRH/BD/122955/2016).

Acknowlegments

This thesis would not have been possible without the contribution of several people, directly involved in the scientific work or not. Therefore, I would like to acknowledge and thank all of them in this small text.

Firstly, and because this thesis would not be written today without her, Prof. Goreti Sales for the opportunity to be a part of the Biomark team and for the guidance through all the years before and while this project was a part of my life. Her guidance and our interactions throughout these years played a key role for me to grow as a professional and I will take these lessons to help me further in my professional and personal lives.

To Prof. Alexandra Pinto, for helping us figure out the best way to proceed in a field that we had little knowledge about and guiding us to a good outcome when our hopes of getting there were low. And to Vânia and Beatriz for helping us with the technical parts of the Fuel Cells.

I want to thank the Biomark@ISEP team for the companionship of all members through this time. But most of all I want to thank the friends that I have made during this time: Liliana, Helena, Manuela, Raquel, and Mariana. This work and time would have been a lot different without you. Thank you for your friendship! A special thank you to Liliana, who was always there for and with me, side by side, on this big step of our lives, being the “proton” and thinking positive, being a friend, and a guide in many ways.

To my friends who even though not involved in this work, but still had an impact in the best way: Marcela, Mariana Martins, and Mariana Raposo. Thank you for everything. You are the best!

To my mother a special thank you for trying to help me see the best in everything that I do and for being always there for me.

To Pedro, the best person I could have on my side as life partner. For bearing with me when I was down, and pushing me to do and be better, for enduring all the big and small things in our lives, with the characteristic sense of humour and positive attitude in life.

At last, to the best part of me and my best accomplishment yet, my daughter Emma. You are the best part of my day in every way!

Resumo

O cancro é uma das principais causas de morte a nível mundial, na qual o diagnóstico precoce e o tratamento adequado podem reduzir a mortalidade associada. É mais provável uma resposta positiva ao tratamento em fases precoces de instalação da doença e há maior probabilidade de sobrevivência quando esta é identificada e tratada no estágio inicial. Uma maneira importante de evitar o diagnóstico tardio de cancro é o rastreio. Atualmente, há já vários dispositivos que visam a deteção seletiva de biomarcadores de cancro e que pretendem contribuir para um diagnóstico precoce. As técnicas mais utilizadas atualmente para o diagnóstico do cancro são biópsias, que podem incluir o recurso a imagem de ressonância magnética, mas estes métodos são invasivos, dolorosos e necessitam de um longo período para que os resultados sejam analisados e facultados aos profissionais de saúde e ao doente.

Portanto, o trabalho desenvolvido nesta tese tem como objetivo o desenvolvimento de dispositivos rápidos, simples, precisos e autónomos para o rastreio e/ou diagnóstico no local de biomarcadores do cancro, usando métodos minimamente invasivos, tendo em vista um diagnóstico rápido e fiável. Para atingir este objetivo, foram desenvolvidos diferentes biossensores, usando anticorpos ou polímeros com impressão molecular como elementos de reconhecimento. Estes biossensores foram integrados numa célula de combustível de metanol passiva, com o objetivo de obter um dispositivo autónomo e para remover a necessidade de equipamentos na altura da medição analítica.

Esta tese demonstra a integração do primeiro imunossensor numa célula de combustível de metanol, trabalhando associados como um dispositivo biossensor autónomo e um sensor baseado na tecnologia de impressão molecular integrado, também, numa célula de combustível de metanol passiva acoplada a um dispositivo electrocrómico. Ambos os biossensores têm em vista a deteção de biomarcadores do cancro, em concreto o *cancer antigen* 15-3 (CA15-3) e a sarcosina. O desenvolvimento dos dispositivos autónomos compreendeu a conversão do ânodo da célula de combustível num elemento sensor. Para este efeito, o tecido de carbono que continha nanopartículas de platina/ruténio em *carbon black* foi modificado com um anticorpo seletivo a CA15-3 ou um MIP para sarcosina. O cátodo foi desenvolvido com nanopartículas de platina em *carbon black*. Estas células de combustível modificadas foram alimentadas com metanol diluído para gerar uma corrente dependente da

concentração e calibradas em diferentes meios (solução tampão e soro diluído), por incubação de concentrações crescentes de soluções do biomarcador alvo.

Em termos de desempenho analítico, foi possível observar uma resposta linear do imunossensor para a deteção com o logaritmo da concentração de CA15-3 entre 281.5 e 563 U/mL, para um limite de deteção de 39.8 U/mL. A seletividade deste biossensor foi também avaliada com biomarcadores do cancro concorrentes, tais como antígeno carcinoembrionário (CEA) e *cancer antigen 125* (CA125), tal como com outros compostos normalmente presentes no plasma sanguíneo (ácido ascórbico, glucose, ureia e ácido úrico), ajustados à concentração normal presente no soro. Os resultados que foram obtidos indicam uma boa seletividade do imunossensor integrado na célula de combustível. O dispositivo que integrava o MIP na célula de combustível apresentou uma resposta linear com o logaritmo da concentração de sarcosina, variando entre 3.2 e 2000 μM em tampão e em soro fetal bovino e com LoD de 0.04 μM, compatível com as concentrações esperadas em amostras reais.

A possibilidade de desenvolver um sistema biossensor sem qualquer equipamento foi explorada pelo acoplamento de uma célula electrocrómica ao dispositivo biossensor/célula de combustível. A célula electrocrómica demonstrou uma coloração azul intensa na energia máxima da célula de combustível e a coloração diminuiu com a diminuição da energia produzida pela célula de combustível, indicando por sua vez o aumento da concentração do biomarcador alvo. Esta abordagem foi testada para o dispositivo de deteção da sarcosina, com o sistema integrado (biossensor, célula de combustível e célula electrocrómica) a revelar a possibilidade de ver a olho nu a alteração de cor na presença de diferentes concentrações de sarcosina. De uma forma geral, esta abordagem confirmou a possibilidade de obter dispositivos que são autónomos e que não requerem equipamento analítico, podendo ser operados sem qualquer apoio energético ou eletrónico externo.

Palavras-chave: Dispositivo autónomo
Imunossensor
Polímero de Impressão Molecular
Biomarcador de cancro
Células de combustível de metanol

Abstract

Cancer is one of the leading causes of death worldwide and early diagnosis and treatment may reduce mortality associated with this disease. It is more likely to respond to treatment and has a better survival rate when identified at an early stage. An important way to avoid a late cancer diagnosis is screening. In current point-of-care (PoC), several devices have been developed with the purpose of detecting specific cancer biomarkers and helping to achieve an early diagnosis. The most used techniques for cancer diagnosis are biopsies, and magnetic resonance imaging (MRI), which are invasive, painful, and need a long time to produce analytical results. However, these methods are invasive, painful, and need a long period of time for result analysis and facilitated to the medical professional.

Therefore, the work in this thesis aims to develop quick, simple, accurate, and autonomous device for PoC cancer biomarker screening and/or diagnosis, by using minimally invasive methods, allowing for a quick and reliable diagnosis. To achieve this goal, different biosensors were developed, using antibodies or molecular imprinted polymers as recognition elements. These biosensors were integrated into a passive direct methanol fuel cell to obtain an autonomous device and to remove the need for any additional equipment.

This thesis shows the integration of the first immunosensor in a passive Direct Methanol Fuel Cell (DMFC) working combined as an autonomous biosensing device and a sensor based on the molecular imprinting technology also integrated into a passive DMFC and coupled to an electrochromic device (EC). Both biosensors have as aim the detection of cancer biomarkers, more concretely Cancer Antigen 15-3 (CA15-3) and sarcosine. The development of the autonomous devices consisted of the transformation of the fuel cell anode into a sensing element. For this, the carbon cloth with platinum/ruthenium nanoparticles on carbon black was modified with a selective CA15-3 antibody or a MIP for sarcosine. The cathode was a commercially available fuel cell electrode with platinum nanoparticles on carbon black. These modified fuel cells were fed with diluted methanol to generate a concentration-dependent current and calibrated in different media (buffer and diluted serum) by incubation of increasing target analyte concentration.

In terms of analytical performance, it was possible to observe a linear response for the immunosensor for CA15-3 detection with the log concentration that ranged from 581.5 to 563 U/mL, and the limit of detection (LoD) was 39.8 U/mL. The selectivity of this biosensor was also evaluated with competing cancer biomarkers, such as carcinoembryonic antigen (CEA), and cancer antigen 125 (CA125), as well as with other compounds normally present in blood plasma (ascorbic acid, glucose, urea, and uric acid), adjusted to the normal range of concentrations present in serum. The obtained results indicate good selectivity of the immunosensor integrated in the fuel cell. The electrochemical performance of the MIP-based DMFC-modified biosensor showed a linear trend with the log concentration of sarcosine ranging from 3.2 to 2000 μM in both buffer and FBS, with a LoD of 0.04 μM, compatible with the concentrations expected in real samples.

The possibility of developing a biosensing system in any equipment was exploited by coupling an EC to the DMFC-EC /biosensor. This EC showed an intense blue coloration at maximum cell power and this coloration decreased with decreasing power values, indicating the increase of the concentration of the target analyte. This approach was tested for the detection of sarcosine with the integrated system (DMFC-EC /biosensor) revealing the possibility of a naked eye-detectable color change in the presence of sarcosine standards. In a general way, this approach confirmed the possibility of developing devices that are autonomous and do not require analytical equipment, that can be operated without any energy requirements or external electrical equipment.

Keywords: Autonomous device
Immunosensor
Molecularly Imprinted Polymer
Cancer biomarker
Direct Methanol Fuel Cells

Table of contents

List of Figures

List of Tables

List of Abbreviations

Ab	Antibody
Acr	Acrylamide
AFCs	Alkaline Fuel Cells
Ag	Antigen
APS	Ammonium Persulfate
ATRP	Atom transfer radical polymerization
BFCs	Biofuel Cells
Bis-Acr	Bis-Acrylamide
BSA	Bovine Serum Albumin
CA125	Cancer Antigen 125
CA15-3	Cancer Antigen 15-3
CB	Carbon Black
CE	Counter Electrode
CEA	Carcinoembryonic Antigen
CLIA	Chemiluminescent immunoassay
CO	Carbon monoxide
CV	Cyclic Voltammetry
DL	Diffusion layer
DMFC	Direct Methanol Fuel Cell
DNA	Deoxyribonucleic acid
DPV	Differential Pulse Voltammetry
DSSC	Dye-Sensitized Solar Cell
EBSD	Electron Backscatter Diffraction
EC	Electrochromic Cell
ECL	Electrochemiluminescent assay
EDC	1-Ethyl-3-(3-dimethylaminopropyl)carbodiimide
EDS	Energy-dispersive X-ray spectroscopy
EIS	Electrochemical Impedance Spectroscopy
ELISA	Enzyme-linked Immunosorbent Assay

FC	Fuel Cell
FBS	Foetal Bovine Serum
FTIR-ATR	Fourier transform infrared spectroscopy - Attenuated total reflectance
GC	Gas Chromatography
hDMFC	hybrid DMFC
Ig	Immunoglobulin
ITO	Indium tin oxide
LC	Liquid Chromatography
LoD	Limit of Detection
LSV	Linear Sweep Voltammetry
MCFC	Molten Carbonate Fuel Cells
MEA	Membrane Electrode Assembly
MeOH	Methanol
MES	2-Morpholinoethanesulfonic acid
MIP	Molecularly Imprinted Polymer
MRI	Magnetic Resonance Imaging
MS	Mass Spectroscopy
MUC1	Mucin 1
NHS	N-Hydroxysuccinimide
NIP	Non-imprinted Polymer
OCP	Open Current Potential
PAFC	Phosphoric Acid Fuel Cells
PC	Propylene Carbonate
PEDOT	Poly(3,4-ethylenedioxythiophene)
PEM	Proton Exchange Membrane
PEMFCs	Proton Exchange Membrane Fuel Cells
PET/ITO	Indium Tin Oxide Coated PET
PNA	Peptide Nucleic Acids
PoC	Point-of-care
PSA	Prostate-specific Antigen
Pt/Ru	Platinum/Ruthenium
QCM	Quartz Cristal Microbalance

RAFT	Reversible addition-fragmentation chain transfer
RNA	Ribonucleic acid
SEM	Scanning Electrode Microscope Analysis
SOFC	Solid Oxide Fuel Cell
SWV	Square Wave Voltammetry
TEMED	Tetramethylethylenediamine
TPB	Triple Phase Boundary
WE	Working Electrode

1. INTRODUCTION

1. Motivation

Biosensors were first demonstrated in 1967 [1], where glucose oxidase was immobilized on a gel to measure glucose concentration in biological samples. Since then, biosensors have been gaining growing popularity, reaching nearly 10000 publications in 2022 [2]. **Figure 1.1** illustrates the evolution of biosensor publications in the last two decades, which reveals a significant increase in biosensor research after the early 2000s. This evolution are an expression of the importance and utility of these devices in the present and future of our society.

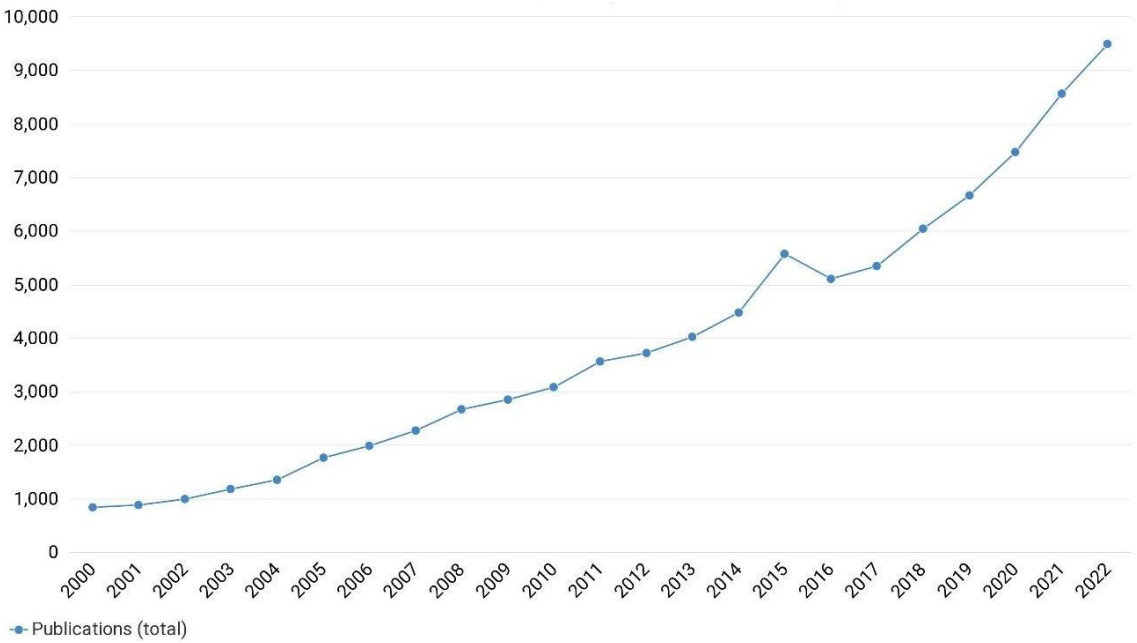

Figure 1.1 - The number of publications in the biosensors research field from 2000 to 2022 (Source: app.dimensions.ai; Criteria: "biosensors" in Title and Abstract).

Biosensors are widely employed in different fields for monitoring, diagnosis, and detection of different analytes. They are used in environmental and food applications, such as the detection of pesticides (both in the environment [3] and food [4]), water contaminants [5], organophosphates [6,7], heavy metals [8–10], and airborne pathogens [11,12], among others. But their main relevance comes from applications in

the health sector, such as glucose monitoring in diabetes patients [13,14], pregnancy tests (detection of hCG protein in urine), measurement of folic acid, biotin, vitamin B12 and pantothenic acid (as alternative to microbiological assays), among others. One of the applications of biosensors with high interest is the detection of different cancer biomarkers for diagnosis. **Figure 1.2** shows the increasing number of published articles since around 2005, achieving nearly 450 publications in 2022 [15]. This tendency implies the need of these kind of sensors as devices for cancer biomarker detection, aiding other methods of cancer diagnosis in the form of a non-invasive approach.

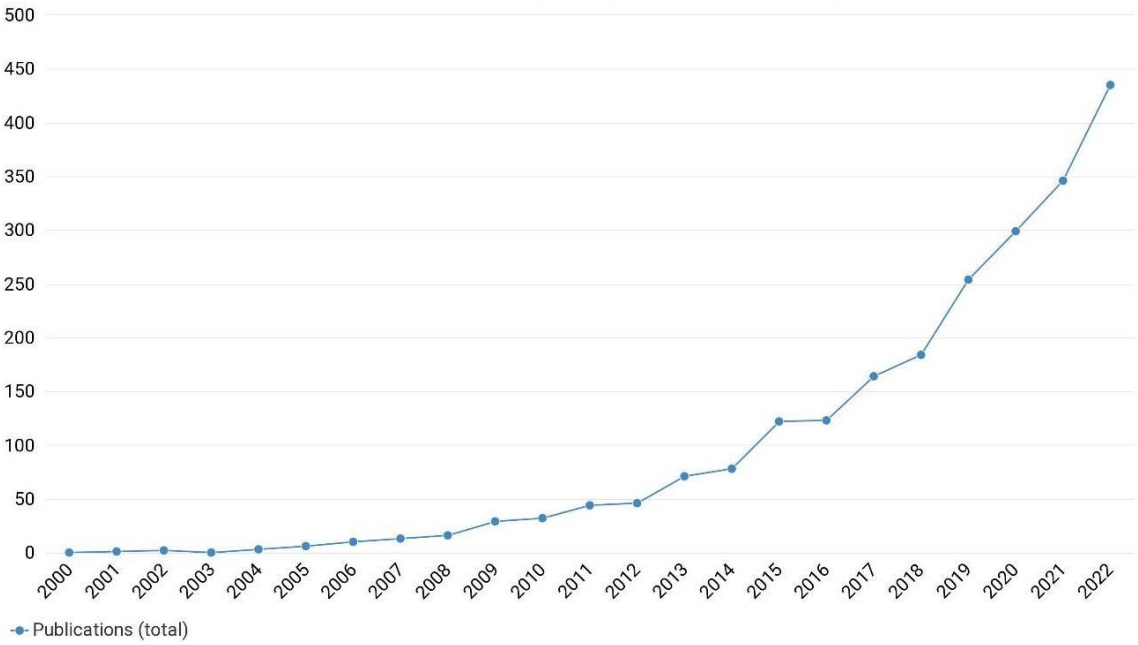

Figure 1.2 - The number of publications in the biosensors for cancer biomarkers detection research from 2000 to 2022 (Source: app.dimensions.ai; Criteria: "cancer biomarkers biosensors" in Title and Abstract).

The obvious need for this type of aid in the diagnosis of different healthcare issues, such as cancer, motivated this work. Cancer is one of the major causes of mortality and morbidity Worldwide. Some countries have already experienced that even when more and more people are diagnosed with cancer, mortality can be decreased and certain cancer diseases may be prevented, when relying on organized and quality-assured cancer screening [16]. A device that detects cancer biomarkers by using only serum and requiring no external power supply to enable the biomarker quantification would be very useful, not only in the day-by-day diagnosis made in the health clinic, but also in

low-income countries. In addition, this would be as a widespread and low-cost method that could be used in difficult scenarios of world crisis, such as we more recently had the chance to witness in form of the COVID-19 pandemic and Wars in different parts of the World.

1.1. Objectives

The work in this thesis had as main objective the development of autonomous biosensing devices, using electrical readings while displaying full autonomy in terms of electrical requirements. To this end, different technologies were integrated, as described next, targeting CA15-3 or sarcosine (both cancer biomarkers).

1) Electrochemical biosensors, focusing particularly upon the recognition element that enables detection of a given biomarker; two different materials were employed for this purpose, namely antibodies (immunosensor) and MIPs (MIP-based biosensor);
2) Fuel cells, by adapting a passive direct methanol fuel cell (DMFC) to enable the integration of the biosensor; the anode of the cell was modified with the recognition element.
3) Electrochromic Cell (EC), by interfacing this cell in the external electrical circuit of the set-up to enable a colour transduction of the electrical power generated by the overall system.

1.2. Outline

This thesis is divided into five chapters, summarized as followed:

- In this chapter, ***Chapter 1***, is where the motivation and objectives of this work are presented.

- In ***Chapter 2***, an overview of both major fields surrounding this work, biosensors and fuel cells, is introduced. A brief state-of-the-art applied to the selected biomarkers and autonomous devices is also presented.
- In ***Chapter 3***, a potentially autonomous immunosensor is described for the detection of CA15-3, by integrating an immunosensor into a DMFC, that may, later on, be used as a power supply.
- In ***Chapter 4***, an innovative electrochemical biosensor is described, which advances its autonomy towards an equipment-free design. The biosensor is powered by a passive direct methanol fuel cell (DMFC) and signals the response via an electrochromic display.
- In ***Chapter 5***, the main conclusions of this work are presented as well as future perspectives.

1.3. List of publications

1.3.1. Published papers

- Nádia S. Ferreira, Alexandra M.F. R. Pinto, M. Goreti F. Sales. Fuel cells operating as an immunosensor for cancer biomarker screening; 2023. Biosensors and Bioelectronics X, Vol. 14, 100344.

- Liliana P.T. Carneiro, Nádia S. Ferreira, Alexandra M.F.R. Pinto and M. Goreti F. Sales, 2023. Chapter 13: Nano-inks for fuel cells application. Smart multifunctional nano-inks: Fundamentals and Emerging Applications. 1st Edition. Elsevier.

- Nádia S. Ferreira, Liliana P. T. Carneiro, Christian Viezzer, Maria J. T. Almeida, Ana C. Marques, Alexandra M.F. R. Pinto, Elvira Fortunato, M. Goreti F. Sales; 2022. Passive direct methanol fuel cells acting as fully autonomous electrochemical biosensors: Application to sarcosine detection. Journal of Electroanalytical Chemistry 922.

- Liliana P. T. Carneiro, Nádia S. Ferreira, Ana P. M. Tavares, Alexandra F. M. R. Pinto, Adélio Mendes, M. Goreti F. Sales; 2021. A passive direct methanol fuel cell as

transducer of an electrochemical sensor, applied to the detection of carcinoembryonic antigen. Biosensors and Bioelectronics 175.

1.3.2. Communications

- Nádia S. Ferreira, Alexandra M.F.R. Pinto and M.G.F. Sales. Autonomous immunosensor employing fuel cells for cancer biomarker screening. Presented at Biosensors 2021 Conference, 26-29 July 2021, online.

- Nádia Ferreira, Lúcia Brandão, Goreti Sales. Glucose fuel cell powered biosensor for acetylcholinesterase using molecular imprinting technology. Presented at the Biosensors 2018 Conference, 12 - 15 June 2018, Miami, USA.

- Nádia S. Ferreira, Liliana P. T. Carneiro, Maria J. T. Almeida and M. Goreti F. Sales. Sensing polymer for sarcosine detection operating in a passive methanol fuel cell. Presented at ANM 2019 Conference, held at Aveiro University, Portugal. 17-19 July 2019.

- Nádia S. Ferreira, Lúcia Brandão, M. Goreti F. Sales. Molecularly imprinted polymer inserted in abiotic glucose fuel cell powered biosensor for acetylcholinesterase. Presented at the 7th Graduate Student Symposium on Molecular Imprinting, held at ISEP, Porto (PT), 8 and 9 June 2017.

- Nádia S. Ferreira, Lúcia Brandão, M. Goreti F. Sales. Carbon Black modification for polymer anchoring targeting fuel cell powered biosensors. Presented in NanoPT, February 16-19, 2016, INL Braga.

1.4. References

[1] S.J. UPDIKE, G.P. HICKS, The Enzyme Electrode, Nature. 214 (1967) 986–988. https://doi.org/10.1038/214986a0.

[2] D.S.& R.S. Inc., Dimensions AI, (2023). https://app.dimensions.ai/analytics/publication/overview/timeline?search_mode=content&search_text=biosensors&search_type=kws&search_field=full_search&year_from=1982&year_to=2021 (accessed March 6, 2023).

[3] N.F. Che Lah, A.L. Ahmad, S.C. Low, Molecular imprinted membrane biosensor for pesticide detection: Perspectives and challenges, Polym. Adv. Technol. 32 (2021) 17–30. https://doi.org/10.1002/pat.5098.

[4] L. Karadurmus, S.I. Kaya, S.A. Ozkan, Recent advances of enzyme biosensors for pesticide detection in foods, J. Food Meas. Charact. 15 (2021) 4582–4595. https://doi.org/10.1007/s11694-021-01032-3.

[5] J.K. Jung, K.K. Alam, M.S. Verosloff, D.A. Capdevila, M. Desmau, P.R. Clauer, J.W. Lee, P.Q. Nguyen, P.A. Pastén, S.J. Matiasek, J.-F. Gaillard, D.P. Giedroc, J.J. Collins, J.B. Lucks, Cell-free biosensors for rapid detection of water contaminants, Nat. Biotechnol. 38 (2020) 1451–1459. https://doi.org/10.1038/s41587-020-0571-7.

[6] J. Kaur, P.K. Singh, Enzyme-based optical biosensors for organophosphate class of pesticide detection, Phys. Chem. Chem. Phys. 22 (2020) 15105–15119. https://doi.org/10.1039/D0CP01647K.

[7] P. Zhang, T. Sun, S. Rong, D. Zeng, H. Yu, Z. Zhang, D. Chang, H. Pan, A sensitive amperometric AChE-biosensor for organophosphate pesticides detection based on conjugated polymer and Ag-rGO-NH 2 nanocomposite, Bioelectrochemistry. 127 (2019) 163–170. https://doi.org/10.1016/j.bioelechem.2019.02.003.

[8] G.E. De Benedetto, S. Di Masi, A. Pennetta, C. Malitesta, Response surface methodology for the optimisation of electrochemical biosensors for heavy metals detection, Biosensors. 9 (2019). https://doi.org/10.3390/bios9010026.

[9] A.S. Maghsoudi, S. Hassani, K. Mirnia, M. Abdollahi, Recent advances in nanotechnology-based biosensors development for detection of arsenic, lead, mercury, and cadmium, Int. J. Nanomedicine. 16 (2021) 803–832. https://doi.org/10.2147/IJN.S294417.

[10] K. Velusamy, S. Periyasamy, P.S. Kumar, G. Rangasamy, J.M. Nisha Pauline, P. Ramaraju, S. Mohanasundaram, D.V. Nguyen Vo, Biosensor for heavy metals detection in wastewater: A review, Food Chem. Toxicol. 168 (2022) 113307. https://doi.org/10.1016/j.fct.2022.113307.

[11] R. Sivakumar, N.Y. Lee, Recent advances in airborne pathogen detection using optical and electrochemical biosensors, Anal. Chim. Acta. (2022) 340297. https://doi.org/10.1016/j.aca.2022.340297.

[12] J. Ma, M. Du, C. Wang, X. Xie, H. Wang, Q. Zhang, Advances in airborne microorganisms detection using biosensors: A critical review, Front. Environ. Sci. Eng. 15 (2021) 1–19. https://doi.org/10.1007/s11783-021-1420-8.

[13] I. Lee, D. Probst, D. Klonoff, K. Sode, Continuous glucose monitoring systems - Current status and future perspectives of the flagship technologies in biosensor research -, Biosens. Bioelectron. 181 (2021) 113054. https://doi.org/10.1016/J.BIOS.2021.113054.

[14] C. Sabu, T.K. Henna, V.R. Raphey, K.P. Nivitha, K. Pramod, Advanced biosensors for glucose and insulin, Biosens. Bioelectron. 141 (2019) 111201. https://doi.org/10.1016/J.BIOS.2019.03.034.

[15] D.S.& R.S. Inc., Dimensions AI, (2023). https://app.dimensions.ai/analytics/publication/overview/timeline?search_mode=content&search_text=cancer biomarker biosensors&search_type=kws&search_field=text_search&year_from=2000&year_to=2021 (accessed March 6, 2023).

[16] World Health Organization (WHO), A short guide to cancer screening., 2022. https://apps.who.int/iris/bitstream/handle/10665/351396/9789289057561-eng.pdf.

2. STATE OF THE ART

2.1. Cancer disease

2.1.1. Cancer, statistics, and diagnostic methods

Cancer is, by definition, a disease where some body cells grow in an uncontrollable manner and spread to other tissues. This happens when the normal cell multiplication process breaks down and abnormal and/or damaged cells multiply, forming tumours (malignant or benign). Malignant tumours invade nearby tissues and may travel to various parts of the body (metastasis) whereas benign tumours don't act in the same way and don't grow back like malignant tumours sometimes do [1].

Cancer is one of the leading causes of death worldwide with lung, breast, colorectal, and prostate cancer being the most diagnosed forms of the disease [2], as shown in **Figure 2.1**. Early diagnosis and treatment may reduce mortality associated with cancer disease, as it is more likely to respond to treatment and have a better survival rate when cancer is identified at an early stage [3,4]. An important way to avoid a late cancer diagnosis is screening. This aims to identify possible cancer or pre-cancer states before the development of symptoms, leading to further tests to confirm the diagnosis. The technique that is most used to diagnose cancer is biopsy, which may be linked or not to magnetic resonance imaging (MRI) [5]. Some biomarker-based expression techniques are also used to complement the imaging data, such as ELISA, radioimmunoassay, and immunohistochemistry. Although all these methods are effective, biopsy is invasive and painful, and the other techniques need a long time to produce analytical results [6].

To avoid time-consuming exams and allow analytical tests in current PoC [7], several devices have been developed with the purpose of detecting specific cancer biomarkers [8–11]. Electrical-based devices are generally very sensitive and provide label-free responses, but they have electrical power requirement. This requirement limits the application of the device to places where an electrical source is present, which may not exist under environmental crisis events and in third-world countries.

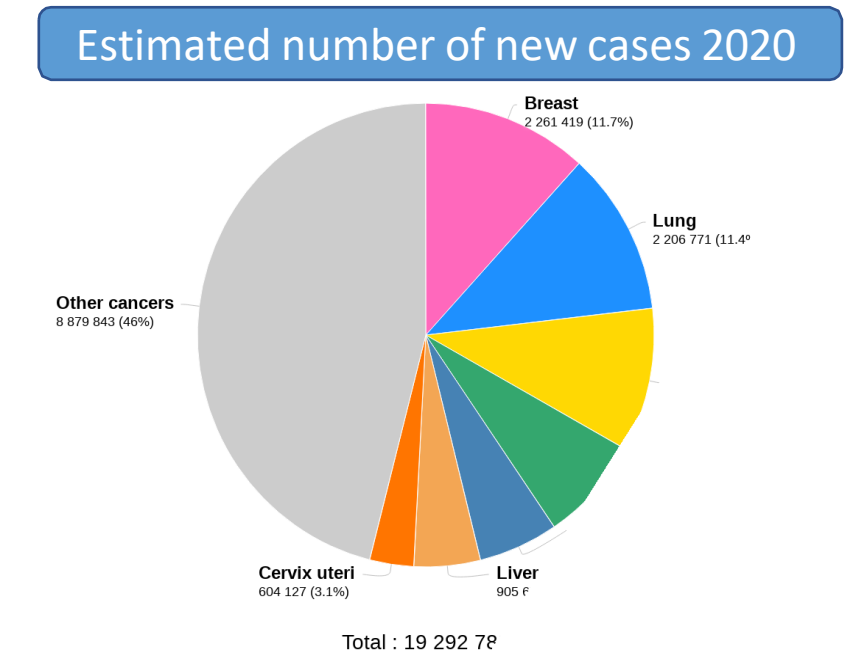

Figure 2.1 - Estimated number of new cancer cases and deaths in 2020 in both sexes, all ages, and worldwide. Data and graph adapted from [2].

2.1.2. Cancer biomarkers

Biomarker is "a defined characteristic that is measured as an indicator of normal biological processes, pathogenic processes or responses to an exposure or intervention", as defined by the Food and Drug Administration (FDA) and National Institute of Health (NIH) joint Biomarker Working Group [12–14]. A cancer biomarker is any "biological molecule produced by a tumour cell or by human tissues in response to a tumour that is objectively measured and evaluated as an indicator of cancerous processes within the body" [13,15]. These molecules may be nucleic acids (DNA, RNA), proteins (enzymes, receptors), peptides, hormones, and even metabolites (**Figure 2.2**) that can be detected in different media, such as in the circulation (blood, serum or plasma), secretions (urine), or in other human biological fluids [13,16].

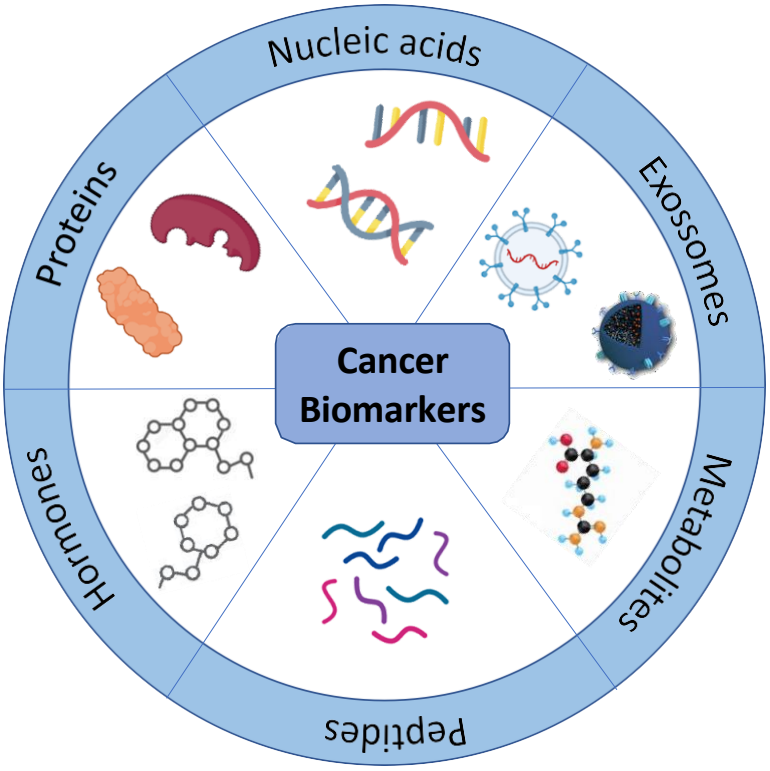

Figure 2.2 - Different molecules that act as cancer biomarkers in the body.

Biomarkers can be used in different clinical settings, such as in risk assessment and screening for early disease, diagnosis of the different types and/or stages of cancer, and monitoring status of the disease (monitoring therapy, detecting recurrence) [16]. In

many cancer types, there is an advantage of cure if diagnosed and treated in an early stage. Thus, early cancer detection in asymptomatic patients is one of the most important goals in cancer research [13,17], leaving the market open for new and innovative sensors to be employed in mass population screening. However, these sensors need to have challenging characteristics, such as adequate diagnostic sensitivity and selectivity, they must be inexpensive and safe to use in populations, and need to have a good analytic reproducibility [17]. Also, biomarker screening is widely used as an aid for cancer diagnosis and/or sub-classification of malignancy state.

Within the scope of this thesis, CA15-3 and sarcosine were selected as target cancer biomarkers, merely as proof-of-concept of the technology to be developed. CA15-3 is a consolidate cancer biomarker of protein nature used in clinical, while sarcosine is an emerging cancer biomarker that corresponds to a small molecule that circulates in body fluids. These biomarkers are described next.

2.1.3. Cancer Antigen 15-3 (CA15-3)

CA15-3, also known as a soluble form of MUC1, is a large trans-membrane glycoprotein (around 400 – 450 kDa) that is expressed on the surface of epithelial tissues including mammary gland, gastrointestinal, respiratory, urinary, and reproductive tracts. Typically, mucins contribute to the protection and lubrication of the epithelial tissues, and are involved in signal transduction and cell adhesion [18–20]. In healthy people, CA15-3 concentration is up to 25 U/mL [21]. Altered expression of this protein is known to reveal cancer formation and metastasis. Although CA15-3 may also be in higher concentrations in individuals with different conditions, such as cirrhosis, hepatitis, benign breast disease, and, most recently, COVID-19 [22]. It is more commonly found in patients with different types of cancer (breast, ovary, lung, gastrointestinal, colorectal cancers) [21] and is widely studied and used as non-invasive biomarker for cancer prognosis, diagnosis and monitoring [18,20]. Even though it is still not known how CA15-3 accumulates in the blood circulation [23], this protein is one of the most established serum biomarkers used for the diagnosis and prognosis of several cancers, mostly for breast cancer.

Different methods have been used for serum CA15-3 level measurements, such as enzyme-linked immunosorbent assay (ELISA), electrochemiluminescent (ECL), chemiluminescence immunoassay (CLIA), and radioimmunoassay [24,25]. ELISA is the most common technique that is used for serum CA15-3 detection (~ 42.9%), which has as advantages requiring less sample pre-treatment, low cost, and high level of selectivity. However, the process requires longer incubation times, and has low sensitivity [23,25]. Therefore, it is important to develop more appropriate analytical methods, that are selective and sensitive for CA15-3 detection in biological samples and at low concentrations. In recent years, increasing numbers of different biosensors for CA15-3 detection have been reported, being considered as alternative approaches for early cancer diagnosis [25].

To date, there are several biosensors for the determination of CA15-3. These include various concepts and approaches, many of which are electrochemical [8–10], optical [26], or lateral flow assays [27–29]. Some biosensors from the literature targeting the detection of CA15-3 were used for comparison with the work that will be described in this thesis, in Chapter 3. **Table 3.2** lists other biosensors for CA15-3 detection from recent years.

2.1.4. Sarcosine

Sarcosine, also known as *N*-methylglycine, is a non-proteinogenic amino acid derivative that occurs in the body as a product of the glycine and creatinine metabolism. It is found predominantly in the skeletal muscles and prostate of the human body. Normal sarcosine levels in serum are 80.8 ng/mL and 102.3 ng/mL in females and males, respectively [30]. Elevated values of this amino acid derivative are implicated with the presence of multiple diseases, like Alzheimer, dementia, colorectal, stomach and prostate cancers, among others. Research demonstrated clinical benefits of using sarcosine in treating mental health disorders [31]. Also, it is considered a promising biomarker for prostate cancer [32]. The research of this amino acid as prostate cancer biomarker was introduced in 2009 in the Journal *Nature* [33]. Since then, a great increase of its levels in body fluids has been associated to prostate cancer progression

and metastatic events [34]. Thus, these can be detected in a non-invasive manner by analysing urine [35,36]. Several studies have indicated the power of diagnosis of sarcosine compared to total Prostate-Specific Antigen (PSA) [37,38]. This trend supports the fact that sarcosine is an important biomarker for prostate cancer diagnosis and could be used successfully for screening tests.

Sarcosine is commonly detected by using different techniques, such as enzymatic assays (colorimetric or fluorometric), gas chromatography (GC), liquid chromatography (LC), mass spectrometry (MS), among others [32,39]. All these techniques have drawbacks: enzymatic colorimetric and fluorometric assays are time consuming and expensive; the chromatographic separation techniques are expensive, and the high cost of instrumental setup, experts in operating the instruments, reagent and high-volume sample consumption, sample pre-treatment, and long-time procedures [32]. Because of the disadvantages of these traditional methods, studies involving biosensors for sarcosine detection have been made, aiming at selective, sensitive, low-cost, rapid, and reproducible methods. Several approaches for screening sarcosine have been described in the literature, including enzymatic assays [40–43], and molecular imprinted polymers (MIPs) [44–46]. However, none of these approaches offers the possibility of complete autonomy when used for PoC. Therefore, in this thesis, we propose a biosensor for sarcosine detection involving an autonomous and potentially portable power source.

Overall, diagnosing and monitoring cancer disease is mostly accomplished by routine examinations such as biopsy, ultrasound, and MRI. These methods, which rely on the physical properties of the tumour and its appearance, have various disadvantages, including invasiveness, complexity, the need for sophisticated instruments and background knowledge, and the long results turn-over [4,50]. The main focus in cancer diagnosis is the development of techniques that are explicitly capable of sensitive detection of different cancer biomarkers, which would be very useful in PoC testing [51]. In this context, biosensors are emerging an alternative methods [52], as they are non-invasive, show good analytical performance and allow the analysis of a biological sample on site. These are described in more detail next.

2.2. Biosensors

Biosensors are analytical devices composed by a biorecognition element (such as cells, enzymes, antibodies, aptamers, among others), and a transducer that translates the information of the analyte recognition (**Figure 2.3**).

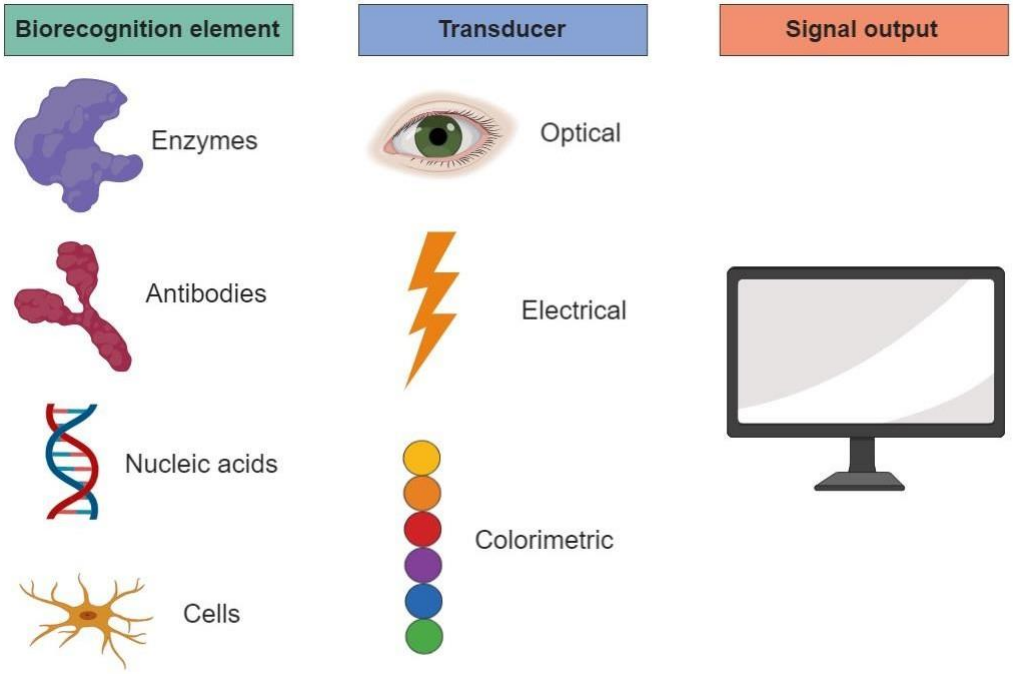

Figure 2.3 - Examples of biorecognition elements, transducers, and signal output linked to biosensors.

The biological recognition element interacts with the target molecule so that the transducer measures and translates this interaction into a measurable signal (optical, colorimetric, piezoelectric, electrochemical, among others).

The first biosensor used glucose oxidase immobilized on a gel to measure glucose concentration in biological samples [53]. Since then, biosensors have evolved tremendously into different technological formats, gaining popularity for different targets and in different fields. The main fields of application include medicine, environmental monitoring, food quality control, and control of industrial processes [54,55]. In medicine and healthcare, one of the major advantages of biosensors is the rapid diagnostics. Since biosensors provide results almost instantly, allowing clinical diagnosis immediately, which greatly decreased the need for lengthy laboratory

procedures. Additionally, these rapid diagnostic products make self-testing at home possible with user-friendly formats and simplified protocols, such as pregnancy tests and COVID-19 rapid tests. They are applicable in PoC systems, such as glucose, lactate, creatinine and cholesterol [50,56,57], cancer screening and diagnosis (analysis in urine and blood plasma) [4,51,58], DNA diagnosis for genetic diseases discovery [59], kits for self-diagnosis at home [54], and detection of infectious diseases [50,57,60,61]. In environmental monitoring these biosensors are widely used for pesticides detection [62,63], heavy metals in ground and wastewater [64,65], and volatile compounds in industrial areas [54]. Furthermore, biosensors can be used to control food quality by detecting microbiological contamination, antibiotics and mycotoxins [66], pesticides [67], food fermentation [68,69], preservatives, and additives [70]. The research and advances in all these fields translate the need for different biosensors for accurate, low-cost, and quick detection of different analytes, may they be in healthcare, food quality control or even environmental monitoring.

From an analytical perspective, a good biosensor should display high selectivity, sensitivity, and reproducibility. High sensitivity is defined as a large measurable change in the biosensor signal when slight changes in analyte concentration occur. High selectivity indicates that the sensor responds majorly to its target rather than other compounds that can be found in the analysed medium. High reproducibility demonstrates the ability to provide similar responses among different units, among other aspects of reproducible operation [71]. In general, these analytical features are mainly related to the biorecognition elements employed when developing the biosensor. There are several materials that may be employed for this purpose, which are described next.

2.2.1.(Bio)Recognition elements

The recognition element is normally a molecular species that uses a biochemical mechanism for the recognition of the selected analytes. The biorecognition element binds the analyte to the sensor surface for reaction/interaction, which is afterwards converted by the transduction mechanism [57,72]. Different types of recognition

elements have been used in the last decades of research, such as animal or plant cells, receptors, organelles, antibodies, tissues, microbes and enzymes. Artificial materials like MIPs, aptamers or Peptide Nucleic Acids (PNAs) have also been widely used [56]. Choosing a recognition element for a biosensor is a critical task and should be performed with the knowledge of the advantages and disadvantages of the different recognition elements that have been used throughout the last decades of biosensor research. In terms of recognition, biosensors may operate by means of a catalytic or an affinity event.

Catalytic biosensors are those in which the recognition is made by means of a catalytic reaction. Typically recognition elements displaying this feature are enzymes, whole cells or tissue slices [54,73,74]. Among these, enzymes are traditionally employed. They interact selectively with a given substrate using non-covalent interactions [75], to create a spatial environment that facilitates the chemical transformation of the substrate, by decreasing the activation energy of the overall reaction [66]. Upon the catalytic reaction, any participating element of the reaction may be monitored (substrate or product or other involved reactants), as its change in concentration is used for analytical purposes. Overall, catalytic-based sensors have simple designs and don't require expensive instrumentation, making them simple to use and inexpensive [76]. But not all recognition elements may trigger a catalytic event, with affinity sensing being an alternative tool of recognition.

Affinity biosensors involve mostly non-covalent interactions with a target analyte upon analyte binding, without its chemical alteration. Typical affinity-based recognition elements are antibodies, nucleic acids (DNA, RNA), aptamers, MIPs, among others [73,74,76]. Antibodies are the most commonly employed affinity recognition elements, giving rise to the production of immunosensors, as they replicate an immunological response. Antibodies are 3D protein structures (~150 KDa) that occur naturally in the body, displaying a unique recognition pattern with high specificity and accuracy for the respective analyte. Although there are widely known limitations when using antibodies, such as animal experimentation, production cost, and limited shelf life, they are widely used and remain an important recognition element in the biosensing community [71,77]. Nucleic acid biosensors, also known as genosensors, are able to bind to a complementary recognition pattern, between the immobilized nucleic acid fragment and the target sequence [78,79]. Genosensors are very versatile because, in principle,

any nucleic acid fragment could be artificially designed and immobilized. PNAs are synthetic oligonucleotides that are uncharged, and therefore create a higher stability when binding. Considering applications, these elements are limited to targeting nucleic acids [71,80], due to the nature of their recognition. Aptamers are like nucleic acids in genosensors, but in which the nucleic acid sequence is designed to interact with another molecule that is not a nucleic acid. In principle, the immobilized aptamer undergoes specific 3D arrangements that involve trapping the target analyte on a specific conformation. MIPs are synthetic polymers tailored around a target compound, and when the target compound exits the polymeric network created vacant sites that should be able to recognize the same analyte. They were originally developed for concentrating specific compounds, but their capacity to undergo selective interactions with a given analyte opened doors into an application in biosensors.

In this thesis, two recognition elements involved in affinity sensing were considered: antibodies and MIPs. Several reasons supported this. Catalytic sensing of CA15-3 or sarcosine would imply indirect and complex approaches. In contrast, the use of antibodies would ensure a simple and effective design, as antibodies have typically high affinities for the target antigen. On the other hand, the design of a synthetic element as a MIP would enable selective readings at low cost, with a stable recognition material. In principle, MIP technology allows a tailor-made design for any intended antigen, making this a versatile option of detecting cancer biomarkers. The next section explains further these specific recognition elements.

2.2.1.1. Molecular Imprinted Polymers (MIPs)

MIPs, also known as 'plastic antibodies' when proteins are being targeted, were firstly reported in 1973 [81] and have raised a lot of interest in the past decades [82]. These polymeric structures act as antibody-like recognition materials and operate by a "lock and key" mechanism, mimicking the antibody-antigen interactions and selective binding to the target molecule used during production. Compared to natural antibodies, these are also less expensive and have higher stability [83]. These are tailored by molecular imprinting technology, where molecular moulds are generated by using a

target molecule and then removing it, leaving cavities where the molecule can rebind, as represented in **Figure 2.4**. There are various advantages in using MIPs, including their high affinity and selectivity, which are similar to natural receptors; great robustness and physical strength, resistance to elevated pressure and temperature, inertness against various chemicals (acids, bases, organic solvents), which are superior to the natural biomolecules characteristics; low cost and simplicity of their preparation, allowing the development of a receptor for an analyte of interest to be available faster and in a less expensive manner; template versatility, since they are able to recognize analytes that are challenging for antibody detection; easy adaptation to practical applications; and long lifetimes [84–86]. An additional and important advantage of these plastic antibodies is the possibility to develop them for almost any target molecule, large or small, which differentiates it from the natural biological systems, where the target must match an available antibody, or an antibody must be specifically produced for that target.

The advantages of MIP materials compared to their natural counterparts led to their use in different applications, such as immunoassays [87], separation [87–90], depollution [91], sensing [92–95], cell imaging and therapy [96–98], drug delivery [99–101], food applications [88,90,102], and industrial applications [103]. Previously described works using plastic antibodies to detect cancer biomarkers show promising results in detecting early stage cancer biomarkers [104,105], obtaining good LoDs and reproducibility.

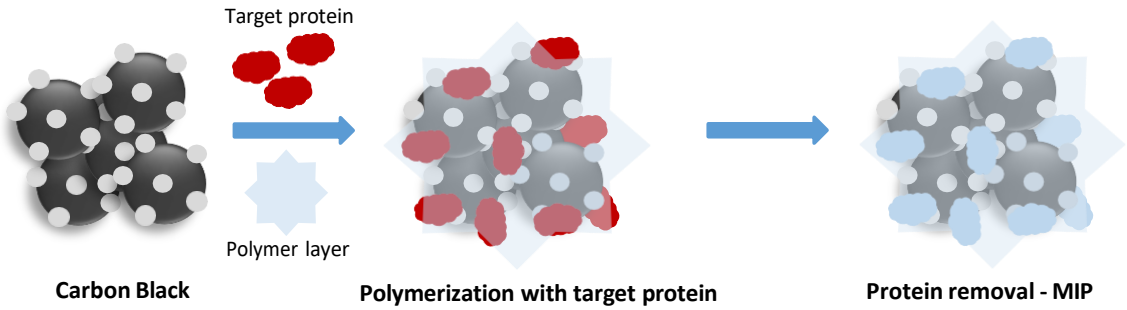

Figure 2.4 - Scheme of the MIP on top of the surface of carbon black with Platinum (Pt) and Ruthenium (Ru) nanoparticles.

MIP-based materials are attracting attention due to the possibility of mass production, simplicity, improved shelf-life, and low cost [106]. The commercialization of these MIPs mostly involves materials for separation, and not sensors. This is mostly because of the occurrence of non-specific binding to the polymer itself due to the adsorbent characteristic and some weak interactions with the target molecule. Also, the need to extract the target molecule from the polymer and its difficulty to ensure the total extraction, compromising the ability to sense the rebinding, may be a reason for the slow commercialization of these sensors. However, the increasing numbers of research articles published in this area, lets speculate the commercialization of more and more sensors with this technology in the near future [82]. These MIPs have been widely used in the biosensors field as recognition elements to achieve more stable, low cost and sensitive sensors for detection of different biomarkers. In recent years, MIP-based biosensors have been developed to detect biomarkers for different diseases and different fields, such as cardiovascular diseases [107,108], cancer [109,110], infectious diseases [111–115], and also for environmental monitoring [116,117]. **Table 2.1** shows some examples of MIP-based biosensors in the different fields, revealing the importance of these biosensors for detection and monitoring of different target compounds.

Table 2.1 - Literature review of MIP-based biosensors in different fields.

	Target	MIP	Support	Detection	Ref
Cardiovascular diseases	Cardiac Troponin T	Polyaniline	CSPE	DPV	[118]
	Cardiac Troponin I	Methylene Blue	GCE	DPV	[119]
	Myoglobin	Methacrylic acid	Au	DPV	[120]
Sepsis	C Reactive Protein	AEDP/DMAA	CSPE	DPV	[121]
	Lactate	3-APBA	CSPE	DPV	[107]
Cancer	PSA	Dopamine	Au	EIS	[122]
	CEA	Toluidine blue	Au	CV	[123]
	CA125	Pyrrole	AuSPE	SWV	[124]
	CA15-3	Toluidine blue	Au	DPV	[125]
Infectious diseases	Influenza A H5N1	AA/MAA/MMA/NVP	QCM electrode	QCM	[114]
	Klebsiella pneumoniae	MAM/AAM/NVP	AuSPE	CV	[115]

Environmental	Tetracycline	Methacrylate	GPUE	DPV	[116]
	Glyphosate	*p*-aminothiophenol	AuNPs	LSV	[126]
	Norfloxacin	*p*-ATP	AuNPs	EIS	[127]

3-APBA: 3-aminophenylboronic acid; **AA/MAA/MMA/NVP:** acrylamide/methacrylic acid/methylmethacrylate/N-vinylpyrrolidone; **AEDP/DMAA:** 2-acryl amidoethyldihydrogen phosphate/N-(4-dimethylaminophenyl)-acrylamide; **Au:** Gold electrode; **AuNPs:** Gold Nanoparticles; **AuSPE:** Gold Screen Printed Electrode; **CA125:** Cancer Antigen 125; **CA15-3:** Cancer Antigen 15-3; **CEA:** carcinoembryonic antigen; **CSPE:** Carbon Screen Printed Electrode; **CV:** Cyclic Voltammetry; **DPV:** Differential Pulse Voltammetry; **EIS:** Electrochemical Impedance Spectroscopy; **GPUE:** graphite-polyurethane composite electrode; **LSV:** Linear Sweep Voltammetry; **MAM/AA/NVP**: poly(methyl methacrylate)/Acrylamide/ N-vinylpyrrolidone; ***p*-ATP:** *p*-aminothiolphenol **PSA:** prostate specific antigen; **QCM:** quartz crystal microbalance; **SWV:** Square Wave Voltammetry.

These MIP-based recognition materials can be obtained by using different methods of polymerization, broadly classified into free-radical polymerization and sol-gel process. In this thesis, the free-radical polymerization procedure was used as the monomers employed contained mostly unsaturated C-C bonds. Free-radical polymerization is a method where the polymeric chains are formed by successive addition of monomers to a growing chain of a radical species. The polymeric chain propagates in a way that each monomer unit is added to the chain in a manner that generates a more stable radical.

Radical polymerization occurs in three steps: initiation, where non-radical species generate radicals; propagation, where the radical addition occurs; and termination, where the polymerization process ends [128]. During initiation, an active centre is created (obtained from the breakdown of the initiator molecule) from where the polymer chain begins to grow. There are many ways to initiate the polymerization process, such as thermal decomposition, chemical initiators, radiation, electrochemical processes, sonication, and other. The propagation phase refers to the addition and linkage of more monomers to the initial chain, which will continue until the termination of this process occurs. The termination process may occur in two ways: by coupling, where the radicals of two growing chain bond together, leaving no free radicals to continue the propagation; or disproportionation, where a hydrogen atom from one radical polymer chain is transferred to another radical polymer chain, terminating the two growing polymeric chains.

There are several free-radical polymerization approaches that can be used to generate a MIP receptor (**Table 2.2**). The most used method is bulk polymerization due

to its simplicity, rapidity, and no need for sophisticated equipment. However, it requires a large amount of template, and the synthesized bulk polymer has to be crushed, grounded, and sieved to the size of interest, which is time consuming and some high-affinity binding sites may be destroyed during this process [92]. Although there are some disadvantages to this technique, the long experience of the literature in this technology allied to its versatility support well its selection for the production of a MIP recognition element for CA15-3, as implemented in this thesis.

Table 2.2 - Overview of polymerization techniques.

Imprinting Methods	Brief description	Reference
Bulk polymerization	Addition of a soluble radical initiator to a pure monomer in the liquid state.	[129]
ATRP	Usually employs a transition metal complex as the catalyst.	[130]
RAFT	Uses a chain-transfer agent in the form of thiocarbonylthio compound – RAFT agent.	[131]
Sol-gel	A colloidal solution is poly-condensed into a solid (gel) phase.	[132]

ATRP: Atom transfer radical polymerization; **RAFT:** Reversible addition fragmentation chain transfer.

One of the approaches in this work is to develop a MIP that uses chemicals to initiate the reaction. This can be very effective in polymerizing vinyl monomers. In addition, free radical polymerization can be performed under mild reaction conditions (water as solvent, low temperatures, etc.), which is an important feature regarding the preparation of MIPs using proteins, such as cancer biomarkers, as target molecules [133]. This process may take few minutes or last few hours, being this duration dependent on the type of monomers and cross-linkers present in the polymer mixture. The obtained MIP should have the properties that are already associated with this kind of materials, as described before [84,85].

2.2.1.1. Immunosensors

Immunosensors are biosensors which are based in interactions between antibody and antigen to form a stable immunocomplex [134]. Either antibody or antigen can be used as immobilized species on the biosensor platform, depending on which target

needs to be analysed. The binding forces between the antibody and the antigen are very strong, and therefore, immunosensors present a high selectivity and sensitivity, making them a very attractive sensor for many different applications in different science fields [135].

Antibodies, also called immunoglobulins (Ig), are naturally secreted by B cells to neutralize antigens such as bacteria and viruses. They are a large family of glycoproteins that are capable of recognize and bind to antigens with high selectivity, composed of one or more copies of the characteristic and well-known unit that can be visualized as a "Y" shape. Each tip of the "Y" contains a paratope, which is a structure analogous to a lock, that is specific for one epitope (analogous to a key) on an antigen. This allows these two structures to bind with a very high precision.

There are two types of antibodies: monoclonal and polyclonal, which depend on the epitope. Monoclonal antibodies are generated by identical B cells, meaning that these antibodies have monovalent affinity and only recognize the same epitope of an antigen, which reduces the chance of cross-reactivity, but also decreases sensitivity. Polyclonal antibodies are produced by different B cell clones in the body, meaning that they can recognize and bind to many different epitopes of a single antigen, showing a heterogeneous immunological response [135,136]. They offer a more sensitive response that may be compromised in terms of selectivity. The choice to use monoclonal or polyclonal antibodies depend on the analytical application.

Immunosensors using electrochemical transducers are ideal biosensing devices for accurate and sensitive detection and quantification of tumour biomarkers. These integrate the advantages of the electrochemical procedures, and the specific reaction between the antibodies and antigens. PoC testing can be very effective using these types of devices due to their high sensitivity, small sample consumption, low sensing expenses, and the easy miniaturization to develop handheld devices [137,138].

There are two types of approaches to develop an immunosensor: direct immunosensor (or label-free), and indirect immunosensor (or labelled). Direct immunosensors measures the presence of the analyte directly through the biochemical reaction that occurs on the biosensor platform, whereas in indirect immunosensors, the analyte is entrapped between the capture agent and labelled agent, which has a specific label (enzymes, quantum dot, fluorophore, or radioisotope) to emit a signal that can be

measured [134,137,138], as explained in the scheme in **Figure 2.5**. Although the indirect immunosensors are more sensitive, they are more complex and not suited for PoC devices. Therefore, the direct immunosensors have been widely studied as a potential alternative due to their simplicity, which was also chosen for this thesis.

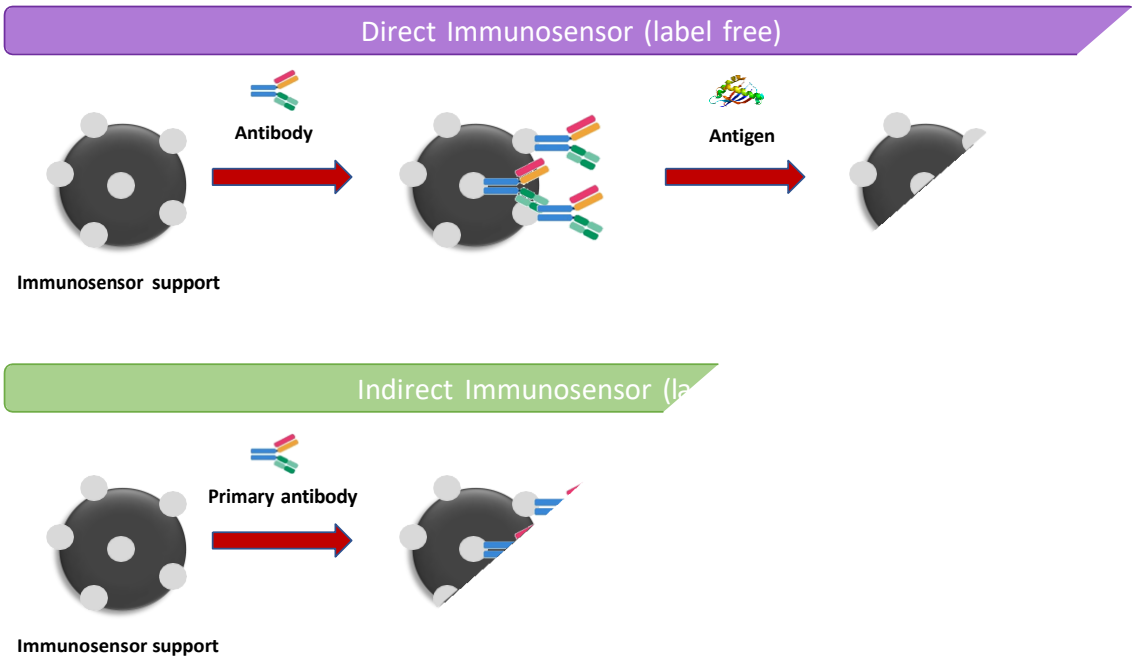

Figure 2.5 - Scheme of the two types of immunosensor development: Direct and indirect immunosensors.

The immobilization procedure of the antibody to the sensor surface is an important step to ensure the specific immunoreaction of the immunocomplex. Therefore, the choice for the immobilization is considered a major step for achieving a high performance and sensitive immunosensor. The selected method needs to maintain the biological activity of the antibody and provide a good orientation in terms of exposed binding sites [139,140]. In addition, a high density of antibody on the electrode surface

can hinder the binding of the antigen. There are different studied methods to immobilize the antibody to the electrode surface.

The simplest method for antibody immobilization is physical adsorption. This is based on non-covalent interactions between the sensing surface and the antibody, and if the antibody concentration is sufficient, a layer of antibodies will be anchored on the sensing surface. However, this method has various limitations, such as the random orientation of the antibody, conformational changes, probability of desorption because of the weak bonds, that may result in low sensitivity and limited reproducibility [141]. Despite these limitations, this method is widely used in immunosensors due to its simplicity and high antibody binding capacity [134].

The most common method is the covalent binding strategy, which is based on the covalent interactions between the modified surface and the functional groups of the antibodies [141]. The covalent attachment of the antibodies to the modified surface depends on various aspects, such as substrate functionality, functional groups present on the antibody, pH, and temperature [142]. Since generally electrode surfaces have no sites for covalent bonding, it is necessary to modify the surface appropriately to bind it covalently to the functional groups of the antibodies. With this procedure a better oriented immobilization is achieved.

Due to the advantages of high sensitivity and selectivity, great precision and accuracy, low cost, simplicity of operation, and requirement of a low quantity of sample, immunosensors have gained considerable interest for the development of cancer diagnostics [143]. Several immunosensors were already addressed for different cancer biomarkers, such as carcinoembryonic antigen (CEA) [144–146], cancer antigen 125 (CA125) [147–149], PSA [150–152], CA15-3 [153–155] for diagnosis of colorectal, ovarian, prostate and breast cancers.

2.2.1. Signal transduction

Another important part of biosensors is the transducer, which converts the (bio)recognition to a measurable signal, converting one form of energy to another. The transducing device may operate on the ground of electrical, optical, mass, thermal,

magnetic and electrochemical signals [156,157]. A scheme explaining the classification of sensors regarding their transducer is shown in **Figure 2.6**.

Figure 2.6 - Scheme of the classification of sensors based on their transducer. Obtained with permission from [157].

Electrochemical biosensors are among the most widely used and studied biosensors [57]. Their operation is based on charge transfer processes that take place at the interface between the electrode and the solution [57,72,158]. The electrochemical properties of the analyte and the transducer, with an electrochemical reaction occurring at the transducer surface between the sensing element and the analyte, causes detectable electrochemical changes in voltage, current, impedance, and/or capacitance [157]. They typically exhibit high sensitivity, selectivity, and analyte detection capability. This type of biosensors convert biochemical information into an electrical signal, as current, voltage, and surface resistance (Rct). They can be used to detect different analytes, such as biomarkers, in different media (sweat, blood, faeces, urine), employed in a vast number of areas, such as food industry, medical sciences, plant biology, among

others [159]. Is it likely that the most relevant feature of electrochemical biosensors is their ability to replace expensive and large instruments, which has led to an increased the number of studies made on this type of sensor in the last decades [160]. They also have low power requirements [161] and operate in an efficient way at room temperature.

In terms of assembly, electrochemical biosensors are made of an electrochemical cell, which is composed by three or two electrodes. The typical three-electrode system is composed of working (chemically stable conductive material, such as carbon, gold, etc.), reference (usually silver metal coated with a layer of silver chloride, Ag/AgCl), and auxiliary (or counter) electrodes (usually platinum or glassy carbon). The two-electrode system has only working and reference electrodes. Both systems are commonly used for biosensor development [76].

Typically, in electrochemical biosensors several types of measurement (**Figure 2.7**) can be used to determine the response of the analyte: amperometric, voltametric, potentiometric, and impedimetric [159,160].

Amperometric techniques measure the current generated by applying a potential to a working electrode against a reference electrode, that is, the potential that is applied is held at a constant value, resulting in a measurement of current as a function of time [162]. In the case of this type of technique, the concentration of the electroactive species is proportional to the obtained current.

Figure 2.7 - Schematic representation of different types of electrochemical biosensors.

Voltametric techniques are characterized by measuring the obtained current when applying a potential to the working electrode against a reference electrode. Voltammetry is used as a term for the techniques where the potential is scanned over a set potential range, such as linear sweep voltammetry (LSV), cyclic voltammetry (CV), square-wave voltammetry (SWV), differential pulse voltammetry (DPV), among others. These methods are commonly used in sensing platforms, since they are cost-effective, high sensitivity, and are useful for low level quantification [76,159]. In this case, the concentration of the analyte in the sample is proportional to a current peak or plateau obtained [73,163]. Normally, the output current of the sensor is analysed and used for the sensing process, which is determined by comparing the obtained current for the different analyte concentrations [159].

Potentiometric techniques determine the potential of the working electrode when compared to the reference electrode, operating under current zero or near-zero. This means that this technique indicates the ion activity in an electrochemical reaction. For this type of measurements, the relation between the analyte concentration and the obtained potential is supported by the Nernst equation:

$$E_{cell} = E^{0}_{cell} - \frac{RT}{nF} \ln Q \quad \textbf{(Eq 1)}$$

In this equation, E_{cell} represents a constant potential (the observed cell potential at zero current), R represents the universal gas constant, *T* the temperature in degrees Kelvin, *n* is the charge number of the electrode reaction, F is the Faraday constant, and *Q* is the ratio of ion concentration between anode and cathode [163,164]. Unlike with the amperometric measurements, the measured species are not consumed, and its response is proportional to the concentration of the studied analyte by comparison of its activity to the reference electrode. The biggest advantages of this kind of measurements are the sensitivity and quickness. The sensors that use potentiometric methods can be easily fabricated in a cost-effective manner, and a reduction of their size does not affect their performance [159].

Impedimetric techniques measure the resistive and capacitive properties of materials upon perturbation of a system. They are powerful methods because of their capability of sampling electron transfer at high frequencies and mass transfer at low frequencies. This kind of detection uses mostly affinity-based biosensors, such as antibody (Ab) – Antigen (Ag) binding on the electrode surface, where there are small changes in impedance that are proportional to concentration changes. During the detection step, the electron transfer resistance at the interface between the electrode and the solution changes when the analyte binds [76]. The most commonly used technique is electrochemical impedance spectroscopy (EIS) where, at slow electron transfer, a semi-circle region is obtained and the resistance of the electron transfer is equal to the diameter of the semi-circle (*Nyquist* plot) [159].

Electrochemical biosensors are particularly suitable in PoC analysis, for being easily miniaturized, simple, and low-cost devices. In addition, relying on electrochemical principles, they are well tuned with regular energy sources as photovoltaic cells or fuel cells, which are also of electrochemical nature. Thus, electrochemical sensing is observed as a main target in this work.

2.2.2. Autonomous biosensors

The development of autonomous bioelectrochemical devices was achieved in the early 21st century by research work conducted on enzymatic biofuel cells (BFCs) that used enzymes as recognition elements [165–167]. In this way, the generated power by the biofuel cell is easily used to enable a self-sustained means of operation, as shown by the first autonomous biosensor applied to the detection of glucose and lactate [168]. Since then, autonomous biosensors have gained considerable attention within various research areas and have been used mainly for sensing applications in the detection of various important analytes [169–172].

Since the first publication, there have been some advances in the field of autonomous biosensors to miniaturize the PoC devices and reduce the cost of analysis. One example is the use of biofuel cells used for implantable devices [173], which is based on the detection of enzyme substrates that act as fuel/oxidant, microbial fuel cells [174]. In addition, autonomous sensors operating with dye-sensitized solar cells were also developed in the research group where this PhD work was implemented [175], as well as a proof-of-concept of this thesis using active direct methanol fuel cells [176].

Fuel cell-based (enzymatic, microbial, and methanol fuel cells) self-powered electrochemical biosensors have several advantages, such as the simplified electronics because no potentiostat is required; improved construction and miniaturization due to the use of two electrodes instead of three; improved stability since a reference electrode is not needed; and the possible development of low-cost screening devices based on printed electronics [177].

Moreover, the implementation of electrochromic devices has facilitated the development of self-powered biosensors. The electrochromic device changes coloration when the current output of an autonomous device reaches in the presence of the analyte, provided that sufficient voltage is achieved by the biodevice. This achieves the possibility of providing sensitive biosensors, even at low power outputs, and for naked eye quantitative discrimination [178–180].

2.3. Fuel Cells

2.3.1. Brief history and basic operating principles

Although the first fuel cell was invented in 1838 by Sir William Grove, when he discovered the generation of electricity by reversing the electrolysis of water using hydrogen and oxygen [181], the term fuel cell was only established nearly 50 years later by Mond and Langer [182]. In 1959, Francis Bacon demonstrated the first fully-operational fuel cell, that was used by NASA in the 1960s in the Apollo and Gemini space programs (Proton Exchange Membrane Fuel Cell, PEMFCs and Alkaline Fuel cells , AFCs) [183,184]. This drove the research in fuel cells to a whole new level, with many research groups starting to focus on fuel cells for different applications, being commercialized since 2007 [185].

Research has been focused to implement Fuel Cell technology in stationary applications, such as the use of Phosphoric Acid Fuel Cells (PAFCs) in cogeneration applications. For small stationary applications, PEMFCs and Solid Oxide Fuel Cells (SOFCs) are being studied [186], although the fuel cell type and size depend on the needed power for the application, ranging from simple back-up systems to large facilities [187].

Currently, the need for better source of power regarding portable electronic devices is rapidly increasing. Therefore, fuel cells are a very good alternative to other sources that are more pollutant, and fossil fuel dependent. A good example for a portable power source is the Direct Methanol Fuel Cell (DMFC), which has gained a lot of attention as the more viable candidate compared to hydrogen feed fuel cells (PEMFC), due to the higher energy density, compact configuration, and convenient operation. These FCs can be easily recharged, which is essential for different electronic devices, such as laptops, mobile phones and power appliances [188].

Fuel Cells are electrochemical devices that convert chemical energy (fuel) into electrical energy. These devices consist of a few main parts: the anode, cathode, and electrolyte, which combined forms the Membrane Electrode Assembly (MEA). In case of a hydrogen supplied fuel cell, at the anode, the supplied hydrogen undergoes an oxidation releasing protons and electrons. The pathway between anode and cathode is separated by a solid electrolyte (in the case of these fuel cells, Nafion®). The presence

of this electrolyte only allows the movement of the positive ions to the cathode, hindering the electrons to migrate by functioning as an insulator. Therefore, the negative charged particles move to the cathode by an external circuit [189,190]. At the cathode, oxygen undergoes a reduction and combined with the positive ions coming from the anode through the electrolyte generates water. Compared to other power sources, fuel cells are environmentally friendly due to the simple and non-toxic products of the chemical reactions.

2.3.2. Types of Fuel Cells

Fuel cells require a fuel and an oxygen source to produce energy. There are different types of fuel cells, already referred in the previous section, as shown in **Table 2.3**, depending on their fuel and function: 1) Alkaline fuel cell (AFC); 2) Phosphoric acid fuel cell (PAFC); 3) Molten carbonate fuel cell (MCFC); 4) Solid oxide fuel cell (SOFC); 5) Proton exchange membrane fuel cell (PEMFC); and 6) Direct methanol fuel cell (DMFC);.

AFCs use an alkaline electrolyte (sodium hydroxide or potassium hydroxide solution) and use pure hydrogen and oxygen as fuel [185]. Although these cells have the best performance, they are very intolerable to impurities and their short lifetimes hinder their role for terrestrial applications [184]. Therefore, they are mainly used for aerospace applications.

Phosphoric acid fuel cells (PAFCs) have an operation very similar to the PEMFC, using platinum or platinum alloys as catalyst at both electrodes, and same anode and cathode reactions. However, the electrolyte is an inorganic acid (concentrated phosphoric acid), which is also a proton conductor. The optimal temperature for PAFCs use is between 180 ^{0}C and 250 ^{0}C, leading to an increase of the anode tolerance to CO poisoning (reduced CO adsorption).

Molten Carbonate Fuel Cells (MCFCs) use a molten mixture of alkali metal carbonates (usually a mixture of lithium and potassium, or lithium and sodium carbonates) in a ceramic matrix as electrolyte. At high temperatures (600 – 700 ^{o}C) the alkali carbonates form a highly conductive molten salt. Unlike all the other fuel cells,

carbon dioxide needs to be supplied to the cathode as well as oxygen, and coal-derived fuel gas, methane, or natural gas as fuel.

Proton Exchange Membrane (or Polymer Electrolyte Membrane) Fuel Cell (PEMFC) use hydrogen gas as fuel and run at a low temperature (30- 100 ^{0}C). The problem of slow reaction rates due to low temperatures is addressed by using catalysts at the electrodes, such as platinum (the most commonly used catalyst) [191]. This type of cells have a problem in terms of fuel delivery processes, since pure hydrogen needs high-cost fuel transmission infrastructure [189]. PEMFCs are the most promising fuel cells because of their low operating temperatures, low noise, quick start-up capability, light mass, and high-power densities. A specific type of PEMFCS – the DMFCs, using methanol or aqueous methanol solutions as the hydrogen source, have been used in portable devices (e.g. laptops, mobile phones, video recorders) because they are lighter and smaller than batteries, have longer operating and faster response time compared to batteries [184,190]. However, PEMFCs that use H_2 as fuel, are mostly used on applications with a need of higher power, such as transportation, and stationary uses.

DMFCs present several advantages over their direct competitors, the hydrogen PEMFC. Due to the difficulty of producing and storing pure hydrogen, DMFCs are a good alternative, since methanol is a readily available and low-cost liquid fuel that has a high energy density. Additionally, for portable applications, mostly due to the lack of effective miniaturizing hydrogen storage technologies, the use a liquid fuel, requiring less ancillary equipment is the best option. Besides this, the system is simpler to use and very quick to refill. In summary, all these advantages of DMFCs assisted in its selection for this thesis. DMFCs have already been studied in the form of active and passive feed, depending on its applications, showing the suitability of these devices in biosensor research. However, the fuel anode reaction rate is low since the oxidation of methanol is a much more complex reaction than the hydrogen oxidation, resulting in fuel cells with lower power. Also, the membrane used as electrolyte is not completely impermeable to the methanol molecules, thus resulting in the crossover of some fuel with a consequent loss of performance [191].

Another main innovative fuel cell technology involves the SOFCs group with a much higher operating temperature range (reaching 1000 °C) and a ceramic electrolyte adapted to this range. Thus, this type of fuel cell requires electrodes composed of

extremely resistant materials, which makes this technology high-cost. Nevertheless, the higher efficiency and performance make it appropriate for stationary applications, when compared to the PEMFCs.

Table 2.3 - Data for the different types of fuel cells. Adapted from [191].

Fuel cell type	Mobile ion	Temperature	Applications
AFC	OH^-	50 – 200°C	Used in space vehicles
PAFC	H^+	~ 220°C	Large number of 200-kW CHP systems
MCFC	CO_3^{2-}	~ 650°C	Suitable for medium to large CHP systems
PEMFC	H^+	30 – 100°C	Vehicles and mobile applications
DMFC	H^+	20 – 90°C	Suitable for portable electronic systems of low power
SOFC	O^{2-}	500 - 1000°C	Suitable for all sizes of CHP systems

AFC: Alkaline Fuel Cell; **DMFC:** Direct Methanol Fuel Cell; **MCFC:** Molten Carbonate Fuel Cell; **PAFC:** Phosphoric Acid Fuel Cell; **PEMFC:** Proton Exchange Membrane Fuel Cell; **SOFC:** Solid Oxide Fuel Cell.

The increasing need for environmental protection, and reduction of fossil-fuel energy sources are leading towards an increase in research on alternative and renewable energy sources. Fuel cells with their advantages of being non-pollutant, and high efficiency are being used in different applications: mostly stationary and portable energies [192].

Combining the characteristics of the types of fuel cells and the requirements for this work, DMFCs were then chosen to develop the biosensor. These features make this fuel cell the best choice for the targeted biosensing device, since it removes the need for an outside power supply to read the signal.

2.3.3. Direct Methanol Fuel Cells (DMFCs)

When comparing to other liquid organic fuels, methanol has an advantage regarding the reactivity at low temperatures, storage, and handling. As referred, a methanol-feed proton exchange membrane fuel cell alleviates the issues of the hydrogen production

and storage. These type of fuel cells are promising to use in portable, transportation, and stationary systems. Methanol is a cheap organic fuel and can be obtained both from fossil fuels (natural gas or coal), and sustainable sources (fermentation of agricultural products and biomass). Some disadvantages such as the sluggish methanol oxidation kinetics and methanol crossover from the anode to the cathode, were already presented in the previous section [193].

In a DMFC, methanol or a methanol aqueous solution is fed to the anode compartment. The reactant diffuses through an anode diffusion layer (AD) toward the anode catalyst layer (AC) where it is converted to carbon dioxide, protons and electrons (**Figure 2.8**) according to

$$CH_3OH + H_2O \rightarrow CO_2 + 6H^+ + 6e^- \quad \textbf{(Eq 2)}$$

The protons obtained in the methanol electro-oxidation reaction are transported through the membrane and the electrons migrate to the cathode through the external circuit. Simultaneously, air (or oxygen) is fed to the cathode and oxygen is transported through the cathode diffusion layer (CD) to the cathode catalyst layer (CC). Here, oxygen combines with the protons and electrons to produce water, according to the reduction reaction represented by:

$$O_2 + 4H^+ + 4e^- \rightarrow 2H_2O \quad \textbf{(Eq 3)}$$

The two electrochemical reactions occurring at each side are combined in an overall reaction given by

$$CH_3OH + \frac{3}{2}O_2 \rightarrow CO_2 + 2H_2O \quad \textbf{(Eq 4)}$$

A proton exchange membrane (commercially called Nafion®) separates the two electrodes. This combination of the two electrodes and the membrane is called Membrane Electrode Assembly (MEA). Each electrode (anode and cathode) is composed of a diffusion layer (AD and CD), which can be an adequate carbon substrate (e.g. carbon paper, carbon cloth, etc.), and a catalytic layer (AC and CC), constituted by carbon with Platinum and Ruthenium particles – anode and carbon with Platinum particles –

cathode. The reactions that occur in the anode (methanol oxidation) and in the cathode (oxygen reduction), can only occur in confined spatial sites where the proton-conducting electrolyte, the fuel, and the electrically connected catalyst nanoparticles are all at the same time in contact, which is called the triple phase boundary (TPB). The optimal electrochemical activity at these sites depend on different factors, namely a good supply of the fuel, a low electronic resistance, and a good ionic conductivity [194].

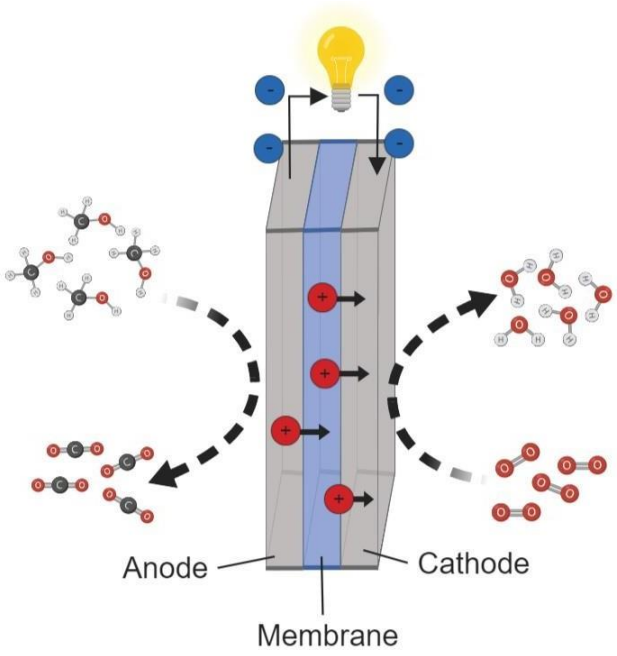

Figure 2.8 - Representation of the MEA and the reactions occurring in both anode and cathode.

The proton exchange membrane typically used in this type of fuel cell is made of perfluorinated-sulfonic acid ionomer which results from the combination of tetrafluorethylene with perfluorosulfonate monomers. These were developed by DuPont and are sold under the commercial name Nafion®, presenting an excellent proton conductivity and chemical stability. This membrane has hydrophilic regions absorbing large amounts of water. Also, these materials are proton conductive because of the H^+ ions movement within the hydrated regions.

The reactions occur at the catalyst layers at both sides and demand for all the involved species. Thus, the electrodes need to be porous to allow the reactants to travel to the reaction sites and provide product removal to keep allowing the reactants access. The electrode supports are named, as previously referred, Diffusion Layers (DL).

Although not actively participating in the reactions, they have important roles. Besides facilitating the reactants access and removal of products they provide mechanical support for the MEA. Additionally, due to their flexibility, these layers help maintaining good electrical contacts with the catalyst particles and to enhance current collection they need to be electrically conductive. The most widely used DL responding to these conditions are carbon-based materials, such as carbon fibre paper and carbon cloths. Carbon cloth is more porous and less tortuous than carbon paper, and both materials are normally hydrophobic by treating them with PTFE (polytetrafluoroethylene) to avoid flooding of the fuel cell.

The theoretical ideal potential (given by thermodynamic principles) of a DMFC is around 1.2 V. However, when a real cell is used, the Open Circuit Potential (OCP) value is much lower, mostly due to the methanol crossover, where the energy is lost due to some methanol passing through the electrolyte toward the cathode where it is oxidised, competing with the oxygen reduction reaction. **Figure 2.9** shows a schematic representation of a typical polarization (Voltage-Current density) curve observed when using a DMFC. The current density is used instead of current for the sake of a better comparison between fuel cells.

There are three major losses responsible for the shape of the real DMFC performance, moving away from the ideal behaviour: activation losses, ohmic losses and mass transport losses. The different types of losses have regions in the curve where their impact is higher. The polarization curve begins by having a high drop in voltage in the so-called activation losses region corresponding to a kinetic control regime, caused by the slow methanol oxidation kinetics at the anode and slow oxygen reduction kinetics at the cathode. Some of the generated voltage is sacrificed while driving the chemical reaction that transfers the electrons from the anode to the cathode. The area where the cell voltage decreases nearly linearly with increasing current density is the ohmic losses control region. At higher current densities, the voltage decreases sharply near a limiting current density. This region called the mass transport control region (with concentration losses) is the result of the high methanol transport rate at the anode and effective oxygen supply at the cathode which at this current density levels are limiting steps [193].

Figure 2.9 - Schematic representation of a typical polarization curve in DMFCs.

Methanol crossover occurs, as referred, due to the inability of the membrane to prevent methanol from permeating through its structure to the cathode platinum catalyst. The methanol reacts with the platinum catalyst from the cathode, leading to a mixed potential, which decreases the cell voltage and the fuel efficiency, lowering the energy density of the system [195,196]. To avoid this, it is necessary to reduce or eliminate the loss of fuel across the membrane.

The effects of methanol crossover have been widely studied in the literature by assessing different conditions, such as methanol concentration, air pressure, temperature, fuel flow rate, membrane thickness and catalyst morphology. One alternative that has been studied to reduce methanol crossover is to obtain a methanol impermeably polymer electrolyte [197–200].

In literature, there is a distinction made between active and passive operation mode. In the active mode, there is an active feed of fuel and air (or oxygen) to both anode and cathode, using auxiliary equipment, such as pumps to supply the reactants and optimize/maintain the working conditions. Under this operating mode, the fuel cells achieve the best efficiency and performance. When using the passive mode, no auxiliary equipment is required for the fuel cell function, and the reactants reach the catalytic sites by natural convection. This system is simpler, and no significant amount of power is dissipated on auxiliaries. The lower efficiency and performance obtained is due to the higher anode activation overpotential due to the slow methanol oxidation reaction

kinetics. This negatively affects the rate of electrochemical reactions, reducing the obtained voltage and efficiency of the system [201]. Also, a passive DMFC needs higher catalyst loading to compensate the slow methanol electro-oxidation reaction kinetics and severe crossover to the cathode side. Since the most used catalyst is a noble metal (platinum), this type of fuel cells tends to have a higher cost and tends to discourage the commercialization of portable devices. There is, however, intense active research in the last years on DMFCs, aiming at developing new and less expensive materials and reduction of the amount of noble catalyst used, together with mass-production methodologies to reach the cost level compatible with commercialization.

In this thesis, passive DMFC were used for the integration of different types of biosensors, since this work aims for autonomous and equipment free biosensing devices. DMFCs were chosen for this project since the power need for an autonomous and functional biosensor is low and achievable with these cells, and as referred they are easier to miniaturize considering the liquid fuel for their operation. Therefore, passive DMFCs, to accommodate the different biosensors, were fabricated according to previous studies [201], and are shown in **Figure 2.10**. The passive DMFC used contained two acrylic plates, one for each electrode, where the anode side contains a specific storage for methanol solution and with easy access for refuelling (**Figure 2.10c**), and the cathode has an open area to allow the oxygen from the atmospheric air to enter the cell (**Figure 2.10b**). The set-up also includes two metallic plates, used as current collectors, and a rubber gasket on each side, acting as insulating elements to avoid electrical short-circuit. These DMFCs were used throughout the presented work in this thesis.

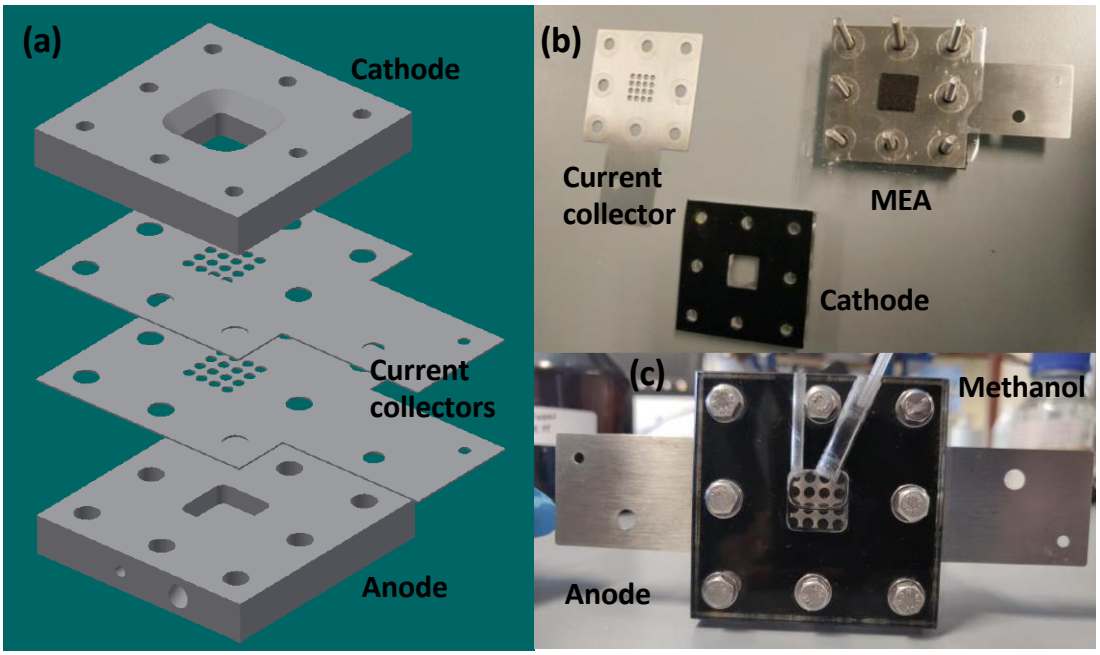

Figure 2.10 - Passive DMFCs to integrate biosensors. (a) Schematic representation of the passive DMFC (cathode, current collectors, and anode); (b) The actual open DMFC produced to integrate the biosensors with a MEA; (c) The actual closed DMFC with methanol in the anode reservoir.

2.4. Scope of the present work

The provided state of the art showed an increasing tendency and need for quick, low-cost and accurate biosensors not only in medicine and healthcare, but also in other fields, such as food quality control, and environmental monitoring. The great advantage of these biosensors is the results of the test are almost instantly (needing only a few minutes of waiting time) and decreasing the need for laboratory procedures. Although this applies mostly in healthcare, this is also advantageous for detecting toxins in food for human/animal consumption (e.g. presence of toxins in shellfish in the Portuguese coast on certain times of year), and for pesticides detection in wastewater and/or agriculture soil.

In this thesis, we will focus on the healthcare field and in the cancer biomarker detection, that is a widespread disease that still lacks quick, non-invasive, and low-cost screening and diagnostic methods.

The main goal of this work was not only to develop biosensors for cancer detection, but also to improve this into a self-powered device, needing no external power,

electricity, solar light, or any external equipment to be fully functional. This would be a very useful tool as a widespread and low-cost device that would be feasible to be used in the day-to-day diagnosis, used in low-income countries, and in world crises as can be now seen all over the World. To accomplish that, we used a passive DMFC as power source so it would be easily miniaturized and used only with a few millilitres of liquid fuel, without any storage problems, that could be used at every moment without the need for solar power or being dependent on electricity.

2.5. References

[1] National Cancer Institute, What is cancer?, (2021). https://www.cancer.gov/about-cancer/understanding/what-is-cancer (accessed August 1, 2022).

[2] International Agency for Reseach on Cancer (WHO), All cancers fact sheet, (2020). https://gco.iarc.fr/today/data/factsheets/cancers/39-All-cancers-fact-sheet.pdf.

[3] World Health Organization, Cancer, (2022). https://www.who.int/news-room/fact-sheets/detail/cancer (accessed August 1, 2022).

[4] L. Wang, Early diagnosis of breast cancer, Sensors (Switzerland). 17 (2017). https://doi.org/10.3390/s17071572.

[5] M. Ahdoot, A.R. Wilbur, S.E. Reese, A.H. Lebastchi, S. Mehralivand, P.T. Gomella, J. Bloom, S. Gurram, M. Siddiqui, P. Pinsky, H. Parnes, W.M. Linehan, M. Merino, P.L. Choyke, J.H. Shih, B. Turkbey, B.J. Wood, P.A. Pinto, MRI-Targeted, Systematic, and Combined Biopsy for Prostate Cancer Diagnosis, N. Engl. J. Med. 382 (2020) 917–928. https://doi.org/10.1056/nejmoa1910038.

[6] S. Mittal, H. Kaur, N. Gautam, A.K. Mantha, Biosensors for breast cancer diagnosis: A review of bioreceptors, biotransducers and signal amplification strategies, Biosens. Bioelectron. 88 (2017) 217–231. https://doi.org/10.1016/j.bios.2016.08.028.

[7] American Cancer Society, American Cancer Society recommendations for early breast cancer detection in women without breast symptoms, (2015). http://www.cancer.org/cancer/breastcancer/moreinformation/breastcancerearlydetection/breast-cancer-early-detection-acs-recs.

[8] I.E. Tothill, Biosensors for cancer markers diagnosis, Semin. Cell Dev. Biol. 20 (2009) 55–62. https://doi.org/10.1016/j.semcdb.2009.01.015.

[9] S.A. Soper, K. Brown, A. Ellington, B. Frazier, G. Garcia-Manero, V. Gau, S.I. Gutman, D.F. Hayes, B. Korte, J.L. Landers, D. Larson, F. Ligler, A. Majumdar, M. Mascini, D. Nolte, Z. Rosenzweig, J. Wang, D. Wilson, Point-of-care biosensor systems for cancer diagnostics/prognostics, Biosens. Bioelectron. 21 (2006)

1932–1942. https://doi.org/10.1016/j.bios.2006.01.006.

[10] M. Perfézou, A. Turner, A. Merkoçi, Cancer detection using nanoparticle-based sensors, Chem. Soc. Rev. 41 (2012) 2606. https://doi.org/10.1039/c1cs15134g.

[11] A.P.M. Tavares, N.S. Ferreira, L.A.A.N.A. Truta, M.G.F. Sales, Conductive Paper with Antibody-Like Film for Electrical Readings of Biomolecules, Sci. Rep. 6 (2016) 26132. https://doi.org/10.1038/srep26132.

[12] A.J. Atkinson, W.A. Colburn, V.G. DeGruttola, D.L. DeMets, G.J. Downing, D.F. Hoth, J.A. Oates, C.C. Peck, R.T. Schooley, B.A. Spilker, J. Woodcock, S.L. Zeger, Biomarkers and surrogate endpoints: Preferred definitions and conceptual framework, Clin. Pharmacol. Ther. 69 (2001) 89–95. https://doi.org/10.1067/mcp.2001.113989.

[13] A. Mordente, E. Meucci, G.E. Martorana, A. Silvestrini, Cancer biomarkers discovery and validation: State of the art, problems and future perspectives, Adv. Exp. Med. Biol. 867 (2015) 9–26. https://doi.org/10.1007/978-94-017-7215-0_2.

[14] Silver Spring (MD): Food and Drug Administration (US); Bethesda (MD): National Institutes of Health (US), BEST (Biomarkers, EndpointS, and other Tools) Resource, BEST (Biomarkers , EndpointS , Other Tools) Resour. (2016). https://www.ncbi.nlm.nih.gov/books/NBK326791/ (accessed March 5, 2023).

[15] A.K. Füzéry, J. Levin, M.M. Chan, D.W. Chan, Translation of proteomic biomarkers into FDA approved cancer diagnostics: Issues and challenges, Clin. Proteomics. 10 (2013). https://doi.org/10.1186/1559-0275-10-13.

[16] N.L. Henry, D.F. Hayes, Cancer biomarkers, Mol. Oncol. 6 (2012) 140–146. https://doi.org/10.1016/j.molonc.2012.01.010.

[17] D. Konforte, E.P. Diamandis, Is early detection of cancer with circulating biomarkers feasible?, Clin. Chem. 59 (2013) 35–37. https://doi.org/10.1373/clinchem.2012.184903.

[18] S. Khorrami, M. Tavakoli, E. Safari, Clinical value of serum S100A8/A9 and CA15-3 in the diagnosis of breast cancer, Iran. J. Pathol. 14 (2019) 104–112. https://doi.org/10.30699/ijp.14.2.104.

[19] M.J. Duffy, D. Evoy, E.W. McDermott, CA 15-3: Uses and limitation as a biomarker for breast cancer, Clin. Chim. Acta. 411 (2010) 1869–1874. https://doi.org/10.1016/j.cca.2010.08.039.

[20] S.J. Gendler, MUC1, The renaissance molecule, J. Mammary Gland Biol. Neoplasia. 6 (2001) 339–353. https://doi.org/10.1023/A:1011379725811.

[21] I. Ghosh, D. Bhattacharjee, A.K. Das, G. Chakrabarti, A. Dasgupta, S.K. Dey, Diagnostic role of tumour markers CEA, CA15-3, CA19-9 and CA125 in lung cancer, Indian J. Clin. Biochem. 28 (2013) 24–29. https://doi.org/10.1007/s12291-012-0257-0.

[22] J.A. Ros-Lucas, D.A. Pascual-Figal, J.A. Noguera-Velasco, Á. Hernández-Vicente, I. Cebreiros-López, M. Arnaldos-Carrillo, I.M. Martínez-Ardil, E. García-Vázquez, M. Aparicio-Vicente, E. Solana-Martínez, S.Y. Ruiz-Martínez, L. Fernández-Mula, R. Andujar-Espinosa, B. Fernández-Suarez, M.D. Sánchez-Caro, C. Peñalver-Mellado, F.J. Ruiz-López, CA 15-3 prognostic biomarker in SARS-CoV-2 pneumonia, Sci. Rep. 12 (2022) 1–8. https://doi.org/10.1038/s41598-022-10726-7.

[23] X. Li, Y. Xu, L. Zhang, Serum CA153 as biomarker for cancer and noncancer diseases, 1st ed., Elsevier Inc., 2019. https://doi.org/10.1016/bs.pmbts.2019.01.005.

[24] S. Jeong, M.J. Park, W. Song, H.S. Kim, Current immunoassay methods and their applications to clinically used biomarkers of breast cancer, Clin. Biochem. 78 (2020) 43–57. https://doi.org/10.1016/j.clinbiochem.2020.01.009.

[25] I.K. Oktaviyanti, D.S. Ali, S.A. Awadh, M.J.C. Opulencia, S. Yusupov, R. Dias, F. Alsaikhan, M.M. Mohammed, H. Sharma, Y.F. Mustafa, M.M. Saleh, Recent advances on applications of immunosensing systems based on nanomaterials for CA15-3 breast cancer biomarker detection, Anal. Bioanal. Chem. (2022). https://doi.org/10.1007/s00216-022-04150-z.

[26] C. Chen, J. Wang, Optical biosensors: An exhaustive and comprehensive review, Analyst. 145 (2020) 1605–1628. https://doi.org/10.1039/c9an01998g.

[27] S. Bayoumy, H. Hyytiä, J. Leivo, S.M. Talha, K. Huhtinen, M. Poutanen, J. Hynninen, A. Perheentupa, U. Lamminmäki, K. Gidwani, K. Pettersson, Glycovariant-based

lateral flow immunoassay to detect ovarian cancer–associated serum CA125, Commun. Biol. 3 (2020) 1–7. https://doi.org/10.1038/s42003-020-01191-x.

[28] F. Di Nardo, M. Chiarello, S. Cavalera, C. Baggiani, L. Anfossi, Ten years of lateral flow immunoassay technique applications: Trends, challenges and future perspectives, Sensors. 21 (2021). https://doi.org/10.3390/s21155185.

[29] T. Mahmoudi, M. de la Guardia, B. Baradaran, Lateral flow assays towards point-of-care cancer detection: A review of current progress and future trends, TrAC - Trends Anal. Chem. 125 (2020) 115842. https://doi.org/10.1016/j.trac.2020.115842.

[30] T.E. Meyer, S.D. Fox, H.J. Issaq, X. Xu, L.W. Chu, T.D. Veenstra, A.W. Hsing, A reproducible and high-throughput HPLC/MS method to separate sarcosine from α- And β-Alanine and to quantify sarcosine in human serum and urine, Anal. Chem. 83 (2011) 5735–5740. https://doi.org/10.1021/ac201003r.

[31] D. Strzelecki, M. Podgórski, O. Kałużyńska, O. Gawlik-Kotelnicka, L. Stefańczyk, M. Kotlicka-Antczak, A. Gmitrowicz, P. Grzelak, Supplementation of antipsychotic treatment with the amino acid sarcosine influences proton magnetic resonance spectroscopy parameters in left frontal white matter in patients with schizophrenia, Nutrients. 7 (2015) 8767–8782. https://doi.org/10.3390/nu7105427.

[32] C.S. Pundir, R. Deswal, P. Kumar, Quantitative analysis of sarcosine with special emphasis on biosensors: a review, Taylor & Francis, 2019. https://doi.org/10.1080/1354750X.2019.1615124.

[33] A. Sreekumar, L.M. Poisson, T.M. Rajendiran, A.P. Khan, Q. Cao, J. Yu, B. Laxman, R. Mehra, R.J. Lonigro, Y. Li, M.K. Nyati, A. Ahsan, S. Kalyana-Sundaram, B. Han, X. Cao, J. Byun, G.S. Omenn, D. Ghosh, S. Pennathur, D.C. Alexander, A. Berger, J.R. Shuster, J.T. Wei, S. Varambally, C. Beecher, A.M. Chinnaiyan, Metabolomic profiles delineate potential role for sarcosine in prostate cancer progression, Nature. 457 (2009) 910–914. https://doi.org/10.1038/nature07762.

[34] H.J. Issaq, T.J. Waybright, T.D. Veenstra, Cancer biomarker discovery: Opportunities and pitfalls in analytical methods, Electrophoresis. 32 (2011) 967–

975. https://doi.org/10.1002/elps.201000588.

[35] B. Cavaliere, B. MacChione, M. Monteleone, A. Naccarato, G. Sindona, A. Tagarelli, Sarcosine as a marker in prostate cancer progression: A rapid and simple method for its quantification in human urine by solid-phase microextraction-gas chromatography-triple quadrupole mass spectrometry, Anal. Bioanal. Chem. 400 (2011) 2903–2912. https://doi.org/10.1007/s00216-011-4960-0.

[36] N. Cernei, Z. Heger, J. Gumulec, O. Zitka, M. Masarik, P. Babula, T. Eckschlager, M. Stiborova, R. Kizek, V. Adam, Sarcosine as a potential prostate cancer biomarker-a review, Int. J. Mol. Sci. 14 (2013) 13893–13908. https://doi.org/10.3390/ijms140713893.

[37] M. Yousefi, D. Qujeq, H. Shafi, K.H. Tilaki, Serum and Urine Levels of Sarcosine in Benign Prostatic Hyperplasia and Newly Diagnosed Prostate Cancer Patients, J. Kermanshah Univ. Med. Sci. 24 (2020) 1–6. https://doi.org/10.5812/jkums.97000.

[38] G. Lucarelli, M. Fanelli, A.M.V. Larocca, C.A. Germinario, M. Rutigliano, A. Vavallo, F.P. Selvaggi, C. Bettocchi, M. Battaglia, P. Ditonno, Serum sarcosine increases the accuracy of prostate cancer detection in patients with total serum PSA less than 4.0 ng/ml, Prostate. 72 (2012) 1611–1621. https://doi.org/10.1002/pros.22514.

[39] L. Bohm, A.M. Serafin, P. Fernandez, G. Van der Watt, P.J.D. Bouic, J. Harvey, Plasma sarcosine does not distinguish early and advanced stages of prostate cancer, South African Med. J. 102 (2012) 677–679. https://doi.org/10.7196/SAMJ.5768.

[40] V. Narwal, P. Kumar, P. Joon, C.S. Pundir, Fabrication of an amperometric sarcosine biosensor based on sarcosine oxidase/chitosan/CuNPs/c-MWCNT/Au electrode for detection of prostate cancer, Enzyme Microb. Technol. 113 (2018) 44–51. https://doi.org/10.1016/j.enzmictec.2018.02.010.

[41] P. Kumar, V. Narwal, R. Jaiwal, C.S. Pundir, Construction and application of amperometric sarcosine biosensor based on SOxNPs/AuE for determination of prostate cancer, Biosens. Bioelectron. 122 (2018) 140–146. https://doi.org/10.1016/j.bios.2018.09.003.

[42] C. Wang, Y. Wang, H. Zhang, H. Deng, X. Xiong, C. Li, W. Li, Molecularly imprinted photoelectrochemical sensor for carcinoembryonic antigen based on polymerized ionic liquid hydrogel and hollow gold nanoballs/MoSe2 nanosheets, Anal. Chim. Acta. 1090 (2019) 64–71. https://doi.org/10.1016/j.aca.2019.09.029.

[43] T. Rajarathinam, M. Kwon, D. Thirumalai, S. Kim, S. Lee, J.H. Yoon, H. jong Paik, S. Kim, J. Lee, H.K. Ha, S.C. Chang, Polymer-dispersed reduced graphene oxide nanosheets and Prussian blue modified biosensor for amperometric detection of sarcosine, Anal. Chim. Acta. 1175 (2021) 338749. https://doi.org/10.1016/j.aca.2021.338749.

[44] T.P. Nguy, T. Van Phi, D.T.N. Tram, K. Eersels, P. Wagner, T.T.N. Lien, Development of an impedimetric sensor for the label-free detection of the amino acid sarcosine with molecularly imprinted polymer receptors, Sensors Actuators, B Chem. 246 (2017) 461–470. https://doi.org/10.1016/j.snb.2017.02.101.

[45] P. Tang, Y. Wang, F. He, Electrochemical sensor based on super-magnetic metal–organic framework@molecularly imprinted polymer for Sarcosine detection in urine, J. Saudi Chem. Soc. 24 (2020) 620–630. https://doi.org/10.1016/j.jscs.2020.06.004.

[46] Z. Ramezani, M. Safdarian, A.A. Ghadiri, Metal-coded hydrogel magnetic molecularly imprinted polymer for preconcentration and cleanup of sarcosine: Determination in urine; coupled to on-column capillary electrophoresis, Talanta. 230 (2021) 122309. https://doi.org/10.1016/j.talanta.2021.122309.

[47] Q. Wang, C. Yang, Q. Yang, S. Yu, H. Yang, Platinum-loaded mesoporous nickel phosphonate and its electrochemical application for sarcosine detection, Anal. Chim. Acta. 1046 (2019) 93–98. https://doi.org/10.1016/j.aca.2018.09.027.

[48] J. Hu, W. Wei, S. Ke, X. Zeng, P. Lin, A novel and sensitive sarcosine biosensor based on organic electrochemical transistor, Electrochim. Acta. 307 (2019) 100–106. https://doi.org/10.1016/j.electacta.2019.03.180.

[49] H. Wang, Y. Qi, D. Wu, Q. Wei, A photoelectrochemical self-powered sensor for the detection of sarcosine based on NiO NSs/PbS/Au NPs as photocathodic material, J. Hazard. Mater. 416 (2021) 126201.

https://doi.org/10.1016/j.jhazmat.2021.126201.

[50] S.K. Metkar, K. Girigoswami, Diagnostic biosensors in medicine – A review, Biocatal. Agric. Biotechnol. 17 (2019) 271–283. https://doi.org/10.1016/j.bcab.2018.11.029.

[51] V.S.P.K.S.A. Jayanthi, A.B. Das, U. Saxena, Recent advances in biosensor development for the detection of cancer biomarkers, Biosens. Bioelectron. 91 (2017) 15–23. https://doi.org/10.1016/j.bios.2016.12.014.

[52] E.B. Bahadir, M.K. Sezgintürk, Applications of commercial biosensors in clinical, food, environmental, and biothreat/biowarfare analyses, Anal. Biochem. 478 (2015) 107–120. https://doi.org/10.1016/j.ab.2015.03.011.

[53] S.J. UPDIKE, G.P. HICKS, The Enzyme Electrode, Nature. 214 (1967) 986–988. https://doi.org/10.1038/214986a0.

[54] A. Pasquarelli, Biosensors and Biochips, 2021. https://doi.org/10.1007/978-3-030-76469-2_11.

[55] P. Bhattarai, S. Hameed, Basics of Biosensors and Nanobiosensors, Nanobiosensors. (2020) 1–22. https://doi.org/10.1002/9783527345137.ch1.

[56] P. Mohankumar, J. Ajayan, T. Mohanraj, R. Yasodharan, Recent developments in biosensors for healthcare and biomedical applications: A review, Meas. J. Int. Meas. Confed. 167 (2021) 108293. https://doi.org/10.1016/j.measurement.2020.108293.

[57] B. Senf, W.H. Yeo, J.H. Kim, Recent Advances in Portable Biosensors for Biomarker Detection in Body Fluids, Biosensors. 10 (2020). https://doi.org/10.3390/BIOS10090127.

[58] H. Sohrabi, N. Bolandi, A. Hemmati, S. Eyvazi, S. Ghasemzadeh, B. Baradaran, F. Oroojalian, M. Reza Majidi, M. de la Guardia, A. Mokhtarzadeh, State-of-the-art cancer biomarker detection by portable (Bio) sensing technology: A critical review, Microchem. J. 177 (2022) 107248. https://doi.org/10.1016/j.microc.2022.107248.

[59] C. chen Li, Z. yue Wang, L. juan Wang, C. yang Zhang, Biosensors for epigenetic

biomarkers detection: A review, Biosens. Bioelectron. 144 (2019). https://doi.org/10.1016/j.bios.2019.111695.

[60] J. Ma, M. Du, C. Wang, X. Xie, H. Wang, Q. Zhang, Advances in airborne microorganisms detection using biosensors: A critical review, Front. Environ. Sci. Eng. 15 (2021) 1–19. https://doi.org/10.1007/s11783-021-1420-8.

[61] R. Sivakumar, N.Y. Lee, Recent advances in airborne pathogen detection using optical and electrochemical biosensors, Anal. Chim. Acta. (2022) 340297. https://doi.org/10.1016/j.aca.2022.340297.

[62] N.F. Che Lah, A.L. Ahmad, S.C. Low, Molecular imprinted membrane biosensor for pesticide detection: Perspectives and challenges, Polym. Adv. Technol. 32 (2021) 17–30. https://doi.org/10.1002/pat.5098.

[63] P. Zhang, T. Sun, S. Rong, D. Zeng, H. Yu, Z. Zhang, D. Chang, H. Pan, A sensitive amperometric AChE-biosensor for organophosphate pesticides detection based on conjugated polymer and Ag-rGO-NH 2 nanocomposite, Bioelectrochemistry. 127 (2019) 163–170. https://doi.org/10.1016/j.bioelechem.2019.02.003.

[64] A.S. Maghsoudi, S. Hassani, K. Mirnia, M. Abdollahi, Recent advances in nanotechnology-based biosensors development for detection of arsenic, lead, mercury, and cadmium, Int. J. Nanomedicine. 16 (2021) 803–832. https://doi.org/10.2147/IJN.S294417.

[65] K. Velusamy, S. Periyasamy, P.S. Kumar, G. Rangasamy, J.M. Nisha Pauline, P. Ramaraju, S. Mohanasundaram, D.V. Nguyen Vo, Biosensor for heavy metals detection in wastewater: A review, Food Chem. Toxicol. 168 (2022) 113307. https://doi.org/10.1016/j.fct.2022.113307.

[66] V. Gaudin, Advances in biosensor development for the screening of antibiotic residues in food products of animal origin – A comprehensive review, Biosens. Bioelectron. 90 (2017) 363–377. https://doi.org/10.1016/j.bios.2016.12.005.

[67] L. Karadurmus, S.I. Kaya, S.A. Ozkan, Recent advances of enzyme biosensors for pesticide detection in foods, J. Food Meas. Charact. 15 (2021) 4582–4595. https://doi.org/10.1007/s11694-021-01032-3.

[68] D.C. Vanegas, L. Patiño, C. Mendez, D.A. de Oliveira, A.M. Torres, C.L. Gomes, E.S. McLamore, Laser scribed graphene biosensor for detection of biogenic amines in food samples using locally sourced materials, Biosensors. 8 (2018). https://doi.org/10.3390/bios8020042.

[69] M. Ghasemi-Varnamkhasti, C. Apetrei, J. Lozano, A. Anyogu, Potential use of electronic noses, electronic tongues and biosensors as multisensor systems for spoilage examination in foods, Trends Food Sci. Technol. 80 (2018) 71–92. https://doi.org/10.1016/j.tifs.2018.07.018.

[70] B. Bhavadharini, M. Kavimughil, B. Malini, A. Vallath, H.K. Prajapati, C.K. Sunil, Recent Advances in Biosensors for Detection of Chemical Contaminants in Food — a Review, Food Anal. Methods. 15 (2022) 1545–1564. https://doi.org/10.1007/s12161-021-02213-y.

[71] M.A. Morales, J.M. Halpern, Guide to Selecting a Biorecognition Element for Biosensors, Bioconjug. Chem. 29 (2018) 3231–3239. https://doi.org/10.1021/acs.bioconjchem.8b00592.

[72] R.B. Reilly, T.C. Lee, Biosensors, Technol. Heal. Care. 19 (2011) 285–293. https://doi.org/10.3233/THC-2011-0625.

[73] J.V. and E.R. Dorothee Grieshaber, Robert MacKenzie, Electrochemical Biosensors - Sensor Principles and Architectures, Sensors. (2008) 1400–1458. https://doi.org/10.3390/s80314000.

[74] H.H. Nguyen, S.H. Lee, U.J. Lee, C.D. Fermin, M. Kim, Immobilized enzymes in biosensor applications, Materials (Basel). 12 (2019) 1–34. https://doi.org/10.3390/ma12010121.

[75] S. Oue, A. Okamoto, T. Yano, H. Kagamiyama, Redesigning the substrate specificity of an enzyme by cumulative effects of the mutations of non-active site residues, J. Biol. Chem. 274 (1999) 2344–2349. https://doi.org/10.1074/jbc.274.4.2344.

[76] N.J. Ronkainen, H.B. Halsall, W.R. Heineman, Electrochemical biosensors, Chem. Soc. Rev. 39 (2010) 1747–1763. https://doi.org/10.1039/b714449k.

[77] C.I.L. Justino, A.C. Freitas, R. Pereira, A.C. Duarte, T.A.P. Rocha Santos, Recent developments in recognition elements for chemical sensors and biosensors, TrAC - Trends Anal. Chem. 68 (2015) 2–17. https://doi.org/10.1016/j.trac.2015.03.006.

[78] B. Zhu, M.A. Booth, P. Shepherd, A. Sheppard, J. Travas-Sejdic, Distinguishing cytosine methylation using electrochemical, label-free detection of DNA hybridization and ds-targets, Biosens. Bioelectron. 64 (2015) 74–80. https://doi.org/10.1016/j.bios.2014.08.049.

[79] J. Labuda, A.M. Oliveira Brett, G. Evtugyn, M. Fojta, M. Mascini, M. Ozsoz, I. Palchetti, E. Paleček, J. Wang, Electrochemical nucleic acid-based biosensors: Concepts, terms, and methodology (IUPAC Technical Report), Pure Appl. Chem. 82 (2010) 1161–1187. https://doi.org/10.1351/PAC-REP-09-08-16.

[80] K.J. Odenthal, J.J. Gooding, An introduction to electrochemical DNA biosensors, Analyst. 132 (2007) 603–610. https://doi.org/10.1039/b701816a.

[81] G. Wulff, A. Sarhan, K. Zabrocki, Enzyme-analogue built polymers and their use for the resolution of racemates, Tetrahedron Lett. 14 (1973) 4329–4332. https://doi.org/10.1016/S0040-4039(01)87213-0.

[82] J.J. Belbruno, Molecularly Imprinted Polymers, Chem. Rev. 119 (2019) 94–119. https://doi.org/10.1021/acs.chemrev.8b00171.

[83] F.T.C. Moreira, S. Sharma, R.A.F. Dutra, J.P.C. Noronha, A.E.G. Cass, M.G.F. Sales, Smart plastic antibody material (SPAM) tailored on disposable screen printed electrodes for protein recognition: Application to myoglobin detection, Biosens. Bioelectron. 45 (2013) 237–244. https://doi.org/10.1016/j.bios.2013.02.012.

[84] G. Vasapollo, R. Del Sole, L. Mergola, M.R. Lazzoi, A. Scardino, S. Scorrano, G. Mele, Molecularly imprinted polymers: Present and future prospective, Int. J. Mol. Sci. 12 (2011) 5908–5945. https://doi.org/10.3390/ijms12095908.

[85] W.J. Cheong, S.H. Yang, F. Ali, Molecular imprinted polymers for separation science: A review of reviews, J. Sep. Sci. 36 (2013) 609–628. https://doi.org/10.1002/jssc.201200784.

[86] O.S. Ahmad, T.S. Bedwell, C. Esen, A. Garcia-Cruz, S.A. Piletsky, Molecularly

Imprinted Polymers in Electrochemical and Optical Sensors, Trends Biotechnol. 37 (2019) 294–309. https://doi.org/10.1016/j.tibtech.2018.08.009.

[87] G. Chen, M. Jin, P. Du, C. Zhang, X. Cui, Y. Zhang, Y. She, H. Shao, F. Jin, S. Wang, L. Zheng, J. Wang, A sensitive chemiluminescence enzyme immunoassay based on molecularly imprinted polymers solid-phase extraction of parathion, Anal. Biochem. 530 (2017) 87–93. https://doi.org/10.1016/j.ab.2017.05.008.

[88] T.S. Anirudhan, J. Christa, J.R. Deepa, Extraction of melamine from milk using a magnetic molecularly imprinted polymer, Food Chem. 227 (2017) 85–92. https://doi.org/10.1016/j.foodchem.2016.12.090.

[89] S. Ansari, M. Karimi, Recent progress, challenges and trends in trace determination of drug analysis using molecularly imprinted solid-phase microextraction technology, Talanta. 164 (2017) 612–625. https://doi.org/10.1016/j.talanta.2016.11.007.

[90] D. Fan, L. Jia, H. Xiang, M. Peng, H. Li, S. Shi, Synthesis and characterization of hollow porous molecular imprinted polymers for the selective extraction and determination of caffeic acid in fruit samples, Food Chem. 224 (2017) 32–36. https://doi.org/10.1016/j.foodchem.2016.12.042.

[91] A. Azizi, C.S. Bottaro, A critical review of molecularly imprinted polymers for the analysis of organic pollutants in environmental water samples, J. Chromatogr. A. 1614 (2020) 460603. https://doi.org/10.1016/j.chroma.2019.460603.

[92] Z. El-Schich, Y. Zhang, M. Feith, S. Beyer, L. Sternbæk, L. Ohlsson, M. Stollenwerk, A.G. Wingren, Molecularly imprinted polymers in biological applications, Biotechniques. 69 (2020) 407–420. https://doi.org/10.2144/btn-2020-0091.

[93] F. Cui, Z. Zhou, H.S. Zhou, Molecularly imprinted polymers and surface imprinted polymers based electrochemical biosensor for infectious diseases, Sensors (Switzerland). 20 (2020). https://doi.org/10.3390/s20040996.

[94] N.S. Ferreira, M.G.F. Sales, Disposable immunosensor using a simple method for oriented antibody immobilization for label-free real-time detection of an oxidative stress biomarker implicated in cancer diseases, Biosens. Bioelectron. 53 (2014) 193–199. https://doi.org/10.1016/j.bios.2013.09.056.

[95] A.R. Cardoso, H.I.A.S. Gomes, A.P.M. Tavares, M.G.F. Sales, Novel electrochemical sensor for Chloramphenicol detection in aquatic medium, (2014) 5400.

[96] S. Piletsky, F. Canfarotta, A. Poma, A.M. Bossi, S. Piletsky, Molecularly Imprinted Polymers for Cell Recognition, Trends Biotechnol. 38 (2020) 368–387. https://doi.org/10.1016/j.tibtech.2019.10.002.

[97] K. Haupt, P.X. Medina Rangel, B.T.S. Bui, Molecularly imprinted polymers: Antibody mimics for bioimaging and therapy, Chem. Rev. 120 (2020) 9554–9582. https://doi.org/10.1021/acs.chemrev.0c00428.

[98] S. Xu, L. Wang, Z. Liu, Molecularly Imprinted Polymer Nanoparticles: An Emerging Versatile Platform for Cancer Therapy, Angew. Chemie - Int. Ed. 60 (2021) 3858–3869. https://doi.org/10.1002/anie.202005309.

[99] S. He, L. Zhang, S. Bai, H. Yang, Z. Cui, X. Zhang, Y. Li, Advances of molecularly imprinted polymers (MIP) and the application in drug delivery, Eur. Polym. J. 143 (2021) 110179. https://doi.org/10.1016/j.eurpolymj.2020.110179.

[100] X.F. Zheng, Q. Lian, H. Yang, X. Wang, Surface molecularly imprinted polymer of chitosan grafted poly(methyl methacrylate) for 5-fluorouracil and controlled release, Sci. Rep. 6 (2016) 1–12. https://doi.org/10.1038/srep21409.

[101] L. Tang, C.Y. Zhao, X.H. Wang, R.S. Li, J.R. Yang, Y.P. Huang, Z.S. Liu, Macromolecular crowding of molecular imprinting: A facile pathway to produce drug delivery devices for zero-order sustained release, Int. J. Pharm. 496 (2015) 822–833. https://doi.org/10.1016/j.ijpharm.2015.10.031.

[102] C.C. Villa, L.T. Sánchez, G.A. Valencia, S. Ahmed, T.J. Gutiérrez, Molecularly imprinted polymers for food applications: A review, Trends Food Sci. Technol. 111 (2021) 642–669. https://doi.org/10.1016/j.tifs.2021.03.003.

[103] J. Wackerlig, R. Schirhagl, Applications of Molecularly Imprinted Polymer Nanoparticles and Their Advances toward Industrial Use: A Review, Anal. Chem. 88 (2016) 250–261. https://doi.org/10.1021/acs.analchem.5b03804.

[104] L.A.A.N.A. Truta, N.S. Ferreira, M.G.F. Sales, Graphene-based biomimetic materials targeting urine metabolite as potential cancer biomarker: Application

over different conductive materials for potentiometric transduction, Electrochim. Acta. 150 (2014) 99–107. https://doi.org/10.1016/j.electacta.2014.10.136.

[105] T.S.C.R. Rebelo, C. Santos, J. Costa-Rodrigues, M.H. Fernandes, J.P. Noronha, M.G.F. Sales, Novel Prostate Specific Antigen plastic antibody designed with charged binding sites for an improved protein binding and its application in a biosensor of potentiometric transduction, Electrochim. Acta. 132 (2014) 142–150. https://doi.org/10.1016/j.electacta.2014.03.108.

[106] L. Uzun, A.P.F. Turner, Molecularly-imprinted polymer sensors: Realising their potential, Biosens. Bioelectron. 76 (2016) 131–144. https://doi.org/10.1016/j.bios.2015.07.013.

[107] Q. Zhang, D. Jiang, C. Xu, Y. Ge, X. Liu, Q. Wei, L. Huang, X. Ren, C. Wang, Y. Wang, Wearable electrochemical biosensor based on molecularly imprinted Ag nanowires for noninvasive monitoring lactate in human sweat, Sensors Actuators, B Chem. 320 (2020) 128325. https://doi.org/10.1016/j.snb.2020.128325.

[108] R.D. Crapnell, N.C. Dempsey-Hibbert, M. Peeters, A. Tridente, C.E. Banks, Molecularly imprinted polymer based electrochemical biosensors: Overcoming the challenges of detecting vital biomarkers and speeding up diagnosis, Talanta Open. 2 (2020) 100018. https://doi.org/10.1016/j.talo.2020.100018.

[109] A.R. Cardoso, M.H. de Sá, M.G.F. Sales, An impedimetric molecularly-imprinted biosensor for Interleukin-1β determination, prepared by in-situ electropolymerization on carbon screen-printed electrodes, Bioelectrochemistry. 130 (2019) 1–9. https://doi.org/10.1016/j.bioelechem.2019.04.017.

[110] J.G. Pacheco, M.S.V. Silva, M. Freitas, H.P.A. Nouws, C. Delerue-Matos, Molecularly imprinted electrochemical sensor for the point-of-care detection of a breast cancer biomarker (CA 15-3), Sensors Actuators, B Chem. 256 (2018) 905–912. https://doi.org/10.1016/j.snb.2017.10.027.

[111] M. Jiang, M. Braiek, A. Florea, A. Chrouda, C. Farre, A. Bonhomme, F. Bessueille, F. Vocanson, A. Zhang, N. Jaffrezic-Renault, Aflatoxin B1 detection using a highly-sensitive molecularly-imprinted electrochemical sensor based on an electropolymerized metal organic framework, Toxins (Basel). 7 (2015) 3540–

3553. https://doi.org/10.3390/toxins7093540.

[112] M. Jia, Z. Zhang, J. Li, X. Ma, L. Chen, X. Yang, Molecular imprinting technology for microorganism analysis, TrAC - Trends Anal. Chem. 106 (2018) 190–201. https://doi.org/10.1016/j.trac.2018.07.011.

[113] M. Golabi, F. Kuralay, E.W.H. Jager, V. Beni, A.P.F. Turner, Electrochemical bacterial detection using poly(3-aminophenylboronic acid)-based imprinted polymer, Biosens. Bioelectron. 93 (2017) 87–93. https://doi.org/10.1016/j.bios.2016.09.088.

[114] T. Wangchareansak, A. Thitithanyanont, D. Chuakheaw, M.P. Gleeson, P.A. Lieberzeit, C. Sangma, A novel approach to identify molecular binding to the influenza virus H5N1: Screening using molecularly imprinted polymers (MIPs), Medchemcomm. 5 (2014) 617–621. https://doi.org/10.1039/c3md00272a.

[115] C. Pintavirooj, N. Vongmanee, W. Sukjee, C. Sangma, S. Visitsattapongse, Biosensors for Klebsiella pneumoniae with Molecularly Imprinted Polymer (MIP) Technique, Sensors. 22 (2022) 1–14. https://doi.org/10.3390/s22124638.

[116] J.E.S. Clarindo, R.B. Viana, P. Cervini, A.B.F. Silva, E.T.G. Cavalheiro, Determination of Tetracycline Using a Graphite-Polyurethane Composite Electrode Modified with a Molecularly Imprinted Polymer, Anal. Lett. 53 (2020) 1932–1955. https://doi.org/10.1080/00032719.2020.1725540.

[117] J. Dong, H. Li, P. Yan, L. Xu, J. Zhang, J. Qian, J. Chen, H. Li, A label-free photoelectrochemical aptasensor for tetracycline based on Au/BiOI composites, Inorg. Chem. Commun. 109 (2019). https://doi.org/10.1016/j.inoche.2019.107557.

[118] M. Karimi, M. Rabiee, M. Tahriri, R. Salarian, L. Tayebi, A graphene based–biomimetic molecularly imprinted polyaniline sensor for ultrasensitive detection of human cardiac troponin T (cTnT), Synth. Met. 256 (2019) 116136. https://doi.org/10.1016/j.synthmet.2019.116136.

[119] Z. Mokhtari, H. Khajehsharifi, S. Hashemnia, Z. Solati, R. Azimpanah, S. Shahrokhian, Evaluation of molecular imprinted polymerized methylene blue/aptamer as a novel hybrid receptor for Cardiac Troponin I (cTnI) detection

at glassy carbon electrodes modified with new biosynthesized ZnONPs, Sensors Actuators, B Chem. 320 (2020). https://doi.org/10.1016/j.snb.2020.128316.

[120] Y. Sun, Y. Yang, S. Li, W. Wang, X. Feng, M. Zhao, Y. Liu, Preparation of Myoglobin Imprinted Polymer via Myoglobin Catalyzed-eATRP on the Surface of Foam-Graphene, J. Electrochem. Soc. 166 (2019) B1251–B1257. https://doi.org/10.1149/2.0231914jes.

[121] D. Kumar, B.B. Prasad, Multiwalled carbon nanotubes embedded molecularly imprinted polymer-modified screen printed carbon electrode for the quantitative analysis of C-reactive protein, Sensors Actuators, B Chem. 171–172 (2012) 1141–1150. https://doi.org/10.1016/j.snb.2012.06.053.

[122] P. Jolly, V. Tamboli, R.L. Harniman, P. Estrela, C.J. Allender, J.L. Bowen, Aptamer-MIP hybrid receptor for highly sensitive electrochemical detection of prostate specific antigen, Biosens. Bioelectron. 75 (2016) 188–195. https://doi.org/10.1016/j.bios.2015.08.043.

[123] P. Abdollahiyan, A. Mohammadzadeh, M. Hasanzadeh, Chemical binding of molecular-imprinted polymer to biotinilated antibody: Utilization of molecular imprinting polymer as intelligent synthetic biomaterials toward recognition of carcinoma embryonic antigen in human plasma sample, J. Mol. Recognit. 34 (2021) e2897. https://doi.org/10.1002/JMR.2897.

[124] T.S.C.R. Rebelo, R. Costa, A.T.S.C. Brandão, A.F. Silva, M.G.F. Sales, C.M. Pereira, Molecularly imprinted polymer SPE sensor for analysis of CA-125 on serum, Anal. Chim. Acta. 1082 (2019) 126–135. https://doi.org/10.1016/J.ACA.2019.07.050.

[125] J.A. Ribeiro, C.M. Pereira, A.F. Silva, M.G.F. Sales, Disposable electrochemical detection of breast cancer tumour marker CA 15-3 using poly(Toluidine Blue) as imprinted polymer receptor, Biosens. Bioelectron. 109 (2018) 246–254. https://doi.org/10.1016/j.bios.2018.03.011.

[126] M.H. Do, A. Florea, C. Farre, A. Bonhomme, F. Bessueille, F. Vocanson, N.T. Tran-Thi, N. Jaffrezic-Renault, Molecularly imprinted polymer-based electrochemical sensor for the sensitive detection of glyphosate herbicide, Int. J. Environ. Anal. Chem. 95 (2015) 1489–1501. https://doi.org/10.1080/03067319.2015.1114109.

[127] O.T. Vu, Q.H. Nguyen, T. Nguy Phan, T.T. Luong, K. Eersels, P. Wagner, L.T.N. Truong, Highly Sensitive Molecularly Imprinted Polymer-Based Electrochemical Sensors Enhanced by Gold Nanoparticles for Norfloxacin Detection in Aquaculture Water, ACS Omega. 8 (2023) 2887–2896. https://doi.org/10.1021/ACSOMEGA.2C04414/ASSET/IMAGES/LARGE/AO2C04414_0006.JPEG.

[128] K. Matyjaszewski, T.P. Davis, Handbook of Radical Polymerization, 2002. https://doi.org/10.1002/0471220450.

[129] X. Ma, G. Wen, Development history and synthesis of super-absorbent polymers: a review, J. Polym. Res. 27 (2020). https://doi.org/10.1007/s10965-020-02097-2.

[130] N.P. Truong, G.R. Jones, K.G.E. Bradford, D. Konkolewicz, A. Anastasaki, A comparison of RAFT and ATRP methods for controlled radical polymerization, Nat. Rev. Chem. 5 (2021) 859–869. https://doi.org/10.1038/s41570-021-00328-8.

[131] F. D'Agosto, J. Rieger, M. Lansalot, RAFT-Mediated Polymerization-Induced Self-Assembly, Angew. Chemie - Int. Ed. 59 (2020) 8368–8392. https://doi.org/10.1002/anie.201911758.

[132] M.M. Moein, A. Abdel-Rehim, M. Abdel-Rehim, Recent applications of molecularly imprinted sol-gel methodology in sample preparation, Molecules. 24 (2019) 1–12. https://doi.org/10.3390/molecules24162889.

[133] A.Z.E. Peter A.G. Cormack, Molecularly imprinted polymers: synthesis and characterization, J. Chromatogr. B. (2004) 173–182. https://doi.org/10.1016/j.jchromb.2004.02.013.

[134] F. Mollarasouli, S. Kurbanoglu, S.A. Ozkan, The Role of Electrochemical Immunosensors in, Biosensors. 9 (2019) 1–19. https://doi.org/10.3390/bios9030086.

[135] F.S. Felix, L. Angnes, Electrochemical immunosensors – A powerful tool for analytical applications, Biosens. Bioelectron. 102 (2018) 470–478. https://doi.org/10.1016/j.bios.2017.11.029.

[136] N.S. Lipman, L.R. Jackson, L.J. Trudel, F. Weis-Garcia, Monoclonal versus

polyclonal antibodies: Distinguishing characteristics, applications, and information resources, ILAR J. 46 (2005) 258–267. https://doi.org/10.1093/ilar.46.3.258.

[137] H. Filik, A.A. Avan, Nanostructures for nonlabeled and labeled electrochemical immunosensors: Simultaneous electrochemical detection of cancer markers: A review, Talanta. 205 (2019) 120153. https://doi.org/10.1016/j.talanta.2019.120153.

[138] O. Hosu, G. Selvolini, C. Cristea, G. Marrazza, Electrochemical Immunosensors for Disease Detection and Diagnosis, Curr. Med. Chem. 25 (2017) 4119–4137. https://doi.org/10.2174/0929867324666170727104429.

[139] P.B. Luppa, L.J. Sokoll, D.W. Chan, Immunosensors—principles and applications to clinical chemistry, Clin. Chim. Acta. 314 (2001) 1–26. https://doi.org/10.1016/S0009-8981(01)00629-5.

[140] N.S. Ferreira, M.G.F. Sales, Disposable immunosensor with simple antibody orientation for label-free real-time detection of a cancer biomarker, (n.d.) 8.

[141] Y. Wan, Y. Su, X. Zhu, G. Liu, C. Fan, Development of electrochemical immunosensors towards point of care diagnostics, Biosens. Bioelectron. 47 (2013) 1–11. https://doi.org/10.1016/j.bios.2013.02.045.

[142] N.G. Welch, J.A. Scoble, B.W. Muir, P.J. Pigram, Orientation and characterization of immobilized antibodies for improved immunoassays (Review), Biointerphases. 12 (2017) 02D301. https://doi.org/10.1116/1.4978435.

[143] R. Laocharoensuk, Development of Electrochemical Immunosensors towards Point-of-care Cancer Diagnostics: Clinically Relevant Studies, Electroanalysis. 28 (2016) 1716–1729. https://doi.org/10.1002/elan.201600248.

[144] M. Hasanzadeh, N. Shadjou, Y. Lin, M. de la Guardia, Nanomaterials for use in immunosensing of carcinoembryonic antigen (CEA): Recent advances, TrAC - Trends Anal. Chem. 86 (2017) 185–205. https://doi.org/10.1016/j.trac.2016.11.003.

[145] M. Jozghorbani, M. Fathi, S.H. Kazemi, N. Alinejadian, Determination of

carcinoembryonic antigen as a tumor marker using a novel graphene-based label-free electrochemical immunosensor, Anal. Biochem. 613 (2021) 114017. https://doi.org/10.1016/j.ab.2020.114017.

[146] G. Manasa, R.J. Mascarenhas, S.J. Malode, N.P. Shetti, Biosensors and Bioelectronics : X Graphene-based electrochemical immunosensors for early detection of oncomarker carcinoembryonic antigen, Biosens. Bioelectron. X. 11 (2022) 100189. https://doi.org/10.1016/j.biosx.2022.100189.

[147] S. Sharma, R. Raghav, R. O'Kennedy, S. Srivastava, Advances in ovarian cancer diagnosis: A journey from immunoassays to immunosensors, Enzyme Microb. Technol. 89 (2016) 15–30. https://doi.org/10.1016/j.enzmictec.2016.03.002.

[148] P. Samadi Pakchin, M. Fathi, H. Ghanbari, R. Saber, Y. Omidi, A novel electrochemical immunosensor for ultrasensitive detection of CA125 in ovarian cancer, Biosens. Bioelectron. 153 (2020) 112029. https://doi.org/10.1016/j.bios.2020.112029.

[149] A.C.H. de Castro, L.M. Alves, A.C.S. Siquieroli, J.M. Madurro, A.G. Brito-Madurro, Label-free electrochemical immunosensor for detection of oncomarker CA125 in serum, Microchem. J. 155 (2020) 104746. https://doi.org/10.1016/j.microc.2020.104746.

[150] H. Medetalibeyoglu, G. Kotan, N. Atar, M.L. Yola, A novel and ultrasensitive sandwich-type electrochemical immunosensor based on delaminated MXene@AuNPs as signal amplification for prostate specific antigen (PSA) detection and immunosensor validation, Talanta. 220 (2020) 121403. https://doi.org/10.1016/j.talanta.2020.121403.

[151] L. Suresh, P.K. Brahman, K.R. Reddy, J.S. Bondili, Development of an electrochemical immunosensor based on gold nanoparticles incorporated chitosan biopolymer nanocomposite film for the detection of prostate cancer using PSA as biomarker, Enzyme Microb. Technol. 112 (2018) 43–51. https://doi.org/10.1016/j.enzmictec.2017.10.009.

[152] M. Zhang, X. Hu, L. Mei, L. Zhang, X. Wang, X. Liao, X. Qiao, C. Hong, PSA detection electrochemical immunosensor based on MOF-235 nanomaterial adsorption

aggregation signal amplification strategy, Microchem. J. 171 (2021) 106870. https://doi.org/10.1016/j.microc.2021.106870.

[153] R.S. Gomes, F.T.C. Moreira, R. Fernandes, M.F. Goreti Sales, Sensing CA 15-3 in point-of-care by electropolymerizing O-phenylenediamine (oPDA) on Au-screen printed electrodes, PLoS One. 13 (2018) 1–19. https://doi.org/10.1371/journal.pone.0196656.

[154] T.S. Martins, J.L. Bott-Neto, O.N. Oliveira, S.A.S. Machado, A sandwich-type electrochemical immunosensor based on Au-rGO composite for CA15-3 tumor marker detection, Microchim. Acta. 189 (2022) 3–9. https://doi.org/10.1007/s00604-021-05145-w.

[155] D. Qin, X. Jiang, G. Mo, J. Feng, C. Yu, B. Deng, A Novel carbon quantum dots signal amplification strategy coupled with sandwich electrochemiluminescence immunosensor for the detection of ca15-3 in human serum, ACS Sensors. 4 (2019) 504–512. https://doi.org/10.1021/acssensors.8b01607.

[156] V. Naresh, N. Lee, A review on biosensors and recent development of nanostructured materials-enabled biosensors, Sensors (Switzerland). 21 (2021) 1–35. https://doi.org/10.3390/s21041109.

[157] A. Navaee, A. Salimi, Chapter 7: Enzyme-based electrochemical biosensors, in: Electrochem. Biosens., Elsevier, 2019: pp. 167–211. https://doi.org/10.1016/B978-0-12-816491-4.00007-3.

[158] G. Evtugyn, Biosensors : Essentials, Springer Berlin Heidelberg, 2014. https://doi.org/https://doi.org/10.1007/978-3-642-40241-8.

[159] A. Singh, A. Sharma, A. Ahmed, A.K. Sundramoorthy, H. Furukawa, S. Arya, A. Khosla, Recent advances in electrochemical biosensors: Applications, challenges, and future scope, Biosensors. 11 (2021) 1–31. https://doi.org/10.3390/bios11090336.

[160] H.A. Abdulbari, E.A.M. Basheer, Electrochemical Biosensors: Electrode Development, Materials, Design, and Fabrication, ChemBioEng Rev. 4 (2017) 92–105. https://doi.org/10.1002/cben.201600009.

[161] L.A.A.N.A. Truta, F.T.C. Moreira, M.G.F. Sales, A dye-sensitized solar cell acting as the electrical reading box of an immunosensor: Application to CEA determination, Biosens. Bioelectron. 107 (2018) 94–102. https://doi.org/10.1016/j.bios.2018.02.011.

[162] T.J. Roussel, D.J. Jackson, R.P. Baldwin, R.S. Keynton, Amperometric Techniques, Encycl. Microfluid. Nanofluidics. (2008) 39–47. https://doi.org/10.1007/978-0-387-48998-8_26.

[163] E.C. Potter, C. V. King, Electrochemistry. Principles and Applications, J. Electrochem. Soc. 104 (1957) 115C. https://doi.org/10.1149/1.2428553.

[164] P.T. Moseley, Fuel Cell Systems Explained, 2001. https://doi.org/10.1016/s0378-7753(00)00571-1.

[165] R.A. Bullen, T.C. Arnot, J.B. Lakeman, F.C. Walsh, Biofuel cells and their development, Biosens. Bioelectron. 21 (2006) 2015–2045. https://doi.org/10.1016/j.bios.2006.01.030.

[166] F. Conzuelo, A. Ruff, W. Schuhmann, Self-powered bioelectrochemical devices, Curr. Opin. Electrochem. 12 (2018) 156–163. https://doi.org/10.1016/j.coelec.2018.05.010.

[167] M.J. Cooney, V. Svoboda, C. Lau, G. Martin, S.D. Minteer, Enzyme catalysed biofuel cells, Energy Environ. Sci. 1 (2008) 320–337. https://doi.org/10.1039/b809009b.

[168] E. Katz, A.F. Bu, M. Weg, Self-Powered Enzyme-Based Biosensors, (2001) 10752–10753.

[169] A.S. Dahiya, J. Thireau, J. Boudaden, S. Lal, U. Gulzar, Y. Zhang, T. Gil, N. Azemard, P. Ramm, T. Kiessling, C. O'Murchu, F. Sebelius, J. Tilly, C. Glynn, S. Geary, C. O'Dwyer, K.M. Razeeb, A. Lacampagne, B. Charlot, A. Todri-Sanial, Review—Energy Autonomous Wearable Sensors for Smart Healthcare: A Review, J. Electrochem. Soc. 167 (2020) 037516. https://doi.org/10.1149/2.0162003jes.

[170] L. Manjakkal, L. Yin, A. Nathan, J. Wang, R. Dahiya, Energy Autonomous Sweat-Based Wearable Systems, Adv. Mater. 33 (2021).

https://doi.org/10.1002/adma.202100899.

[171] F.T.C. Moreira, M.G.F. Sales, Autonomous biosensing device merged with photovoltaic technology for cancer biomarker detection, J. Electroanal. Chem. 855 (2019) 113611. https://doi.org/10.1016/j.jelechem.2019.113611.

[172] M.H. de Sá, L. Brandão, Non-enzymatic direct glucose fuel cells (DGFC): A novel principle towards autonomous electrochemical biosensors, Int. J. Hydrogen Energy. 45 (2020) 29749–29762. https://doi.org/10.1016/j.ijhydene.2019.09.105.

[173] C. Gonzalez-Solino, M. Di Lorenzo, Enzymatic fuel cells: Towards self-powered implantable and wearable diagnostics, Biosensors. 8 (2018). https://doi.org/10.3390/bios8010011.

[174] G. Pasternak, J. Greenman, I. Ieropoulos, Self-powered, autonomous Biological Oxygen Demand biosensor for online water quality monitoring, Sensors Actuators, B Chem. 244 (2017) 815–822. https://doi.org/10.1016/j.snb.2017.01.019.

[175] L.A.A.N.A. Truta, F.T.C. Moreira, M.G.F. Sales, A dye-sensitized solar cell acting as the electrical reading box of an immunosensor: Application to CEA determination, Biosens. Bioelectron. 107 (2018) 94–102. https://doi.org/10.1016/j.bios.2018.02.011.

[176] M.G.F. Sales, L. Brandão, Autonomous electrochemical biosensors: A new vision to direct methanol fuel cells, Biosens. Bioelectron. 98 (2017) 428–436. https://doi.org/10.1016/j.bios.2017.07.021.

[177] M. Zhou, Recent Progress on the Development of Biofuel Cells for Self-Powered Electrochemical Biosensing and Logic Biosensing: A Review, Electroanalysis. 27 (2015) 1786–1810. https://doi.org/10.1002/elan.201500173.

[178] P. Pinyou, F. Conzuelo, K. Sliozberg, J. Vivekananthan, A. Contin, S. Pöller, N. Plumeré, W. Schuhmann, Coupling of an enzymatic biofuel cell to an electrochemical cell for self-powered glucose sensing with optical readout, Bioelectrochemistry. 106 (2015) 22–27. https://doi.org/10.1016/j.bioelechem.2015.04.003.

[179] A. Zloczewska, A. Celebanska, K. Szot, D. Tomaszewska, M. Opallo, M. Jönsson-Niedziolka, Self-powered biosensor for ascorbic acid with a Prussian blue electrochromic display, Biosens. Bioelectron. 54 (2014) 455–461. https://doi.org/10.1016/j.bios.2013.11.033.

[180] A.P.M. Tavares, L.A.A.N.A. Truta, F.T.C. Moreira, L.P.T. Carneiro, M.G.F. Sales, Self-powered and self-signalled autonomous electrochemical biosensor applied to cancinoembryonic antigen determination, Biosens. Bioelectron. 140 (2019) 111320. https://doi.org/10.1016/j.bios.2019.111320.

[181] W.R. Grove, LXXII. On a gaseous voltaic battery, London, Edinburgh, Dublin Philos. Mag. J. Sci. 21 (1842) 417–420. https://doi.org/10.1080/14786444208621600.

[182] C. L, L. R, R.S. Sec, Downloaded from https://royalsocietypublishing.org/ on 23 August 2022 Downloaded from https://royalsocietypublishing.org/ on 23 August 2022, 8 (1889) 296–304.

[183] L. Carrette, K.A. Friedrich, U. Stimming, Fuel Cells: Principles and Applications, (2000).

[184] O.Z. Sharaf, M.F. Orhan, An overview of fuel cell technology: Fundamentals and applications, Renew. Sustain. Energy Rev. 32 (2014) 810–853. https://doi.org/10.1016/j.rser.2014.01.012.

[185] U. Lucia, Overview on fuel cells, Renew. Sustain. Energy Rev. 30 (2014) 164–169. https://doi.org/10.1016/j.rser.2013.09.025.

[186] R.A. Felseghi, E. Carcadea, M.S. Raboaca, C.N. Trufin, C. Filote, Hydrogen fuel cell technology for the sustainable future of stationary applications, Energies. 12 (2019). https://doi.org/10.3390/en12234593.

[187] V. Cigolotti, M. Genovese, P. Fragiacomo, Comprehensive review on fuel cell technology for stationary applications as sustainable and efficient poly-generation energy systems, Energies. 14 (2021). https://doi.org/10.3390/en14164963.

[188] D.M. Fadzillah, S.K. Kamarudin, M.A. Zainoodin, M.S. Masdar, Critical challenges in the system development of direct alcohol fuel cells as portable power supplies:

An overview, Int. J. Hydrogen Energy. 44 (2019) 3031–3054. https://doi.org/10.1016/j.ijhydene.2018.11.089.

[189] N. Sazali, W.N.W. Salleh, A.S. Jamaludin, M.N.M. Razali, New perspectives on fuel cell technology: A brief review, Membranes (Basel). 10 (2020). https://doi.org/10.3390/membranes10050099.

[190] W.R.W. Daud, R.E. Rosli, E.H. Majlan, S.A.A. Hamid, R. Mohamed, T. Husaini, PEM fuel cell system control: A review, Renew. Energy. 113 (2017) 620–638. https://doi.org/10.1016/j.renene.2017.06.027.

[191] J. Larminie, A. Dicks, Fuel cell systems explained, 2003. https://doi.org/10.1002/9781118878330.

[192] G. Karanfil, Importance and applications of DOE/optimization methods in PEM fuel cells: A review, Int. J. Energy Res. 44 (2020) 4–25. https://doi.org/10.1002/er.4815.

[193] A.M.F.R. Pinto, V.B. Oliveira, D.S. Falcão, Direct alcohol fuel cells for portable applications: Fundamentals, engineering and advances, Elsevier, 2018. https://doi.org/10.1016/C2016-0-00632-0.

[194] I. Fouzaï, S. Gentil, V.C. Bassetto, W.O. Silva, R. Maher, H.H. Girault, Catalytic layer-membrane electrode assembly methods for optimum triple phase boundaries and fuel cell performances, J. Mater. Chem. A. 9 (2021) 11096–11123. https://doi.org/10.1039/d0ta07470e.

[195] M. Ahmed, I. Dincer, A review on methanol crossover in direct methanol fuel cells: challenges and achievements, Int. J. Energy Res. 35 (2011) 1213–1228. https://doi.org/10.1002/er.

[196] N.K. Shrivastava, S.B. Thombre, R.B. Chadge, Liquid feed passive direct methanol fuel cell: challenges and recent advances, Ionics (Kiel). 22 (2016) 1–23. https://doi.org/10.1007/s11581-015-1589-6.

[197] S. Feng, G. Yang, D. Zheng, A. Rauf, U. Khan, R. Cheng, L. Wang, W. Wang, F. Liu, Completely eliminating the metal barrier cracks on Nafion for suppressing methanol crossover with anodic aluminum oxide substrates, Int. J. Hydrogen

Energy. 47 (2022) 18496–18503. https://doi.org/10.1016/j.ijhydene.2022.04.002.

[198] M. Tawalbeh, A. Al-Othman, M. El Haj Assad, Graphene oxide - Nafion composite membrane for effective methanol crossover reduction in passive direct methanol fuel cells, 5th Int. Conf. Renew. Energy Gener. Appl. ICREGA 2018. 2018-Janua (2018) 192–196. https://doi.org/10.1109/ICREGA.2018.8337596.

[199] Z. Zakaria, S.K. Kamarudin, A review of quaternized polyvinyl alcohol as an alternative polymeric membrane in DMFCs and DEFCs, Int. J. Energy Res. 44 (2020) 6223–6239. https://doi.org/10.1002/er.5314.

[200] J. Zhou, J. Cao, Y. Zhang, J. Liu, J. Chen, M. Li, W. Wang, X. Liu, Overcoming undesired fuel crossover: Goals of methanol-resistant modification of polymer electrolyte membranes, Renew. Sustain. Energy Rev. 138 (2021) 110660. https://doi.org/10.1016/j.rser.2020.110660.

[201] B.A. Berns, M.F. Torres, V.B. Oliveira, Performance of passive Direct Methanol Fuel Cell : modelling and experimental studies, U.Porto J. Eng. 1 (2015) 89–103. https://journalengineering.fe.up.pt/article/view/110/111.

3. FUEL CELLS AS AN IMMUNOSENSOR FOR CANCER BIOMARKER SCREENING

3.1. Introduction

Biosensor research dates back several decades and has now established itself as a growing area of interest for point-of-care (PoC) health monitoring. These are analytical devices that convert a response obtained through a biological or biomimetic material - biorecognition element - into a measurable electrical signal-transducer [1]. The need for PoC biosensors is increasing day by day and is becoming more and more important for quick, easy, and cost-effective screening of various diseases. In response to the specific needs of underdeveloped countries and in case of global crisis or war scenarios, it is important that biosensors can operate autonomously and use readily available energy.

In search for autonomous devices, some research works make use of microbial fuel cells [2], enzymatic fuel cells [3], Dye-sensitized solar cells [4] or Direct Methanol Fuel Cells (DMFCs) [5]. Although these approaches offer autonomy features, microbial and enzymatic fuel cells are very delicate systems that require specific conditions of operation and have difficulties in terms of reproducibility, limiting their application to quantitative measures. Moreover, dye-sensitized solar cells (DSSCs) are not functional at night limiting their operation in places where there is no electrical power.

A power source that favours the operation of autonomous biosensors at any time and with higher performance are DMFCs. DMFCs convert chemical energy into electrical energy and are now widely used, including in commercial applications. These cells are simple, environmentally friendly, highly efficient, reliable, have a long lifetime and can be easily miniaturized. They use methanol as fuel, which can be easily stored and transported compared to hydrogen-fed fuel cells, which simplifies the fuel cell system [6]. In addition, they offer high power, meaning that only a small volume of methanol (few mL) is enough for their operation. To date, DMFCs have been interfaced with plastic antibodies as biorecognition layer [7–10] but no work has been conducted with antibodies, which in general are a guarantee of the production of a selective response.

Thus, this work presents for the first time a combination of antibodies and DMFCs aimed at producing an autonomous immunosensor. This principle was applied to cancer

antigen 15-3 (CA15-3), a cancer biomarker circulating in the blood. Healthy individuals contain 25 U/ml of CA15-3 [11], and higher levels indicate a cancer diagnosis, including breast cancer, the most common cancer in women worldwide [12]. To date, there are several biosensors for the determination of CA15-3. These include various concepts and approaches, many of which are electrochemical [13–16], optical [17], or lateral flow assays [18–20]. Electrochemical sensors offer high sensitivity but are electrically powered devices, thereby being energy dependent. This limits their use to locations where a power source is available, which may not always be the case. Excluding coloured systems detected by naked eye, optical sensors are also powered by an electrical device to measure the generated signal [21]. Lateral flow assays are energy independent, but they provide a simple "yes" or "no" response and are not able to quantify the concentration of the biomarker, which is important in this case to determine whether a particular individual has a normal or high CA15-3 level.

In detail, this work describes the design of a hybrid DMFC system (hDMFC) consisting of two carbon-based electrodes on commercial carbon cloth, one of which is modified with antibodies against CA15-3. In this way, the performance of the cell becomes concentration dependent, because when more CA15-3 is bound to the antibodies, less energy is generated by the hDMFC. The system was optimised with respect to key variables and calibrated under buffered conditions to define the linear reaction range and detection limit (LoD) of the hDFMC. Selectivity studies and calibration in serum-based solutions were also performed to anticipate the behaviour of the hDMFC under realistic conditions.

3.2. Experimental section

3.2.1. Reagents, solutions, and materials

All chemicals were of analytical grade and water was ultrapure. MES buffer, 1 mM, pH 6.0, was obtained by dissolving 2-morpholinoethanesulfonic acid (MES, AppliChem) in water. The immunosensor was prepared using the following solutions: cysteamine (50 mM, Merck, prepared in ultrapure water), EDC (1-Ethyl-3-(3-dimethylaminopropyl)carbodiimide, 25 mM, Alfa Aesar, prepared in MES buffer), NHS

(N-Hydroxysuccinimide, 50 mM, Merck, prepared in MES buffer), Anti-CA15-3 (10× diluted in MES buffer, St Johns Lab), ethylenediamine (20 mM, VWR, prepared in ultrapure water), BSA (1 mg/mL, Sigma-Aldrich, prepared in MES buffer). To purify the antibody, Amicon® Ultra-2 mL Centrifugal Filters for DNA and Protein Purification and Concentration (Merck) were used.

The fuel cell was constructed using a commercial carbon cloth with a carbon black PtRu catalyst (40:20 wt%, 2 mg/cm^2) as the anode and a commercial carbon cloth with a carbon black Pt catalyst (0.5 mg/cm^2) as the cathode (both from Fuel Cells Etc The membrane electrode assembly (MEA) contained a Nafion® 115 membrane (Fuel Cells Etc) between the anode and cathode. The fuel cell was operated with a methanol solution of 0.5 or 0.1 M prepared in ultrapure water.

To obtain the ferrocyanide redox probe for three-electrode analysis, Potassium hexacyanoferrate III ($K_3[Fe(CN)_6]$) and potassium hexacyanoferrate II ($K_4[Fe(CN)_6]$) trihydrate (Riedel-de Haen) were used at concentration of both intervenient species of 5 mM, prepared in PBS at pH 7.3.

Stock solutions of 750 U/mL CA15-3 (17.42 kU/mL, MyBioSource) were prepared in MES buffer, and less concentrated standards were obtained by accurate dilution of the previous solution, also in MES. For selectivity studies, CA125 (150 U/mL, HyTest), CEA (100 ng/mL, EastCoastBio), glucose (1.3 mg/mL, Alfa Aesar), and ascorbic acid (0.02 mg/mL, Riedel-de-Haen) were prepared in MES buffer.

The antibody solution was purified before use, by diluting a small amount of commercial antibody solution (30 µL) in MES buffer (1.0 mL). The antibody solution was then purified using dedicated centrifuge filters (Amicon® Ultra-2 mL Centrifugal Filters) and centrifuged according to the centrifuge filter instructions. In this case, a 10-minute centrifugation at 7500× g was performed to capture the antibody in the filter network. To recover the purified antibody from the filter, it was inverted and a 2-minute centrifugation at 1000× g was performed. This procedure was repeated twice to ensure the purity of the antibody.

3.2.2. Immunosensor assembly

The anode electrode was used as support for the antibodies to create an immunosensitive region. For this purpose, it was first oxidized to remove impurities and reduce the hydrophobic properties of the surface. This oxidation was performed by cyclic voltammetry (CV, 10 cycles, -0.3 V to 1.2 V, scan rate 0.1 V/s) in 0.5 M of H_2SO_4.

The overall structure of the immunosensor is shown in **Figure 3.1a**. This included the binding of the antibody to the Pt/Ru metal nanoparticles on the carbon cloth. First, a cysteamine solution was added to the support surface for 1 hour (to bind -SH groups to Pt). The antibody was modified before it was anchored to the Pt surface. To do this, the antibody solution (1 µL for each electrode) was mixed with EDC/NHS (1 µL of 25 mM EDC and 1 µL of 50 mM NHS) and MES buffer (7 µL) to obtain a final volume of 10 µL for each electrode (final concentration of 25 mM EDC and 50 mM NHS and a 10-fold dilution of the antibody). This mixture was allowed to react for 30 min to activate the carboxyl groups of the antibody. The third step was incubation of the activated antibody on the aminated support surface for 2 hours. Then, ethylenediamine was added to the carbon cloth for 1 hour to deactivate the reactive carboxyl groups. BSA was then added to the carbon cloth for 1 hour to minimize non-specific binding. Between each of these immunosensor assembly steps, the carbon electrode was washed with ultra-pure water and dried with nitrogen.

3.2.3. Apparatus

Electrochemical measurements were performed using a Metrohm Autolab potentiostat/galvanostat and a PGSTAT302N equipped with the FRA module and controlled by the NOVA 2.1 software. Scanning electrode microscope analysis (SEM) was performed using a Quanta 400 FEG ESEM from FEI, and energy dispersive X-ray spectroscopy (EDS) was performed using a Genesis X4M from EDAX. This analysis was performed with Electron Backscatter Diffraction (EBSD) analysis. Raman spectroscopy was performed using a Thermo Scientific DXR Raman microscope system with a 532 nm excitation laser. Spectra were acquired with a 50× objective magnification, a maximum laser power of 5 mW, and a slit aperture of 50 µm. The photobleaching time was set to 10 minutes. Data analysis was performed using OMNIC software.

3.2.4. Hybrid Fuel Cell assembly and operation

The hDMFC was constructed in a single cell, shown in **Figure 3.1b**, operating at steady state, as previously described [3]. The cell was constructed with a commercial cathode (0.5 mgPt/cm^2 - used area: 2.25 cm^2), a Nafion® membrane (115), and the previously modified Carbon Cloth with Carbon Black PtRu (40:20 wt%) as anode (used area: 2.25 cm^2). Fuel cell measurements were performed at room temperature and atmospheric pressure. The anode was fed with a 0.5 M methanol solution inside the reservoir during cell activation (see **Figure 3.1b**) and with a 0.1 M methanol solution for sensor calibration. The excess methanol that was in the fuel cell after activation was removed by soaking the cell in ultrapure water overnight (the initial OCP reduces to almost zero).

To evaluate the response of the fuel cell with the immunosensor, electrochemical measurements were made. The electrochemical technique used to evaluate the fuel cell was Sampled DC. This measurement was performed starting from the OCP value of the fuel cell to 0.1 V, with time interval of 30s, and step of -0.05 V. The fuel cell activation was accomplished by measuring the cell consecutively until stabilization of the signal.

Figure 3.1 – (a) Schematic representation of the immunosensor assembly: integration of the immunosensor on the anode of the Membrane Electrode Assembly (MEA) from the passive Direct Methanol Fuel Cell (DMFC); **(b)** Real passive DMFC that was used throughout this work, where the immunosensor was assembled.

3.2.5. Three-electrode system

To evaluate the immunosensor construction, a three-electrode system was used. For this, an Ag/AgCl reference electrode and a platinum counter electrode were used. As working electrode, a fuel cell anode electrode (as described in section 2.4) was used for the construction and analysis of the immunosensor. All electrodes were emerged in 10 mL of a ferrocyanide redox probe of $[Fe(CN)_6]^{3-}$ and $[Fe(CN)_6]^{4-}$ to measure Electrochemical Impedance Spectroscopy (EIS) on all immunosensor construction steps. EIS assays were performed at open current potential (OCP), using a perturbation amplitude of 0.01 V and a frequency range from 0.1 to 100 kHz in ferrocene redox probe

(5 mM). An Ag/AgCl reference electrode and a platinum counter electrode were used. As working electrode, a fuel cell anode electrode (as described in section 3.2.2) was used for the construction and analysis of the immunosensor. Firstly, the fuel cell anode was cleaned with 0.5 M H_2SO_4, Cysteamine (0.05 M) was incubated on the electrode. During this incubation, the antibody was incubated with EDC/NHS (0.025 M and 0.05 M, respectively) for 30 minutes (previous to the incubation on the working electrode). The antibody was incubated for 2h, and afterwards, the reaction was blocked by incubating 1h with ethylenediamine (0.02 M). The final step was an incubation of BSA (1 mg/mL) for 1h. Measurements were performed between each step. Analysis of Nyquist plots was performed by using an equivalent electric circuit fit. Obtained Rct values after the different construction stages are shown in the table next to the Nyquist plots. The obtained data was analysed by NOVA Software, by Metrohm.

3.2.6. Calibration of the immunosensor

The calibration curves of the hDMFC used sampled DC measurements, made in 0.1 M methanol solution. Calibration was performed by first cleaning the sample reservoir with MES buffer, incubating the lowest concentration of the target protein for 15 minutes, cleaning the reservoir again with MES buffer, and then measuring the signal output of the cell by adding the methanol solution in the reservoir. This procedure was repeated for each target protein concentration from the lowest concentration (46.8 to 750 U/mL of CA15-3) prepared in MES buffer. All standards in the calibration were incubated on the same electrode, as this is a cumulative calibration.

3.3. Results and discussion

3.3.1. Assembly of the immunosensor electrode

The immunosensor electrode was constructed as described in the experimental section, having each modification step followed by a three-electrode system with a ferrocyanide redox probe and EIS measurements. The first step of the modification

consisted of the addition of cysteamine, which binds to the Pt nanoparticles. This binding decreases the intrinsic conductivity properties of Pt, leading to an increase in charge transfer resistance. The positive charge on the surface generated by the cysteamine could also have reduced the resistance to charge transfer of the negatively charged probe, but this effect was less pronounced than the effects on reducing the conductivity properties of Pt. Then the activated antibodies, previously modified with EDC/NHS chemistry, were added to the electrode with the amine layer. The activated carboxyl groups were capable of mild reaction with the amine groups and covalently bound the antibodies to the electrode surface. This modification contributed to an additional increase in resistance. Deactivation of the activated carboxylic groups that did not react was necessary to stabilize the electrode, and this was done by adding ethylenediamine. Since ethylenediamine carries positively charged amino groups, the resistance to charge transfer of the negatively charged probe decreased. The final step of the modification was the addition of BSA to reduce the nonspecific binding of CA15-3 to the electrode surface. The presence of BSA contributed to an additional increase in resistance to charge transfer (**Figure 3.2**). Overall, these results showed a similar trend to a previous immunosensor construction using a similar strategy [22], indicating that the immunosensor was successfully constructed. The amplitude of the observed resistance changes was smaller than when an immunosensor was built on commercial carbon electrodes, but this was already observed by us when Pt nanoparticles were added to these commercial carbon electrodes.

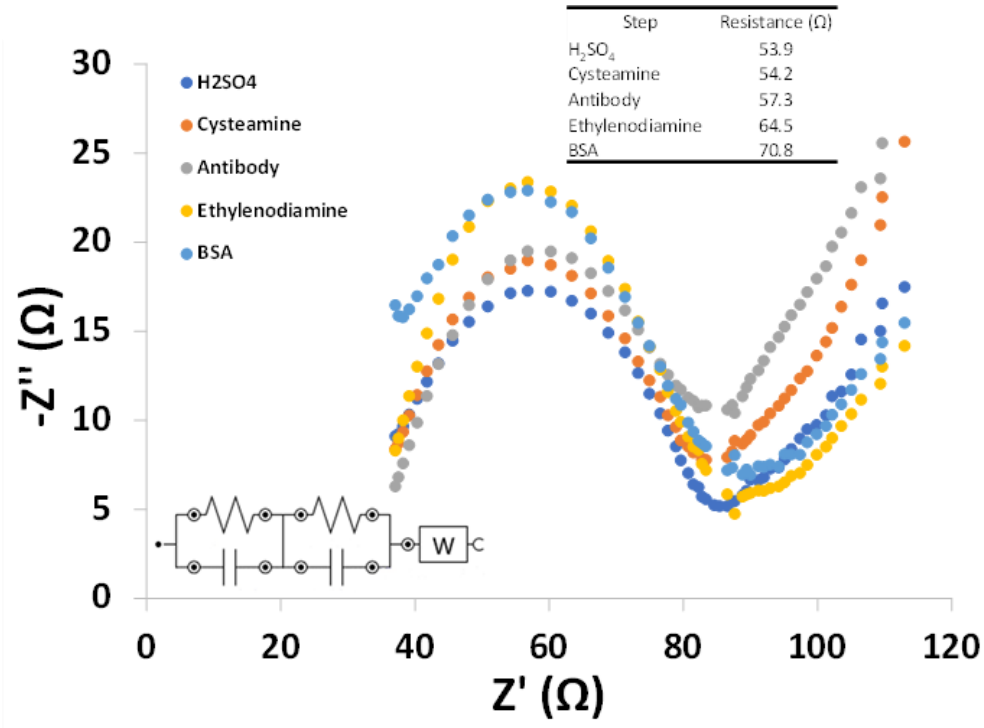

Figure 3.2 - Construction of the immunosensor followed by Electrochemical Impedance Spectroscopy (EIS) at open current potential (OCP). Analysis of Nyquist plots was performed by using an equivalent electric circuit fit (used circuit in Figure). Obtained Rct values after the different construction stages are shown in the table next to the Nyquist plots.

3.3.1.1. SEM and EDS analysis

Figure 3.3 shows the results of SEM (**Figure 3.3a, b**) and EDS (**Figure 3.3c, d**) analysis of the Carbon Cloth/PtRu carbon black electrode before (**Figure 3.3a**) and after modification with the antibody (**Figure 3.3b**). As expected, the SEM images showed different light contrasts [18,19], because when the platinum is more exposed (control sample – **Figure 3.3a**) the brightness is more intense than when the antibody is bound to the platinum nanoparticles (**Figure 3.3b**). These differences in image contrast indicate that a change has occurred at the electrode, due to the attachment of the antibody to the platinum on the electrode surface. When analysing the EDS spectra (**Figures 3.3c, d**), the control sample shows similar results to previous studies [20, 21] with high Pt and Ru element peaks, mostly between 2 and 3 keV. For the electrode with the antibody, a slight increase in nitrogen (N) is observed in the modified sample. This indicated that an increased amount of this component was present, due to the presence of the amino

groups (-NH_2) of the antibody and the cysteamine on the surface. Overall, the data obtained confirmed the modification of the electrode, both in terms of image contrast and changes in EDS.

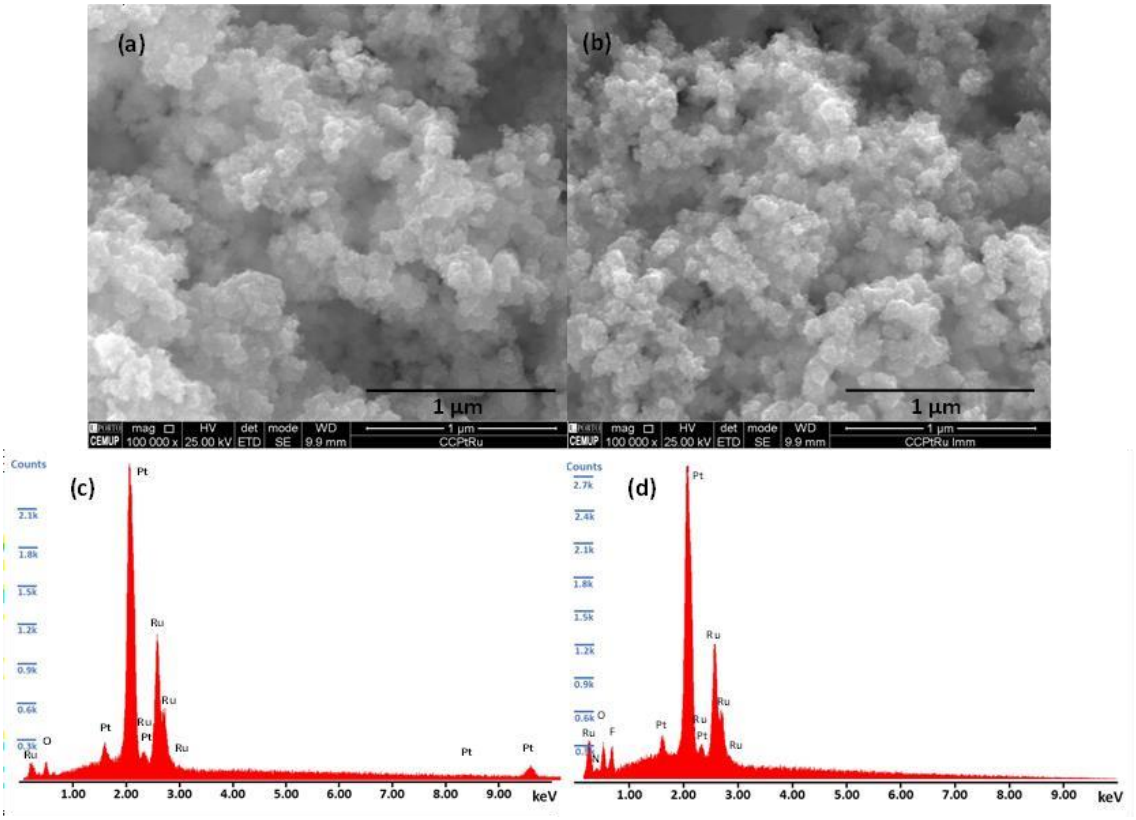

Figure 3.3 - SEM images of the Carbon Cloth PtRu carbon black (CCPtRu) anode electrode using Electron Backscatter Diffraction (EBSD) analysis of: **(a)** without any modification, **(b)** after binding the immunosensor construction protocol (H_2SO_4 cleaning, cysteamine bin binding the immunosensor construction protocol (H_2SO_4 cleaning, cysteamine binding to cleaned surface, and antibody anchorage to cysteamine after EDC/NHS activation), and **(c)** and **(d)** the corresponding EDS spectra.

3.3.1.2. Raman Spectroscopy

When excited at a wavelength in the visible region of the Raman spectrum, both D and G bands are typically found in graphite spectra, and the D band indicates defects or disorder in the carbon structure. Quantification of disorder is obtained by calculating the ratio between the G (related to the sp^2 carbon bonding) and D (related to the sp^3 carbon bond) bands (ID/IG) [22,23]. Looking at the overall spectra, the Raman intensity

was low compared to similar spectra from carbon black only, which was already expected [24]. This was consistent with previous studies of the group, which indicated that the presence of Pt/Ru quenches the Raman signal. In terms of ID/IG ratio, there are small differences between the immunosensor assembly steps (**Figure 3.4**). Since the overall intensity was low, it meant that the assembly of the immunosensor was successful, which is consistent with the SEM and EIS data.

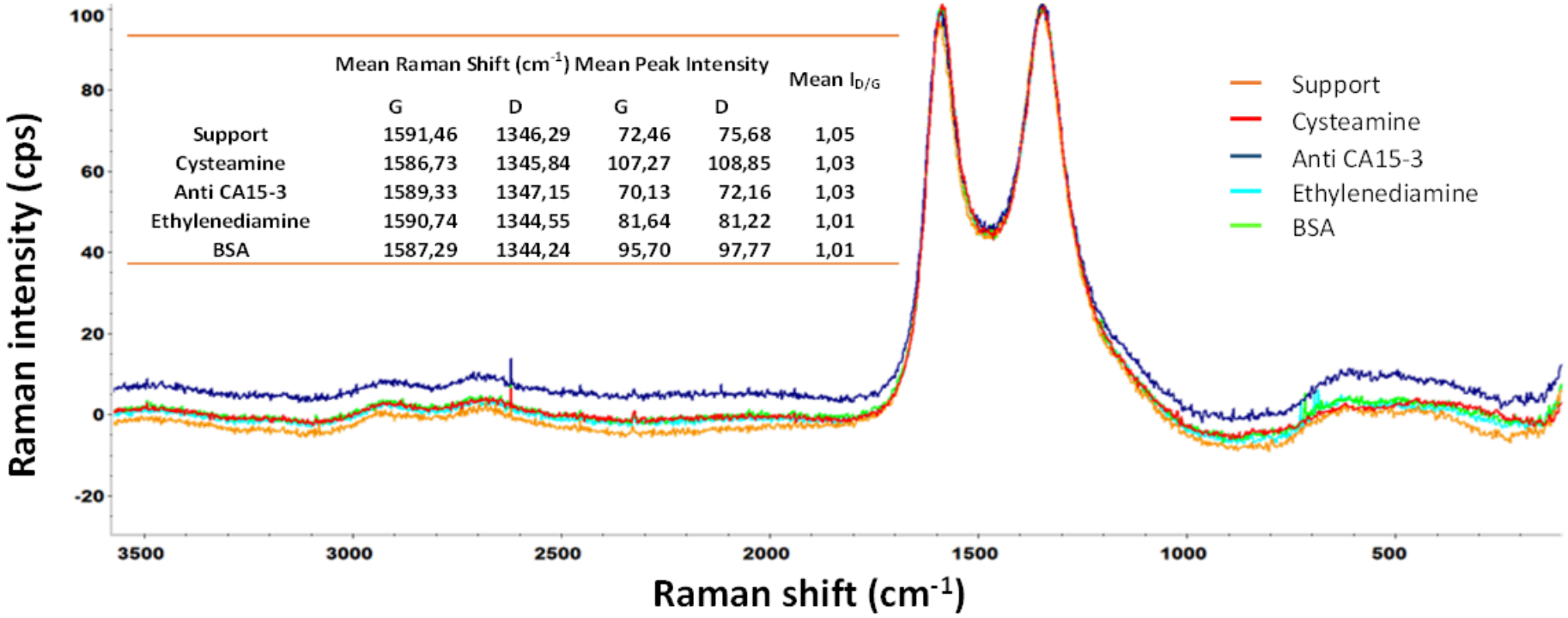

Figure 3.4 - Raman spectra obtained during immunosensor construction. All immunosensor construction steps were analysed (support without any modification, after cysteamine binding, after antibody binding to the surface, ethylenediamine, and BSA). The quantification of the disorder of each immunosensor construction was obtained by calculating the ratio between the G and D bands (I_D/I_G), which is shown in the table.

3.3.2. Selection of methanol concentration

An optimally functioning passive DMFC using the same design as in this work achieves power densities and currents around 2.5 mW/cm^2 when operated at high methanol concentrations (3 to 4 M) [3,25]. These high concentrations ensure that the cell also delivers the maximum possible energy because the amount of methanol is in excess compared to what can be consumed by the cell. However, while high concentrations promote high electrical output from the cell, high methanol concentrations can compromise the quality of the hDMFC analytical response for two reasons. One reason is that if the cell is operated with an excess of methanol, it will not detect when a small amount of methanol has not reached the PtRu particles, making it insensitive to CA15-3 binding.

The other reason is the possible denaturation of the antibody in the presence of a large amount of methanol, which in turn impairs the ability of the antibody to bind its target antigen. Therefore, in order to maintain the antibody-antigen reaction and ensure electrical autonomy and operational sensitivity, a medium methanol concentration had to be used. In addition, two methanol concentrations should be considered, one for the activation phase and the other for the operation of the cell. In this work, methanol was not in direct contact with the serum that was incubated in the fuel cell, since the reservoir was thoroughly washed with water between each step, leaving, only the antibody and antigen in direct contact with methanol. However, there are already some studies regarding the denaturation of proteins in methanol mixtures (with water or with other solvents) that show little effect of methanol on proteins conformation on concentrations lower than 25-30% (v/v),~ 6 M [31–34], indicating that our molecules are not denatured in the low methanol concentrations used in this work.

In previous studies 0.05 M of methanol was shown to be the best performing methanol concentration to achieve a functional and sensitive biosensor, which is why in this work this concentration was firstly tested. Since 0.05 M methanol was not enough to power the DMFC with the immunosensor, 0.1 M methanol was therefore tested to obtain the achieved results. It was the minimal methanol concentration to be used for DMFC powering without losing the biosensor response [7].

Initially, the DMFC was activated with a methanol concentration of 0.5 M. This activation is done by leaving the fuel cell with the methanol solution for several hours (3-4h), so that the liquid penetrates through the fibres of the carbon fabric and starts to react with the platinum particles. Then several sampled DC measurements were performed until the stability of the system was reached. Higher concentrations lead to an excessive amount of methanol adsorbed on the electrodes, which is subsequently very difficult to remove.

The performance and difference between an unmodified and a modified cell after the first activation (with 0.5 M) are shown in **Figure 3.5**. **Figure 3.5a** shows a clear difference in the starting potential of the cell with or without the immunosensor electrode. The presence of the sensor material at the anode hindered the access of methanol to the platinum and consequently the initial OCP and power densities were lower than for the unmodified cell (**Figure 3.5b**). After completing fuel cell activation with 0.5 M methanol, the excess was removed by filling the anode reservoir with Milli-Q water overnight. As a result, the fuel cells had near zero OCP at the start of calibration.

At this point, a compromise had to be made between fuel cell performance and a sensitive biosensor for methanol concentration during calibration. The methanol concentration had to be high enough for the fuel cell to provide consistent performance and stable readings, but low enough to ensure antibody activity and selectivity. To find the best compromise, two different methanol concentrations were tested: 0.050 and 0.10 M. At 0.05 M, the fuel cell showed no response and kept its OCP close to zero, as at start-up (**Figure 3.6a**). When 0.10 M methanol was used, the cell began to produce energy until stable readings were obtained (**Figure 3.6b, c**). Since the fuel cell did not generate current signals when 0.05 M was used, a concentration of 0.1 M methanol was used in the calibrations in this work.

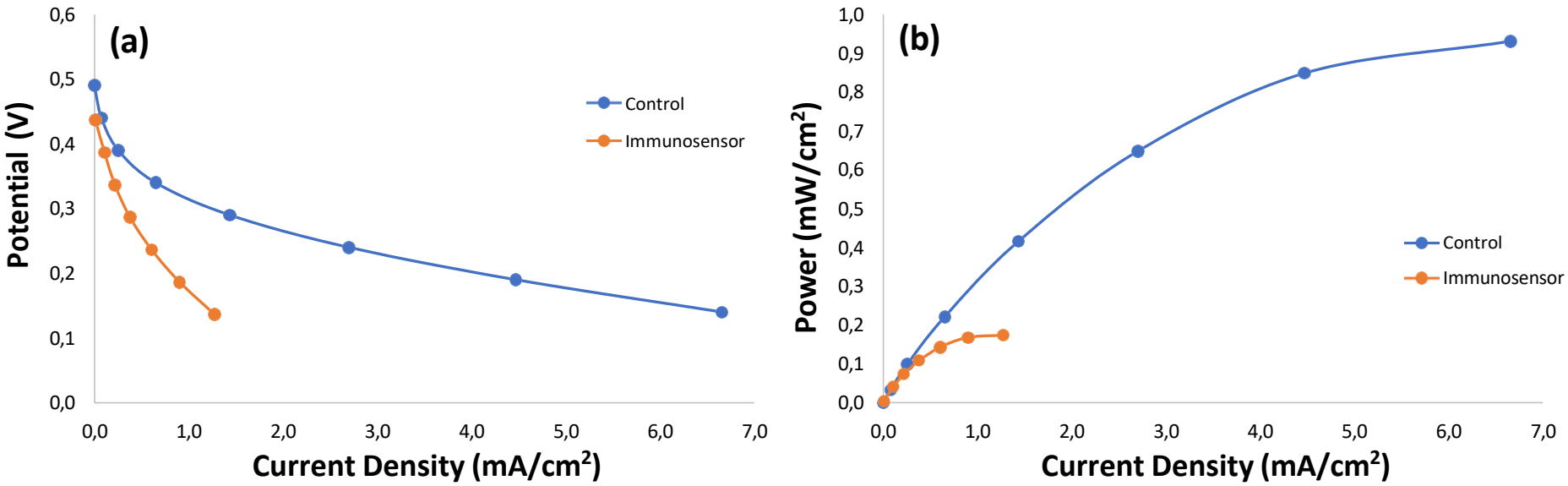

Figure 3.5 - Obtained performance and differences between a non-modified (control) and a modified cell (immunosensor) after initial activation (with 0.5 M). **(a)** clear difference in the starting potential of the cell, which hindered the access of the methanol to the platinum and consequently the initial OCP and **(b)** clear difference in power densities: lower with the immunosensor.

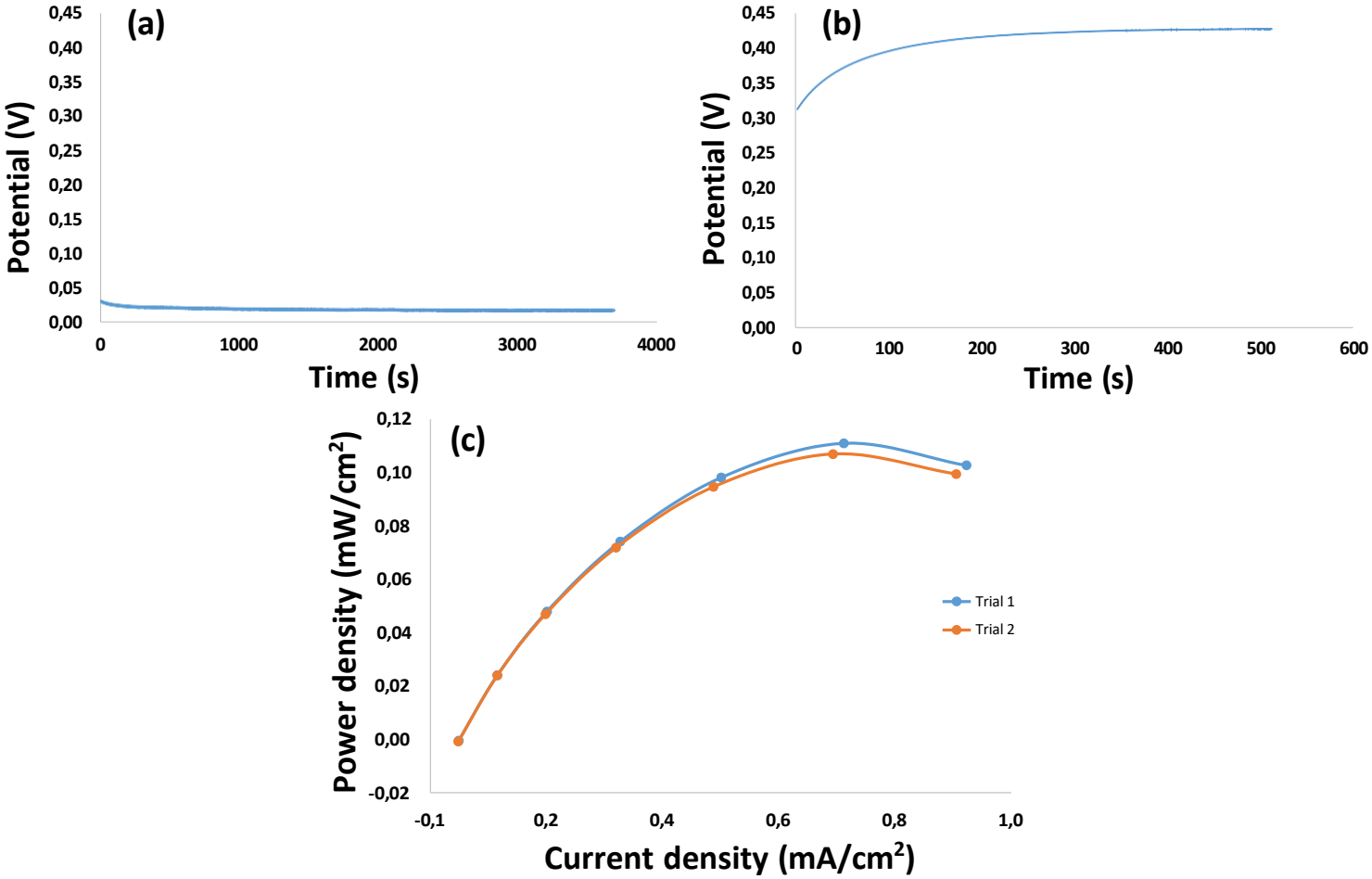

Figure 3.6 - Results obtained with 0.05 and 0.1 M methanol solution: (a) response of the fuel cell with 0.05 M methanol solution, maintaining its OCP near zero as when started; (b) response of the fuel cell with 0.1 M methanol solution; (c) stable readings of the fuel cell output with 0.1 M methanol solution.

3.3.3. Calibrations in buffer

The calibration of the system consisted in incubating consecutively standard solutions of increasing concentration and checking the electrical output of the hDMFC. After each incubation, the system reservoir was washed with ultra-pure water and the measurements of sampled DC were performed using the selected methanol solution. To be sure that the hDMFC was providing stable readings, various incubations in measuring buffer were performed first (three to four times), until a stable response was achieved. Having standard solutions prepared in MES buffer, the first incubations were made with MES. About 3 to 4 incubations were necessary prior to calibration.

Several calibrations of CA15-3 were performed with independent electrodes to determine the typical analytical characteristics of the calibration of hDMFC. The typical data obtained in one calibration run of the sample DC are shown in **Figure 3.7a** and the calibration curve is shown in **Figure 3.7b**, where the normalized values of the power density of hDMFC are plotted against the log concentration of CA15-3 (U/mL) and each standard of each concentration value (in the form of error bars). The lower concentrations of CA15-3 are able to reduce the power signal, but not with sufficient sensitivity to produce a linear trend. The linear trend is observed only from 281.5 and 562.5 U/mL. The average power density changed within this linear range from 0.078 to 0.042 mW/cm^2, with this last value obtained by incubating the highest protein concentration. This corresponded to a deviation of about 54% between the initial and final power output, which was consistent across the different calibrations with buffered standard solutions. This decrease in power with increasing CA15-3 concentration reflects decreasing methanol oxidation at the platinum surface. The increasing number of CA15-3 proteins bound to the antibody increases the steric hindrance of methanol at the metal catalyst. This decreases the power generated by the cell as the electron flow is restricted by the external circuit.

The representative calibration curve obtained by normalizing the power curve values (power sample/power blank) had a slope of -0.6105 and a squared correlation coefficient (R^2) of 0.9773, as shown in **Figure 3.7b**. The system was highly reproducible,

with standard deviations of individual standards ranging from 0.04% to 5.0%. The detection limit achieved was 39.8 U/mL.

3.3.4. Calibrations in Cormay® serum

To verify the functionality of the fuel cell integrated immunosensor in the analysis of human samples, CA15-3 standard solutions were prepared in diluted Cormay® serum. This is a commercially available human serum that can be used to evaluate the effects of a real serum on the operation of the immunosensor. The high quantity of salts and ions present in this matrix made it difficult to test this sample and avoid poisoning of the catalyst and membrane of the fuel cell. Therefore, this serum was 1000x diluted in MES buffer, to minimize the poisoning of the system due to the small molecules that are not of interest for our biosensor. The concentrations of CA15-3 used for this purpose ranged from 46.8 to 750 U/mL. The results obtained are shown in **Figure 3.8**. The response of the sensor in serum was similar to that obtained in buffer. In this case, the initial concentrations of CA15-3 used in the calibrations showed no or very little response and an initial plateau, followed by a decreasing in the power of the fuel cell as the standard concentration was increased, with linear response from 187.5 to 750U/mL. The system was also highly reproducible when calibrated with this sample, resulting in low standard deviations between 1.1% and 3.6%.

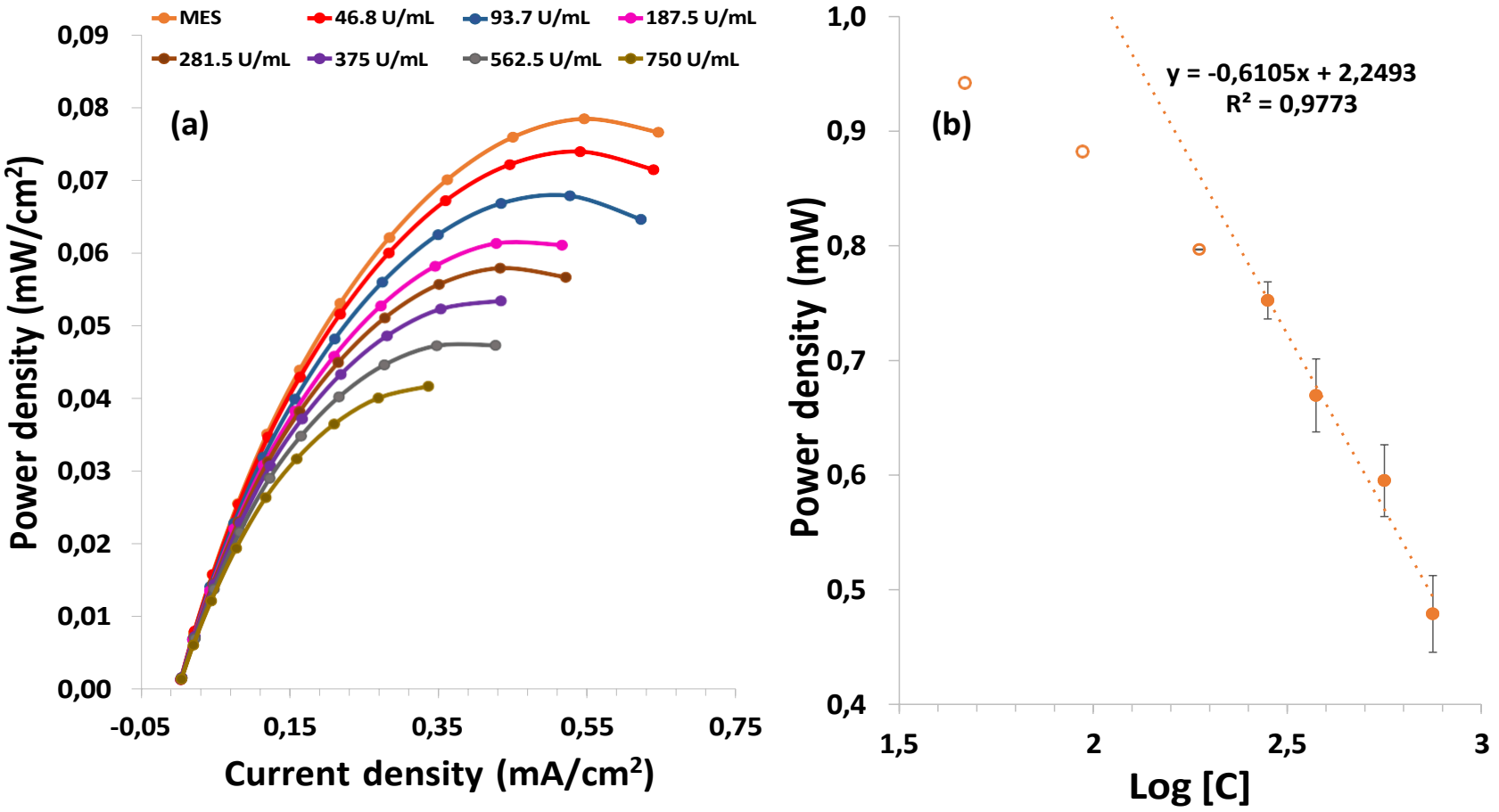

Figure 3.7 - (a) Representation of a typical calibration plot obtained from the polarization curves from the Fuel Cell when using MES buffer as medium; **(b)** Calibration curves with normalized values of the obtained power curves of the modified fuel cells and its respective standard deviation (error bars; *n*=3). Standards from 46.8 U/mL to 750 U/mL of CA15-3 in MES buffer were used.

3.3.5. Analytical recovery

Recovery is defined by IUPAC as the "Proportion of the amount of analyte, present in or added to the analytical portion of the test material, which is extracted and presented for measurement" [35]. In electrochemical sensors this is usually estimated by spiking, meaning that known amounts of analyte are added to the blank or suitable medium. These are then analysed an unspiked portion of the medium. The difference of these two allows to estimate the recovered part of the added analyte. This is called the "surrogate recovery" [36,37].

In this work the analytical recovery was determined by the surrogate recovery, by spiking buffer and Cormay® serum with known amounts of analyte. The obtained calibration curves were then used to calculate the % of recovery that are shown in **Table 3.1**. The immunosensor shows a good performance in detection of CA15-3 with a very good recovery values (ranged from 98.5% to 104.7%) suggesting the possibility of the proposed sensor for real sample analysis.

Table 3.1 - Recovery study in Buffer and Cormay® serum calibrations.

	Buffer		**Cormay® serum**		
Added CA15-3 (U/mL)	Calculated CA15-3 (U/mL)	% Recovery	Added CA15-3 (U/mL)	Calculated CA15-3 (U/mL)	% Recovery
187.5	239.4	104.7	187.5	204.9	101.7
281.5	283.1	100.1	281.5	260.5	98.6
375.0	387.0	100.5	375.0	344.7	98.6
562.5	512.3	98.5	562.5	580.7	100.5
750.0	794.3	100.9	750.0	778.9	100.6

3.3.6. Selectivity studies

To evaluate the selectivity of the immunosensor response, tests were performed in which potentially interfering species that may be present in human serum (at biological concentrations) were added to a known concentration of CA15-3. This selectivity study was made against common species in serum, such as glucose and ascorbic acid, and

other cancer biomarkers, such as CA125 and CEA. For this purpose, different independent fuel cells were assembled and tested with different species: a known CA15-3 concentration and the same known CA15-3 concentration spiked with an interfering substance (one fuel cell for each interfering substance). The concentrations of each interfering cancer biomarker was high, implying illness, concentrations that would be found in a cancer patient: 100 ng/mL CEA, and 150 U/mL CA125. For the interferents that are a part of the human blood, the used concentrations were within the normal range in the blood: 1.3 mg/mL glucose, 0.02 mg/mL ascorbic acid, 0.2 mg/mL urea, and 0.06 mg/mL uric acid.

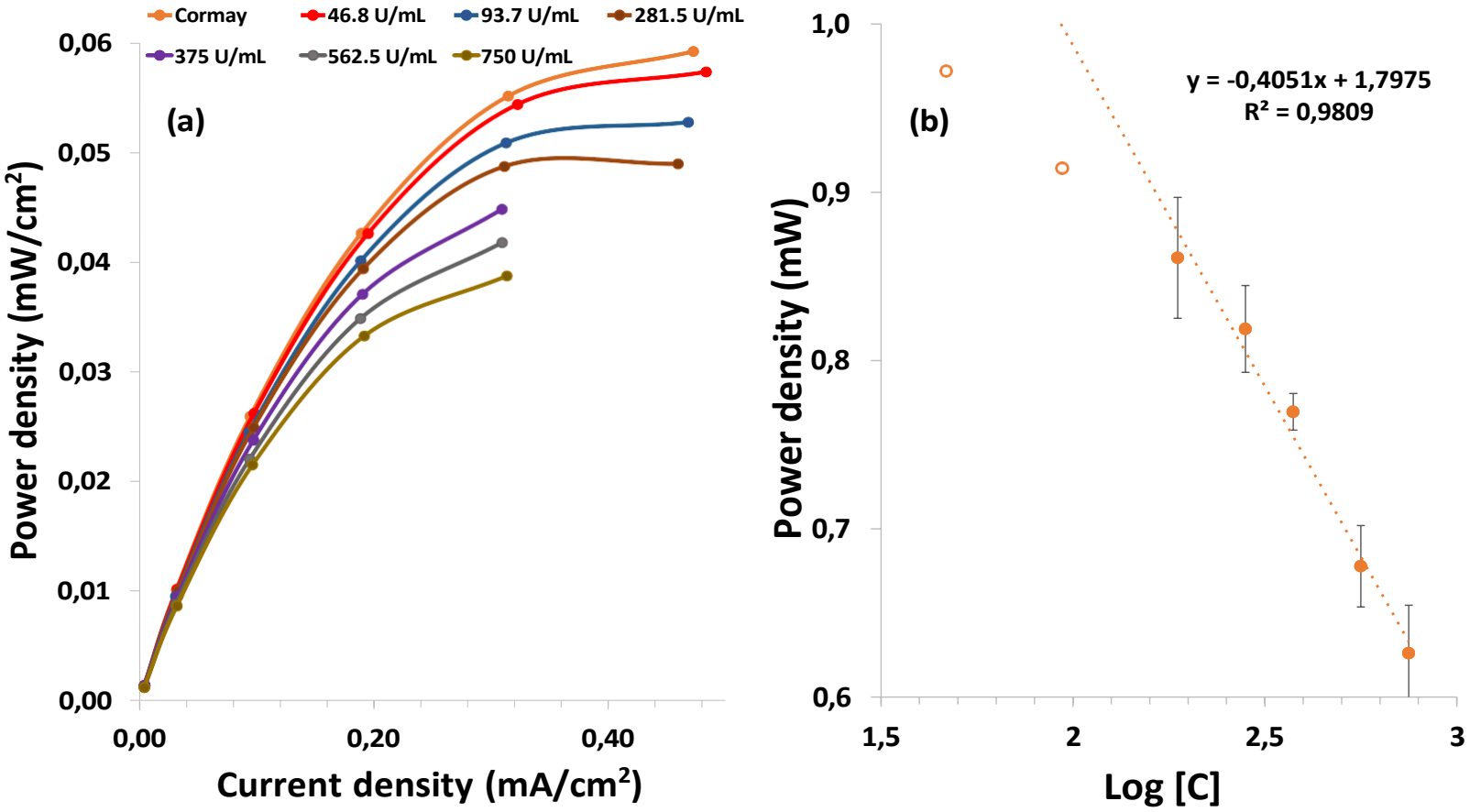

Figure 3.8 - (a) Representation of a typical calibration plot obtained from the polarization curves from the Fuel Cell when using Cormay® serum as medium; **(b)** Calibration curves, obtained with Cormay® serum, with normalized values of the obtained power curves of the modified fuel cells and its respective standard deviation (error bars; n=3). Standards from 46.8 U/mL to 750 U/mL of CA15-3 in serum were used.

As expected, the results reveal the selectivity of the immunosensor for CA15-3, with the interfering substance changing the signal between 0.7 and 5.9. **Figure 3.9** shows the influence of the interfering species on the fuel cell signal, with the smallest influence observed in the analysis with ascorbic acid (0.7% decrease in signal compared to control - fuel cell with only CA15-3 standard). The interfering species that had a greater effect on fuel cell power output was the use of CA125 (5.9% increase in signal) and urea (5.2% increase in signal), which can be explained by the similarity of CA125 to CA15-3 in terms of structure, since they are both members of the mucin family glycoproteins. Urea is an interfering species for this system, since it also is used in electrocatalysis, and can be used as fuel in fuel cells with platinum catalyst. Therefore, it is expectable to have a change in fuel cell power when adding urea to the system [38]. CEA was also tested and had a minor effect on fuel cell power output (2.2% decrease in signal). Overall, these results show that the interfering species had a small effect on fuel cell performance.

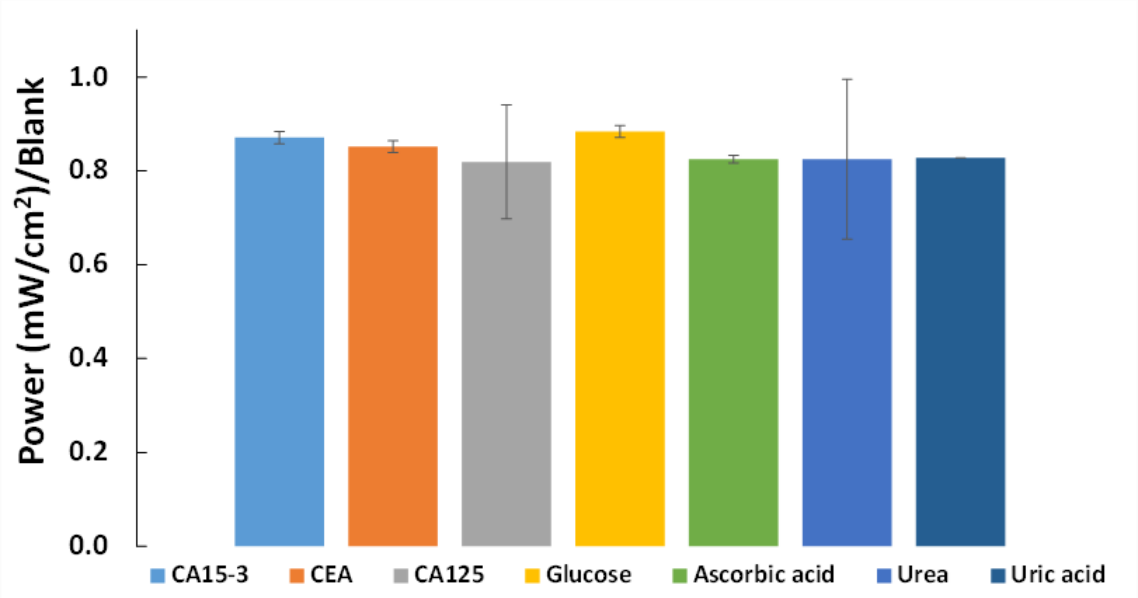

Figure 3.9 - Response of the immunosensor for potential interfering species: other cancer biomarkers (CA125, CEA) and common interfering substances found in the Human serum (ascorbic acid, glucose, urea, uric acid). All values were normalized against the blank (MES buffer), and standard deviation (error bars; *n*=2) were added for each interfering species.

3.3.7. Comparison to previous CA15-3 biosensors

Some biosensors from the literature targeting the detection of CA15-3 were used for comparison with this work. **Table 3.2** lists other immunosensors from recent years and their differences from this work. Although we can see that the analytical performance of the other immunosensors is superior to this work (LoD values and linear response), this work has a broader linear range for CA15-3 concentrations, and this range includes the concentration of interest in the clinical setting (patients with cancer). Another novel feature of this work is the ability to turn the system into an autonomous sensor, which has the great advantage of being able to be used anytime, anywhere, without the need for power or other devices. The potential autonomy and response to the biomarker CA15-3 in the clinical setting are beneficial for PoC analysis.

Table 3.2 - Previous works reporting biosensors for CA15-3 detection in the literature.

Type	Detection	Support	Bioreceptor element	Autonomy	Linear response	LOD	Reference
MIP	Electrochemical	Au SPE	MIP	No	0.25 to 10.00 U/mL	0.05 U/mL	[29]
MIP	Electrochemical	Au SPE	MIP	No	5 and 50 U/mL	1.5 U/mL	[30]
MIP/Immunosensor	Fluorescence	Magnetic graphene oxide	MMIP Anti-CA15-3	No	0.0005–40 U/mL	50 µU/mL	[31]
Immunosensor	Electrochemical	RGO and CuS placed on a SPGE	Anti CA15-3	No	1.0 to 150 U/mL	0.3 U/mL	[32]
Immunosensor	Electrochemiluminescence (ECL)	PAMAM-QDs	Anti CA15-3	No	0.1 to 100 U/mL	10 µU/mL	[33]
Immunosensor	Electrochemical	CysA/GQDs	Anti CA15-3	No	0.16–125 U/mL	0.11 U/mL	[34]
Immunosensor	Electrochemical	CoS2-GR and AuNPs composites	Anti CA15-3	No	0.1 to 150 U/mL	0.03 U/mL	[35]
Immunosensor	Electrochemical	Dual SPCE	Anti CA15-3	No	0 to 70 U/mL	5.0 U/mL	[36]
Immunosensor	Electrochemical	Gold electrode	Anti CA15-3	No	15 to 50 µU/mL	15 µU/mL	[37]
Immunosensor	Electrochemical	Graphite ink	Anti CA15-3	No	15 to 250 U/mL	15 U/mL	[38]
Immunosensor	Electrochemical	Cu-MOF	Anti CA15-3	No	10 µU/mL to 10 mU/mL 10 mU/mL to 100 U/mL	5.06 µU/mL	[39]
Immunosensor	Electrochemical	CBPtRu	Anti-CA15-3	Yes	187.5 to 562.5 U/mL	39.8 U/mL	**Chapter 3 work**

Au SPE: Gold Screen Printed Electrode**; MMIP:** Magnetic molecularly imprinted polymer; **RGO:** Reduced Graphene Oxide; **CuS:** Copper Sulfide; **SPGE:** Screen Printed Graphene Electrode; **PAMAM-QDs:** Polyamidoamine dendrimer-quantum dots; **CysA/GQDs:** thiolated graphene quantum dots; **SPCE:** Screen Printed Carbon Electrode; **Cu-MOF:** Copper-based metal-organic framework nanoparticles; **CBPtRu:** Carbon Black with Platinum and Ruthenium nanoparticles.

3.4. Conclusions

In conclusion, the hDMFC exhibits a concentration-dependent response to the presence of the target molecule, such that the fuel cell can be used as an autonomous sensing device in conjunction with an electrochromic device that changes colour in the presence of the target analyte. This was demonstrated by using different background media and assessing the selectivity of this sensor with molecules in blood plasma and other relevant cancer biomarkers. The results obtained demonstrate a well-functioning immunosensor that responds to higher CA15-3 concentrations relevant to early cancer detection, and the selectivity performed showed negligible interference by other molecules present in blood plasma.

This work demonstrates a biosensor that can be used as a potentially autonomous device and still be able to detect relevant concentrations of cancer biomarkers and a response of interest for PoC analysis with high selectivity and reproducibility. This setup can be further improved for a point-of-care device by adding an electrochromic cell to indicate the presence and/or amount of the biomarker in the sample.

3.5. References

[1] P. Mehrotra, Biosensors and their applications - A review, J. Oral Biol. Craniofacial Res. 6 (2016) 153–159. https://doi.org/10.1016/j.jobcr.2015.12.002.

[2] G. Pasternak, J. Greenman, I. Ieropoulos, Self-powered, autonomous Biological Oxygen Demand biosensor for online water quality monitoring, Sensors Actuators, B Chem. 244 (2017) 815–822. https://doi.org/10.1016/j.snb.2017.01.019.

[3] C. Gonzalez-Solino, M. Di Lorenzo, Enzymatic fuel cells: Towards self-powered implantable and wearable diagnostics, Biosensors. 8 (2018). https://doi.org/10.3390/bios8010011.

[4] L.A.A.N.A. Truta, F.T.C. Moreira, M.G.F. Sales, A dye-sensitized solar cell acting as the electrical reading box of an immunosensor: Application to CEA determination, Biosens. Bioelectron. 107 (2018) 94–102. https://doi.org/10.1016/j.bios.2018.02.011.

[5] M.G.F. Sales, L. Brandão, Autonomous electrochemical biosensors: A new vision to direct methanol fuel cells, Biosens. Bioelectron. 98 (2017) 428–436. https://doi.org/10.1016/j.bios.2017.07.021.

[6] H. Liu, C. Song, L. Zhang, J. Zhang, H. Wang, D.P. Wilkinson, A review of anode catalysis in the direct methanol fuel cell, J. Power Sources. 155 (2006) 95–110. https://doi.org/10.1016/j.jpowsour.2006.01.030.

[7] L.P.T. Carneiro, A.M.F.R. Pinto, A. Mendes, M. Goreti, An all-in-one approach for self-powered sensing: A methanol fuel cell modified with a molecularly imprinted polymer for cancer biomarker detection, J. Electroanal. Chem. 906 (2022) 116009. https://doi.org/10.1016/j.jelechem.2022.116009.

[8] L.P.T. Carneiro, N.S. Ferreira, A.P.M. Tavares, A.M.F.R. Pinto, A. Mendes, M.G.F. Sales, A passive direct methanol fuel cell as transducer of an electrochemical sensor, applied to the detection of carcinoembryonic antigen, Biosens. Bioelectron. 175 (2021) 1–9. https://doi.org/10.1016/j.bios.2020.112877.

[9] M.G.F. Sales, L. Brandão, Autonomous electrochemical biosensors: A new vision to direct methanol fuel cells, Biosens. Bioelectron. 98 (2017) 428–436. https://doi.org/10.1016/j.bios.2017.07.021.

[10] N.S. Ferreira, L.P.T. Carneiro, C. Viezzer, M.J.T. Almeida, A.C. Marques, A.M.F.R. Pinto, E. Fortunato, M.G.F. Sales, Passive direct methanol fuel cells acting as fully autonomous electrochemical biosensors: Application to sarcosine detection, J. Electroanal. Chem. 922 (2022). https://doi.org/10.1016/j.jelechem.2022.116710.

[11] F.G. Ebeling, P. Stieber, M. Untch, D. Nagel, G.E. Konecny, U.M. Schmitt, A. Fateh-Moghadam, D. Seidel, Serum CEA and CA 15-3 as prognostic factors in primary

breast cancer, Br. J. Cancer. 86 (2002) 1217–1222. https://doi.org/10.1038/sj.bjc.6600248.

[12] Globocan, Source: Globocan 2020, 419 (2020) 119–120.

[13] I.E. Tothill, Biosensors for cancer markers diagnosis, Semin. Cell Dev. Biol. 20 (2009) 55–62. https://doi.org/10.1016/j.semcdb.2009.01.015.

[14] S.A. Soper, K. Brown, A. Ellington, B. Frazier, G. Garcia-Manero, V. Gau, S.I. Gutman, D.F. Hayes, B. Korte, J.L. Landers, D. Larson, F. Ligler, A. Majumdar, M. Mascini, D. Nolte, Z. Rosenzweig, J. Wang, D. Wilson, Point-of-care biosensor systems for cancer diagnostics/prognostics, Biosens. Bioelectron. 21 (2006) 1932–1942. https://doi.org/10.1016/j.bios.2006.01.006.

[15] M. Perfézou, A. Turner, A. Merkoçi, Cancer detection using nanoparticle-based sensors, Chem. Soc. Rev. 41 (2012) 2606. https://doi.org/10.1039/c1cs15134g.

[16] A.P.M. Tavares, N.S. Ferreira, L.A.A.N.A. Truta, M.G.F. Sales, Conductive Paper with Antibody-Like Film for Electrical Readings of Biomolecules, Sci. Rep. 6 (2016) 26132. https://doi.org/10.1038/srep26132.

[17] C. Chen, J. Wang, Optical biosensors: An exhaustive and comprehensive review, Analyst. 145 (2020) 1605–1628. https://doi.org/10.1039/c9an01998g.

[18] S. Bayoumy, H. Hyytiä, J. Leivo, S.M. Talha, K. Huhtinen, M. Poutanen, J. Hynninen, A. Perheentupa, U. Lamminmäki, K. Gidwani, K. Pettersson, Glycovariant-based lateral flow immunoassay to detect ovarian cancer–associated serum CA125, Commun. Biol. 3 (2020) 1–7. https://doi.org/10.1038/s42003-020-01191-x.

[19] T. Mahmoudi, M. de la Guardia, B. Baradaran, Lateral flow assays towards point-of-care cancer detection: A review of current progress and future trends, TrAC - Trends Anal. Chem. 125 (2020) 115842. https://doi.org/10.1016/j.trac.2020.115842.

[20] F. Di Nardo, M. Chiarello, S. Cavalera, C. Baggiani, L. Anfossi, Ten years of lateral flow immunoassay technique applications: Trends, challenges and future perspectives, Sensors. 21 (2021). https://doi.org/10.3390/s21155185.

[21] V. Naresh, N. Lee, A review on biosensors and recent development of nanostructured materials-enabled biosensors, Sensors (Switzerland). 21 (2021) 1–35. https://doi.org/10.3390/s21041109.

[22] N.S. Ferreira, M.G.F. Sales, Disposable immunosensor using a simple method for oriented antibody immobilization for label-free real-time detection of an oxidative stress biomarker implicated in cancer diseases, Biosens. Bioelectron. 53 (2014) 193–199. https://doi.org/10.1016/j.bios.2013.09.056.

[23] O.C. Wells, L.M. Gignac, C.E. Murray, A. Frye, J. Bruley, Use of backscattered electron detector arrays for forming backscattered electron images in the

scanning electron microscope, Scanning. 28 (2006) 27–31. https://doi.org/10.1002/sca.4950280105.

[24] N. Brodusch, H. Demers, R. Gauvin, Imaging with a commercial electron backscatter diffraction (EBSD) camera in a scanning electron microscope: A review, J. Imaging. 4 (2018). https://doi.org/10.3390/jimaging4070088.

[25] M.S. Nashner, A.I. Frenkel, D.L. Adler, J.R. Shapley, R.G. Nuzzo, Structural characterization of carbon-supported platinum-ruthenium nanoparticles from the molecular cluster precursor PtRu5C(CO)16, J. Am. Chem. Soc. 119 (1997) 7760–7771. https://doi.org/10.1021/ja971039f.

[26] X. Zhang, K.Y. Chan, Water-in-oil microemulsion synthesis of platinum-ruthenium nanoparticles, their characterization and electrocatalytic properties, Chem. Mater. 15 (2003) 451–459. https://doi.org/10.1021/cm0203868.

[27] M.S. Dresselhaus, A. Jorio, A.G. Souza Filho, A.R. Saito, Defect characterization in graphene and carbon nanotubes using Raman spectroscopy, Phil. Trans. R. Soc. A. 368 (2010) 5355–5377. https://doi.org/10.1098/rsta.2010.0213.

[28] T. Jawhari, A. Roid, J. Casado, Raman spectroscopic characterization of some commercially available carbon black materials, Carbon N. Y. 33 (1995) 1561–1565. https://doi.org/10.1016/0008-6223(95)00117-V.

[29] C. Cerezo-Navarrete, Y. Mathieu, M. Puche, C. Morales, P. Concepción, L.M. Martínez-Prieto, A. Corma, Controlling the selectivity of bimetallic platinum-ruthenium nanoparticles supported on N-doped graphene by adjusting their metal composition, Catal. Sci. Technol. 11 (2021) 494–505. https://doi.org/10.1039/d0cy02379e.

[30] B.A. Berns, M.F. Torres, V.B. Oliveira, Performance of passive Direct Methanol Fuel Cell : modelling and experimental studies, U.Porto J. Eng. 1 (2015) 89–103. https://journalengineering.fe.up.pt/article/view/110/111.

[31] A. Fernández, O. Sinanoğlu, Denaturation of proteins in methanol/water mixtures, Biophys. Chem. 21 (1985) 163–166. https://doi.org/10.1016/0301-4622(85)80002-8.

[32] Q. Shao, Methanol concentration dependent protein denaturing ability of guanidinium/methanol mixed solution, J. Phys. Chem. B. 118 (2014) 6175–6185. https://doi.org/10.1021/jp500280v.

[33] K.R. Babu, D.J. Douglas, Methanol-induced conformations of myoglobin at pH 4.0, Biochemistry. 39 (2000) 14702–14710. https://doi.org/10.1021/bi001265t.

[34] K. Yamazaki, T. Iwura, R. Ishikawa, Y. Ozaki, Methanol-induced tertiary and secondary structure changes of granulocyte-colony stimulating factor, J. Biochem. 140 (2006) 49–56. https://doi.org/10.1093/jb/mvj133.

[35] A. International, P. Willetts, M. Thompson, S.L.R. Ellison, R. Wood, HARMONISED GUIDELINES FOR THE USE OF RECOVERY INFORMATION IN ANALYTICAL information in analytical measurement (Technical Report), 71 (1999) 337–348.

[36] D. Elio, B. Brunetti, Data Treatment of Electrochemical Sensors and Biosensors Chapter 18 Data Treatment of Electrochemical Sensors and Biosensors, (2015). https://doi.org/10.1007/978-1-4939-1301-5.

[37] E. Desimoni, B. Brunetti, Presenting Analytical Performances of Electrochemical Sensors . Some Suggestions, (2013) 1645–1651. https://doi.org/10.1002/elan.201300150.

[38] W. Xu, Z. Wu, S. Tao, Urea-Based Fuel Cells and Electrocatalysts for Urea Oxidation, Energy Technol. 4 (2016) 1329–1337. https://doi.org/10.1002/ente.201600185.

4. PASSIVE DIRECT METHANOL FUEL CELLS ACTING AS FULLY AUTONOMOUS ELECTROCHEMICAL BIOSENSORS: APPLICATION TO SARCOSINE DETECTION

4.1. Introduction

Electrochemical biosensors provide analytical data by combining a biorecognition unit with an electrochemical transduction element [1,2]. They are among the most popular biosensors because they are low cost, offer fast response,are potentially portable, and can be miniaturised - all attractive features for point-of-care (PoC) applications [3,4]. Despite all these advantages, the direct application of biosensors remains challenging for many reasons. One of them is their lack of autonomy [5,6].

This lack of self-sufficiency has been addressed in the past by the development of several approaches to self-powered biosensors described in the literature, including biosensors powered by dye-sensitised solar cells [7–10], and microbial/enzymatic fuel cells [11–14]. Despite the advantages of these transduction methods, there are still limitations in their application. Dye-sensitized solar cells cannot be operated at night and their performance is still low. Microbial and enzymatic fuel cells are very delicate systems that require more care in handling, and the performance to date is so low that this hinders their application, even for a small device.

Another approach for self-powered biosensors is the use of direct methanol fuel cells (DMFCs). DMFCs are electrochemical devices that generate electricity from methanol fuel and oxygen with high efficiency and vestigial emissions [15–17], which can be used for portable applications [15,18,19]. The first approach consisted of a heavy/large cell operated with flowing methanol solutions [20]. This operation under flow conditions provides good electrochemical performance of the fuel cell but hinders its application in PoC. Therefore, this design was recently developed into a cell that operates under steady-state conditions. It was designed in a previous report [21] and optimized to operate in passive mode, requiring only a few mL of a methanol solution. Although it had a lower electrochemical output, it provided enough energy to evaluate the effect of

a target analyte, a cancer biomarker [22]. In this configuration, the biosensor was placed as an external element of the cell to reduce its impact on fuel cell performance.

Therefore, the work developed here is an innovative approach to the latest configuration in which the biosensor layer is integrated into the stationary DMFC [23]. This biosensor was directly attached to the surface of the anode catalyst that is commonly used in this type of Fuel Cell [24] and contains a molecularly imprinted polymer (MIP) as a sensing element for a target compound. This polymer was tailored by radical polymerization with suitable vinyl monomers (acrylamide, bis-acrylamidevinyl phosphonichonic acid) and radical initiators [25,26]. Upon removal of sarcosine, a potential cancer biomarker, from the polymeric network, binding sites are formed. As expected, these sites have a complementary shape to the imprinted molecule and allow complementary electrostatic interactions [27]. Since this MIP layer was located on the carbon-based anode electrode, which contained carbon fabric and Pt/Ru as metal catalysts, the sarcosine bond prevented the methanol from accessing the catalysts and thus hindered the fuel cell performance. This makes the operation of the DMFC concentration-dependent, leading to a new integrated DMFC biosensor device.

The autonomy of this platform also requires the elimination of all electronic components, since they require additional energy, and the electrochemical readings are usually collected by potentiostats. This limitation of autonomy has been solved in the past by coupling an electrochromic cell to the external circuit of the platform [8,9]. This cell has a colour that depends on the energy that passes through it. Since the energy arriving from the hybrid DMFC/biosensor depends on the concentration of sarcosine, the observed colour is concentration dependent. The electrochromic cell (EC) used in these works was organic and was made from PEDOT. However, we aimed at a more stable system for which we used an EC of inorganic nature prepared from tungstate, as tungsten oxide nanoparticles, as previously reported [28]. Since the inorganic ECs require more energy to show a colour change, the DMFC/biosensor cells were arranged in a 4-stack configuration.

As a proof-of-concept, this stand-alone biosensor was used to detect sarcosine, which has been reported in the literature as a potential biomarker for early detection of prostate cancer [29–31]. Sarcosine can be measured in urine and serum and can be used to study the progression of prostate cancer, as it is absent or present in negligible

concentrations in healthy individuals [29]. Several approaches for screening sarcosine have been described in the literature (Table), including enzymatic assays [32–35], and molecular imprinted polymers (MIPs) [36–38]. None of these approaches offers the possibility of complete autonomy when used at the PoC.

Thus, this is the first work reporting on a DMFC/biosensor hybrid in a 4-stack configuration and in conjunction with an EC for visual transmission. This approach has been optimized under various conditions, with particular attention to the composition of the MIP layer, which is a novel material that has not been described before. The setup was characterized for analytical performance against sarcosine using two different media (buffer and synthetic serum). Operation of the system was tested with a single passive DMFC connected to a potentiostat and a 4-stack DMFC using the EC.

Table 4.1 - Literature review of Sarcosine biosensors with electrochemical detection.

Type	Detection	Support	Bioreceptor element	Autonomy	Linear response	LOD	Reference
Enzymatic	Electrochemical	Gold electrode	Sarcosine oxidase	No	0.1 – 100 µM	0.01 µM	[51]
Enzymatic	Electrochemical	Gold electrode	Sarcosine oxidase	No	0.1 – 100 µM	0.10 pM	[50]
Enzymatic	Electrochemical	Pt/MNP	Sarcosine oxidase	No	5 - 40 µM	0.24 µM	[60]
Enzymatic	Electrochemical	OECTs	Sarcosine oxidase	No	50 nM - 100 µM	50.0 nM	[61]
Enzymatic	Photoelectrochemical	ITO/NiO/PbS/Au electrode	Sarcosine oxidase	Yes	50 nM – 0.05 M	17.0 nM	[62]
Enzymatic	Electrochemical	CSPE	Sarcosine oxidase	No	10 – 400 µM	0.66 µM	[53]
MIP	Electrochemical	AuSPE	Electropolymerization of p-ATP	No	0.12 – 1.2 µM	8.50 nM	[54]
MIP	Electrochemical	Au electrode	MOFs	No	1 - 100 pM	0.40 pM	[55]
MIP	Electrochemical	Hydro-MeC-M	Electropolymerization of MAA	No	0.56– 22.5 µM	0.11 µM	[56]
MIP	Electrochemical	CB/PtRu	Acr/Bis-Acr/VPA	Yes	3.2 - 2000 µM	0.04 µM	**Chapter 4 work**

Pt/MNP: platinum loaded mesoporous nickel phosphonate; **OECTs:** Organic electrochemical transistors; **CSPE:** Carbon Screen Printed Electrode; **AuSPE**: Gold Screen-Printed Electrode; **p-ATP:** poly-aminothiophenol; **MAA:** Methacrylamide; **MOFs:** metal–organic frameworks; **Hydro-MeC-M:** metal-coded hydrogel magnetic; **CB/PtRu:** Carbon Black/Platinum Ruthenium; **Acr/Bis-Acr/VPA:** Acrylamide/Bis-Acrylamide/Vinylphosphonic Acid.

4.2. Experimental section

4.2.1. Reagents and solutions

All chemicals were of analytical grade and the water was ultra-pure Milli-Q laboratory water. Measurements were performed in a buffer consisting of 2-morpholinoethanesulfonic acid (MES, AppliChem), 10 mM, pH 6.0. Sarcosine (Acros Organics) was used as the target compound, and standard solutions were prepared in MES buffer. For polymerization, 0.1 mM acrylamide (Acr - 99%, Sigma Aldrich) and 0.5 mM bis-acrylamide (Bis-Acr - 99%, Sigma Aldrich) in MES buffer were used, including 0.1 mM vinyl phosphonic acid (VPA - 97%, Sigma-Aldrich) as a negatively charged monomer. Ammonium persulfate (APS, VWR Chemicals) and tetramethylethylenediamine (TEMED - from TCI) were used as initiators at a concentration of 1% of the total concentration of monomers. For selectivity studies, fetal bovine serum (FBS) from Gibco was used at a 1000-fold dilution.

Carbon Black (CB) with PtRu (CB /PtRu, 40:20 wt%) catalyst (from Vulcan XC -72R, Quintech) was used as polymerization support. Liquid Nafion® (20 wt% in alcohols, Quintech) and 2-propanol (99.8%, Panreac) were used for ink preparation. Solutions of 2.0 and 0.5 M methanol (Merck, HPLC grade) were used in the activation and calibration phases, respectively. Untreated plain carbon cloth (FuelCellsEtc) was used to apply the modified biosensor material (the anode of DMFC) and Pt carbon cloth (10 wt% Pt on Vulcan XC -72R, 1 mgPt/cm2, Nafion coated, Quintech) was used as the cathode.

The EC material was prepared as WO_3 nanoparticles obtained with 0.15 M sodium tungstate dihydrate (99%, ACROS Organics) and 3.0 M hydrochloric acid (37%, Fluka). The resulting nanoparticles were dispersed in a 1:1 mixture of distilled water/ethylene glycol butyl ether. The electrolyte for the EC was a solution containing 1.0 M lithium perchlorate and propylene carbonate (PC).

4.2.2. Fuel Cell units

The passive DMFC devices were developed following [18] and are shown in **Figure 4.1**. The single cell configuration includes the anode side (**Figure 4.1a**) with a container to feed the methanol solution and the cathode side (**Figure 4.1b**) with an "open" grid region to allow reaction with atmospheric oxygen. These electrodes were part of a MEA containing the MIP-modified anode and a commercial cathode (Pt carbon mesh), separated by a solid Nafion® 115 membrane. The active area of this MEA was 2.25 cm^2. The DMFC also contained two metal plates that acted as current collectors and a rubber plate to insulate the system and prevent an electrical short. The 4-stack fuel cell configuration was achieved by connecting four DMFCs in series (**Figure 4.1c**).

Both passive systems use natural capillary forces, diffusion, and convection for their operation, without the additional power consumption and without additional components such as pumps to feed the reactants. These features and advantages of this type of systems make them suitable for portable applications, as they can be manufactured in a small and compact structure.

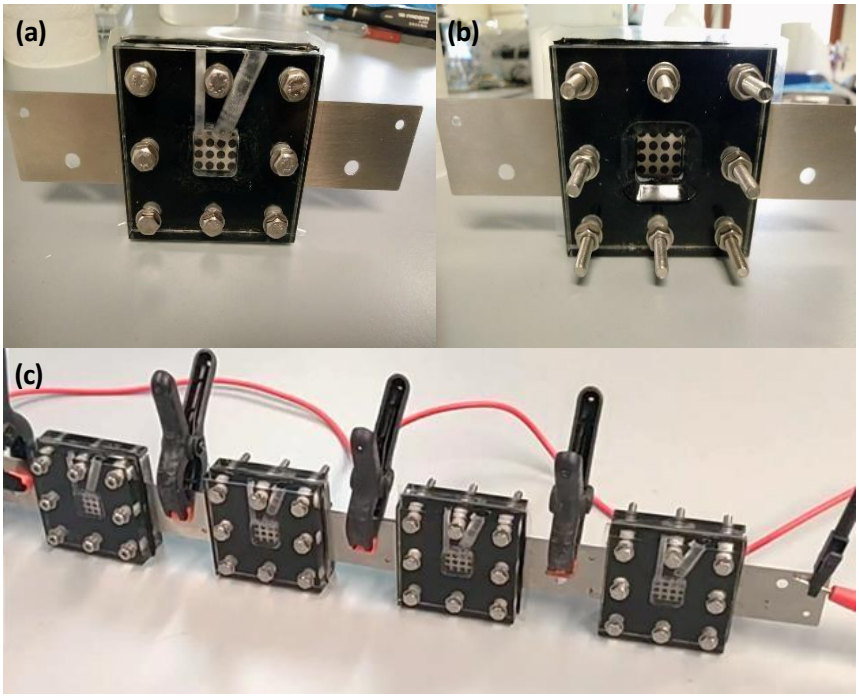

Figure 4.1 - Pictures of the passive DMFC device: **(a)** anode side of the fuel cell, containing a reservoir for introducing the methanol solution into the system; **(b)** cathode side of the fuel cell, with a grid opened to the atmosphere to allow the O_2 present in the atmospheric air to reach the electrode; **(c)** cell stack with the devices placed in series.

The CB containing PtRu (40:20 wt%) catalyst (1 mg/mL) was suspended in MES buffer (pH ~ 6.0) by sonicating the mixture for 15 minutes. The target molecule (0.1 mM), sarcosine, and the negatively charged monomer (vinyl phosphonic acid) were previously incubated together for 1 hour at 30 ºC, then added to the previous mixture of CB and MES and incubated for 1 hour at 30 ºC with agitation. The polymerization mixture was then added to the flask. To initiate polymerization, both APS and TEMED were added to this suspension and stirred at 30 ºC for 1 hour. After the polymerization time, the mixture was centrifuged (so that the sensor material settled) and the supernatant was removed. The solid was washed by stirring in 0.5 M H_2SO_4 for 30 min to remove the template protein. To remove and neutralize residual monomers/proteins, the sensor material was washed with Milli-Q water (4×) and ethanol (1×) and dried overnight at 60 ºC.

A control non-imprinted polymer (NIP) was also synthesized under the same conditions as the biosensor material, but without the template protein.

Special care was taken in the addition of the polymer layer around the catalytic particles because of its effect on the electrochemical activity of methanol. The polymer obtained should be permeable enough to allow some of the methanol to reach the catalytic particles, thus maintaining the operation of the fuel cell and the function of the biosensor.

4.2.3. Ink and electrode preparation

The MIP-CB -Pt/Ru nanoparticles were cast onto a carbon cloth support by incorporating them into a suitable ink formulation, spraying and drying. The ink suspension consisted of the biosensor material, 20 wt% Nafion® in alcohols (relative to the biosensor material), and 2-propanol. To apply the material with an airbrush, the solid should only make up to 10% of the suspension to avoid clogging. The obtained suspension was sonicated for 30 minutes and applied to the support.

The application of the ink to the gas diffusion layer (GDL) of the fuel cell - the carbon cloth - was done by heating the carbon cloth to 60ºC (on a hot plate), applying the

material to it with an airbrush, and letting it dry. The mass of the catalyst on the carbon cloth was controlled by weighing the support before and after deposition.

4.2.4. Electrochemical cell (EC)

The electrochromic device was produced according to Marques, et al. [7] with minor modifications. Briefly, the device was designed in image processing software (Adobe Illustrator, Adobe Systems Software, San Jose, CA, USA) with a planar 2-electrode configuration defined as working and counter electrodes (WE and CE, respectively). To pattern these electrodes and the electrical tracks, a CO_2 laser device with a wavelength of 10.6 µm (VLS3.50, Universal Laser Systems, Scottsdale, AZ, USA) was used to selectively remove the ITO layer from a PET/ITO foil with a sheet resistance of 30 Ω/square (Kintech Company, Shenzhen, China) with 10 W laser power at a scan rate of 1.27 m/s. Silver ink (Conductive compounds, Inc., New Hampshire, USA) was applied to the electrical tracks, followed by a curing process at 120 ºC for 20 min, for ink's solvent evaporation. Then, 3 µL of 0.04 g/L WO_3 nanoparticles dispersed in water: ethylene glycol butyl ether were drop casted onto the WE and allowed to dry at 50 ºC for 20 min. The WO_3 nanoparticles were prepared using an oven-assisted hydrothermal method according to Santos, et al [19] and Marques, et al. [7]. Finally, the EC device was encapsulated using a home-version laminator with a hydrophilic Whatman paper grade 4 (GE Healthcare, Chicago, IL, USA) placed on top of the WE/CE electrodes to obtain a simple configuration for easy integration into the DMFC/biosensor. A lithium-based electrolyte ($LiClO_4$: PC 1 M) was used in the EC.

The EC was integrated into an external circuit connected to the 4-stack DMFCs. At the time of use, the electrolyte was dropped onto the paper pad to first perform a control test (blank). In this case, the unit EC renders a blue colour at ≥ 1.5 V when fuel is added to the fuel cells. To test this unit, MeOH was removed from the container and replaced with the buffer solution, which was incubated there for 30 minutes. This solution was then removed and replaced again with methanol to check the electrical properties of the system. Then the MeOH solution was removed, and the container was filled with the less concentrated sarcosine standard solution; this solution was incubated

for 30 minutes, then removed and replaced with MeOH to recheck the electrical properties and operation of EC. Then a bleaching process of the device was performed, followed by the test with the sarcosine sample. With increasing sarcosine incubation concentration, the fuel cell was unable to generate 1.5 V and the EC device could not achieve a colored state.

4.2.5. Apparatus and Fuel Cell assembly

Electrochemical measurements were performed using a Metrohm Autolab Potentiostat/Galvanostat and a PGSTAT302N equipped with an FRA module and controlled by Nova software (NOVA 2.1). The cells were monitored at room temperature and atmospheric pressure. The anode was fed with 2.0 or 0.5 M MeOH solution (depending on whether it was used during activation or calibration) deposited on the reservoir, and the cathode used the O_2 of air.

The DMFC/biosensor assemblies are shown in **Figure 4.2**. The biosensor element was first developed by free radical polymerization (**Figure 4.2a**) and then placed on the anode side of the 4-stack DMFCs (**Figure 4.2b-c**). These 4-stack/ DMFCs integrate the electrochemical cell (EC), which is electrically connected to simulate a single device without connecting a potentiostat. The generated energy powers the EC and promotes color change according to the concentration of the biomarker present.

Generally, the polymer layer at the anode slows MeOH penetration, which limits access to the Pt/Ru nanoparticles that are trapped in the polymeric network and influences the rate of the electrochemical process. This outcome is also seen when a protein blocks the MeOH molecule's path to the Pt catalyst by entering the imprinted cavity, which is schematically represented in **Figure 4.3**.

4.2.6. Electrochemical assay

For DMFC measurements, the cell was used at room temperature and atmospheric pressure. To evaluate the response of the DMFC with the modified imprinted anode,

electrochemical measurements were performed using Sampled DC. This technique can be used to generate polarization curves, which are typically used for characterization when studying DMFCs. This involves entering a series of potentials and recording the corresponding current values. All measurements obtained were normalized to the catalyst mass (Pt/Ru) on the surface of the carbon cloth. The polarization curves of the DMFC and the DMFC/biosensor were normalized to obtain the maximum output of the system.

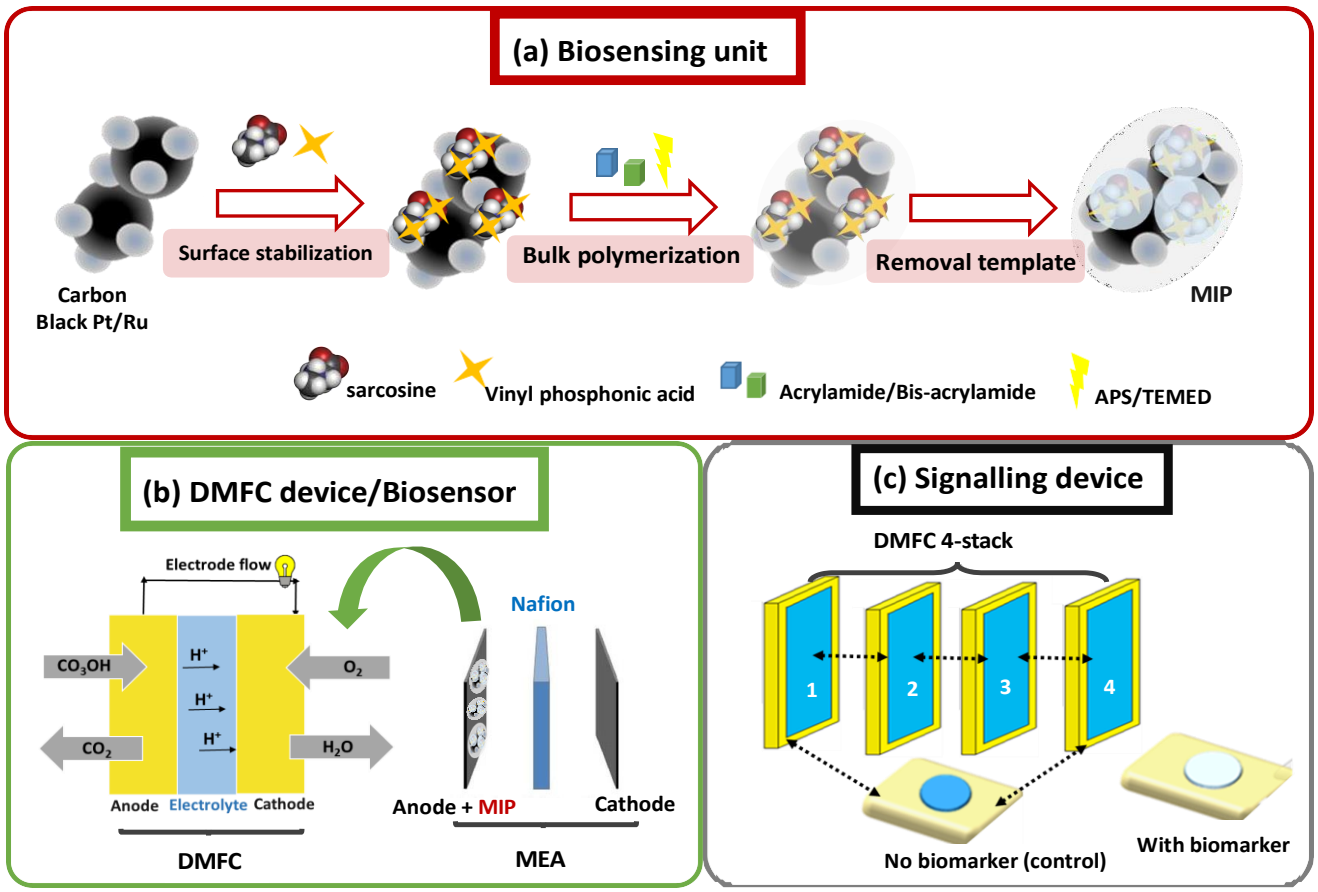

Figure 4.2 - Schematic representation of the various components of the final biosensor device, including **(a)** the synthesis of the MIP material around the CB-Pt/Ru; **(b)** the methanol fuel cell

device and the membrane electrode unit (MEA); **(c)** and the 4-stack DMFC cells with biosensor, coupled with the signaling electrochromic cell.

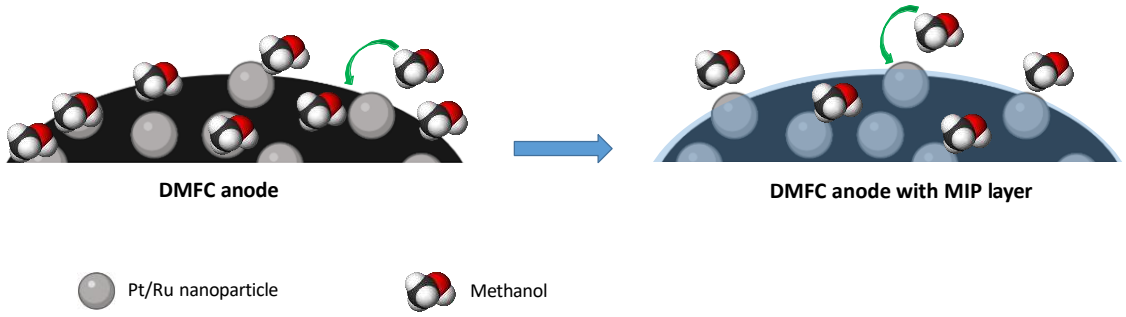

Figure 4.3 - Simple schematic representation of Pt/Ru blocking by the MIP layer, conditioning the access of MeOH, and consequent oxidation, reducing the power output of the system.

The fuel cell was previously activated by recording the polarization curves with 2.0 M MeOH solution until the power of the cell reached a stable value. Then, the fuel cell was left in Milli-Q water overnight to remove the excess MeOH on the electrode surface.

Calibration curves in buffered media were established by Sampled DC in sarcosine standard solutions (3.2, 16.0, 80.0, 400, 2000 µM) prepared in MES buffer. During calibration, each solution was incubated on the sensor surface (in the fuel cell anode reservoir) for 30 minutes, starting with the lowest concentration. After each incubation period, the sensor surface was washed with MES buffer; electrochemical measurements were performed with 0.5 M methanol. Selectivity studies were performed by calibrations in 1000-fold diluted FBS and spiked sarcosine standard solutions to evaluate the influence of serum on electrochemical readings.

4.3. Results and discussion

4.3.1. Operation of the passive Fuel Cell device and optimization

The performance of the passive DMFCs systems was evaluated prior to MIP assembly to identify the most suitable conditions. For this purpose, several polarization curves were measured with two different MeOH concentrations of 0.5 and 2.0 M, respectively, until signal stabilization. The polarization curves monitored the variation of cell potential against current density.

Figure 4.7 shows the typical polarization curves of the DMFCs used in this work compared to the results obtained with different concentrations of MeOH. As expected, both current and power density were strongly affected by the MeOH concentration. However, considering that this system will function as a biosensor and the overall influence of the MIP film on the fuel cell results from it hindering the access of methanol to the Pt/Ru catalyst, using too much MeOH would result in a less sensitive system (experimental data not shown). Since MeOH is a small molecule, it can easily diffuse through the catalyst surface at higher concentrations and consequently affect the sensitivity of the final sensor (it would become insensitive to low concentrations of CEA).

With respect to the use of the DMFC with the MIP film as a biosensor, it is important that the signal is stable and that the power generated by the DMFC with the MIP can trigger the EC, which requires at least 1.5 V. **Figure 4.4** shows that the DMFC with the sensing polymer on the anode operated with a 0.5 M MeOH solution and generates enough cell power to feed the EC when operated in stack mode. It was important to note that the system did not require a high MeOH concentration and the MeOH solution was only fed at specific times. The DMFC/biosensor device was very stable with a low MeOH concentration (**Figure 4.4**), which was also confirmed by calibrations with sarcosine solutions from independent cells.

4.3.2. Biosensing unit characterization

4.3.2.1. Spectroscopy analysis

To confirm the presence of the polymer on the surface of the carbon black catalyst (CB-Pt/Ru), the MIP films and the control materials (NIP) were analyzed by FTIR-ATR spectroscopy (**Figure 4.5a**) and Raman analysis (**Figure 4.5b**).

Quite similar spectra were obtained in the analysis of FTIR-ATR (**Figure 4.5a**), which was expected since these materials are mainly carbon-based, making it difficult to visualize the functional groups that might be present in the MIP/NIP samples [40]. However, the spectra of the polymerized MIP/NIP samples show significant differences compared to the unmodified CB-Pt/Ru. The observed differences are related to the vibrations of the functional groups of the monomers used in the polymerization and can be approximately assigned to the acrylate and amide groups (N-H, C-N, C=O) at 647 cm-1,750 cm-1, 870 cm-1 and 1000-1100 cm-1 At 1260 cm-1, a small band can be seen in the MIP/NIP samples, which can be associated with the P=O group of the vinylphosphonic acid, and at about 1400 cm-1, a band with strong intensity appears in the modified polymer samples, which can be assigned to the carbonyl group insertion (C=O) [41]. The observed spectra differences are consistent and provide evidence for significant modification of the CB -Pt/Ru matrix support with the sensitive polymer.

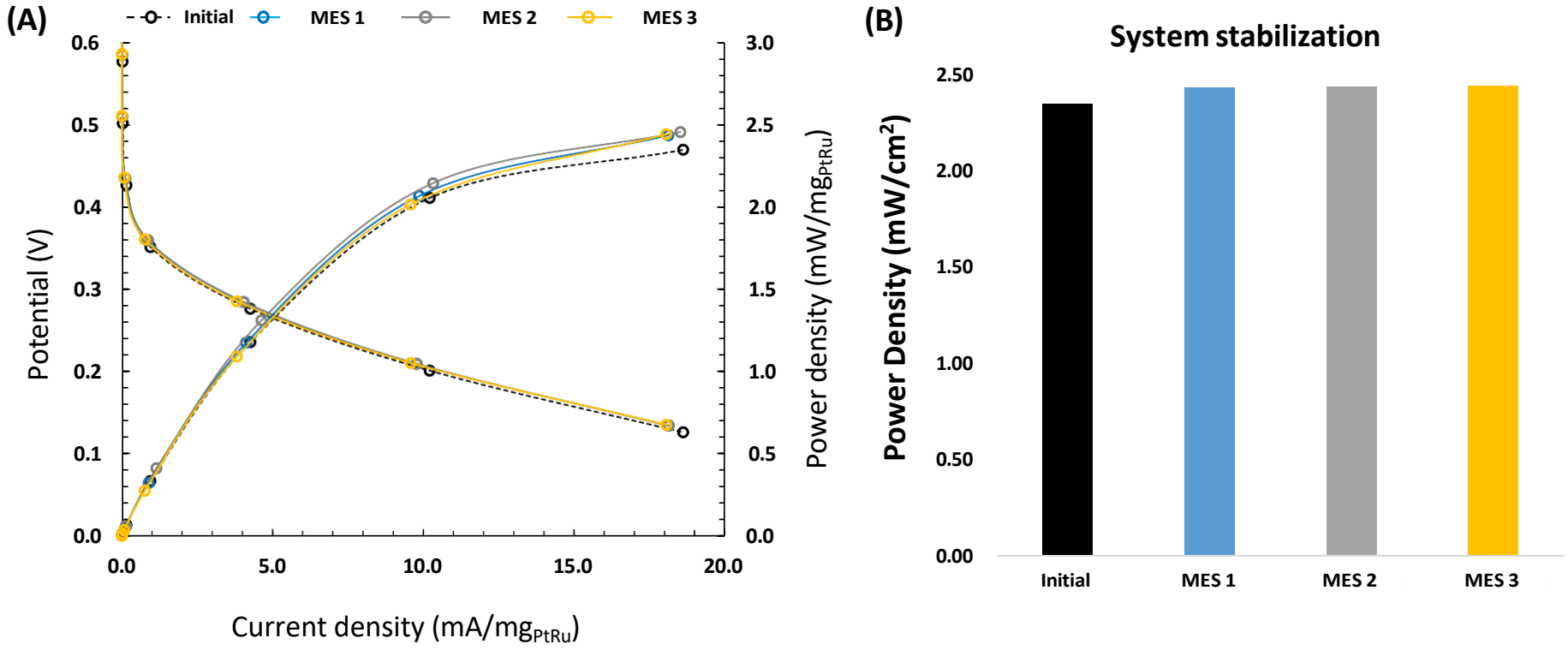

Figure 4.4 - Polarization curves of the DMFC-Biosensor assembly after MES buffer incubations using 0.5 M MeOH. Bar chart to show the stability of the electrical signal obtained after consecutive MES buffer incubations.

Raman spectroscopy analysis (**Figure 4.5b**) also proves the presence of the polymer on the surface of CB -Pt/Ru. All the samples examined showed the D and G peak of carbon. The D peak was located between 1200 and 1400 cm-1 and G peak between 1500 and 1600 cm-1. The D peak is related to the disorder of the carbon structure (structural defects), while the G peak is related to the graphite present in the structure. In addition to these two peaks, one can observe other peaks between 100 and 800 cm-1 that probably indicate the presence of platinum [42] and ruthenium [43] in the samples. The ratio between the intensity of the D and G peaks was used to evaluate the carbon surface modifications [44]. The obtained ID /IG values can be found in the attached table in **Figure 4.5b**. Analysis of these results shows that the ratio (ID /IG) of the MIP and NIP samples was significantly lower than that of the control sample, indicating that the presence of the polymer affects the Raman spectra of CB-Pt/Ru.

4.3.2.2. Calibration in a single passive cell

Prior to calibration, the DMFC was activated with 2.0 M MeOH, as the use of a high concentration of MeOH allowed for rapid activation of the fuel cell. However, since the quantity of MeOH used for activation (2 M) was higher than the one used for calibrations (0.5 M), some of the adsorbed MeOH on the carbon cloth electrode was removed. The complete removal of MeOH that was absorbed on the carbon cloth was not possible. Therefore, the partial removal of adsorbed MeOH was accomplished by leaving the activated cell with water in the fuel compartment, as shown in **Figure 4.6**.

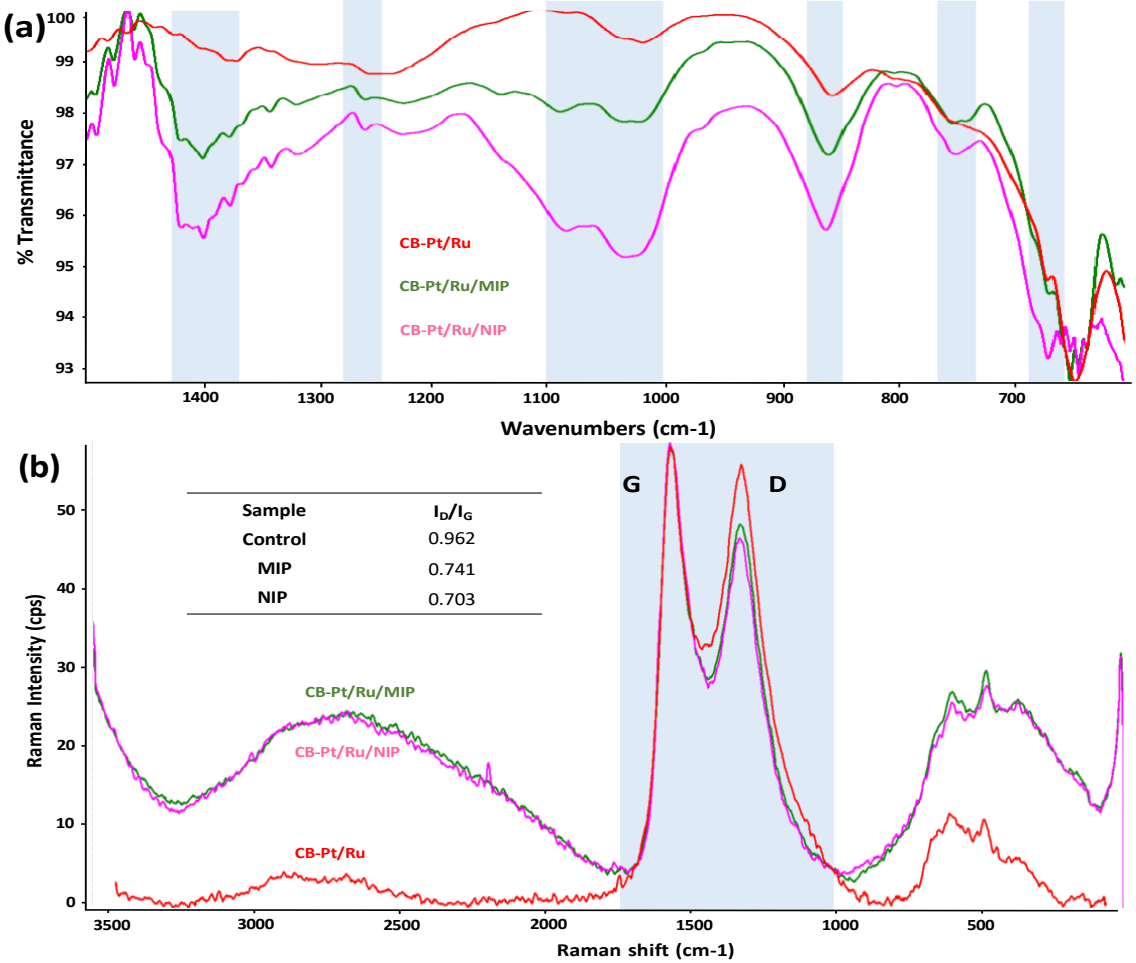

Figure 4.5 - FTIR **(a)** and Raman **(b)** spectra of the materials CB -Pt/Ru (control) and polymerized (MIP and NIP) CB -Pt/Ru. Important areas are highlighted in blue.

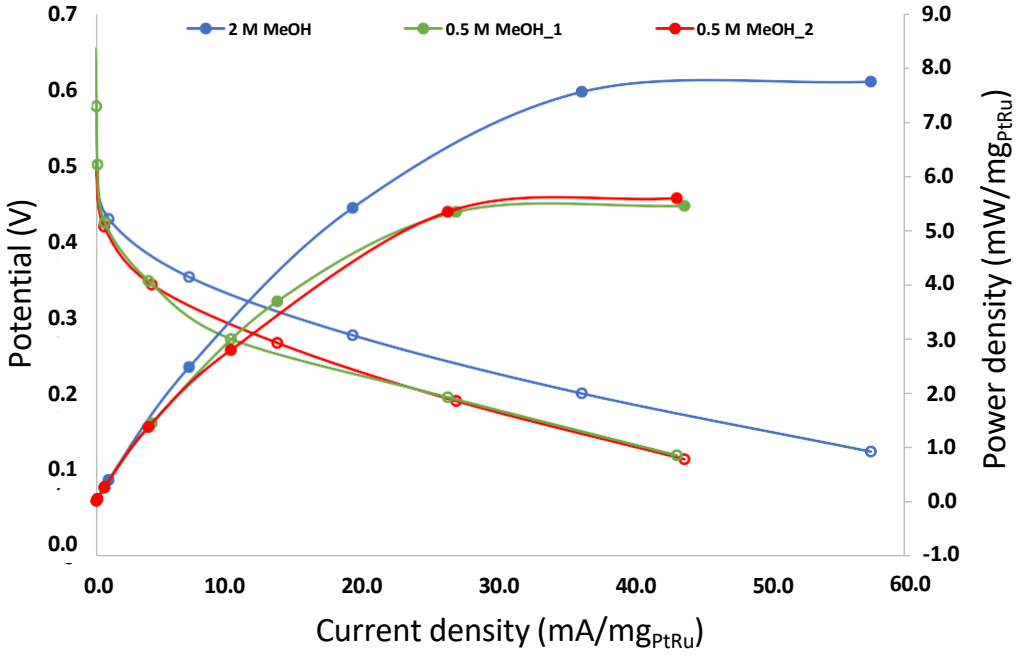

Figure 4.6 - Polarization and power curves of the DMFC after activation with 2 M MeOH, and after removal of the excess amount of MeOH and stabilization with 0.5 M MeOH.

4.3.2.3. Calibration in buffer

Calibrations were always performed using sampled DC as electrochemical measurement and with sarcosine standard solutions prepared in MES buffer. Initially, only MES was incubated two to three times to check the influence of buffer solution on DMFC performance. This procedure was repeated until signal stability was achieved. The results obtained are shown in **Figure 4.7** and confirm the good stability of the system after several buffer incubations.

Each standard solution was incubated in the fuel cell for 30 minutes, after which the cell was washed with buffer. The performance of the cell was then measured using a 0.5 M MeOH solution at the anode compartment. The standard solutions incubated there had increasing sarcosine concentrations, namely 3.2, 16, 80, 400 and 2000 µM.

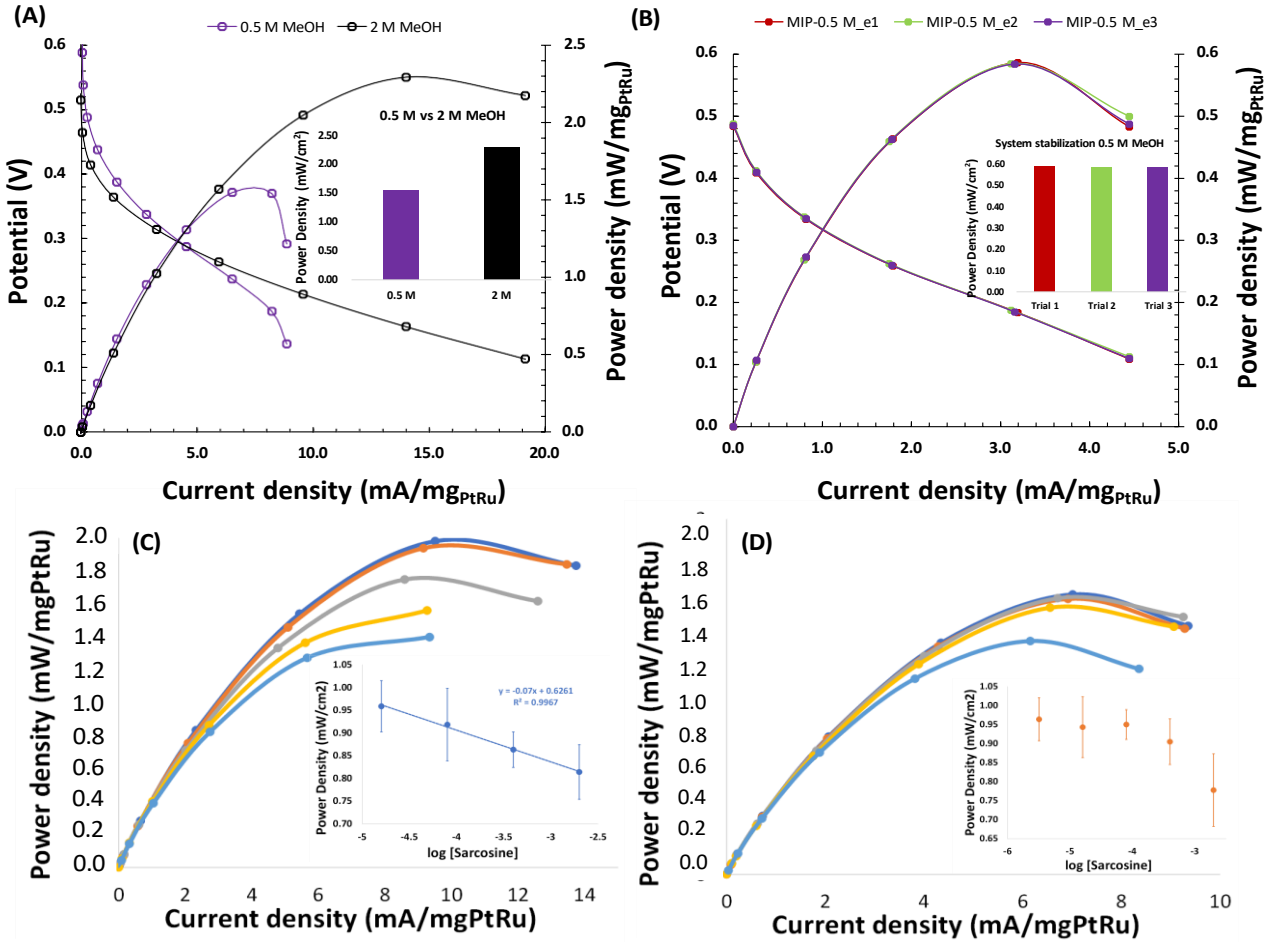

Figure 4.7 - Polarization curves of the passive DMFC device with **(a)** different MeOH concentrations (2M and 0.5M); **(b)** stability of a DMFC with a printed anode using 0.5 M MeOH solution. The bar graphs are representative of the data obtained in both plots to better observe the stability of the system. Calibration data show **(c)** and **(d)** normalized calibration curve for the MIP shown compared to a control (NIP) obtained under the same conditions, and typical polarization curves of the DMFC biosensor device (MIP and NIP, respectively) for sarcosine with increasing concentrations ranging from 3.2 to 2000 µM in buffer.

Figure 4.7a shows the current and power densities obtained when calibrating a MIP, and **Figure 4.7b** shows the calibration curve of the same MIP compared to the control (NIP). The MIP shows decreasing power with increasing sarcosine concentration and exhibits a logarithmic concentration-dependent behavior from 3.2 to 2000 µM. This concentration interval mainly encompasses the sarcosine concentration in the blood of prostate cancer patients, which ranges from 2.0 to 10 µM, whereas the normal sarcosine level in healthy individuals is approximately 1.4±0.6 µM. [12]. The NIP also showed decreasing performance like the MIP, but with lower intensity and only at higher concentrations. This different response of the MIP proves the binding of sarcosine to the imprinted binding sites and the subsequent blocking of the access of MeOH to the catalyst for its oxidation.

An additional control was performed to evaluate possible nonspecific adsorption of sarcosine on the carbon material. For this purpose, a calibration was performed using only the catalyst material (CB -Pt/Ru) under the same conditions as described previously. **Figure 4.8** shows the results of this control calibration. There is no significant change in the obtained performance after the incubation of sarcosine. These results show that the non-specific adsorption of sarcosine on the carbon surface is negligible. The limit of detection (LOD) was determined as described in [45], using linear regression method. In this case, LOD can be expressed as:

$$\boldsymbol{LOD = 3\,(\frac{Sa}{b})}$$

Where, Sa means the standard deviation of the response of the curve, which can be obtained by the standard deviation of the regression line, and b is the slope of the calibration curve obtained from the equation of the calibration line. The calculation of LOD was performed using this equation, and the obtained LOD for this work was 0.04 µM.

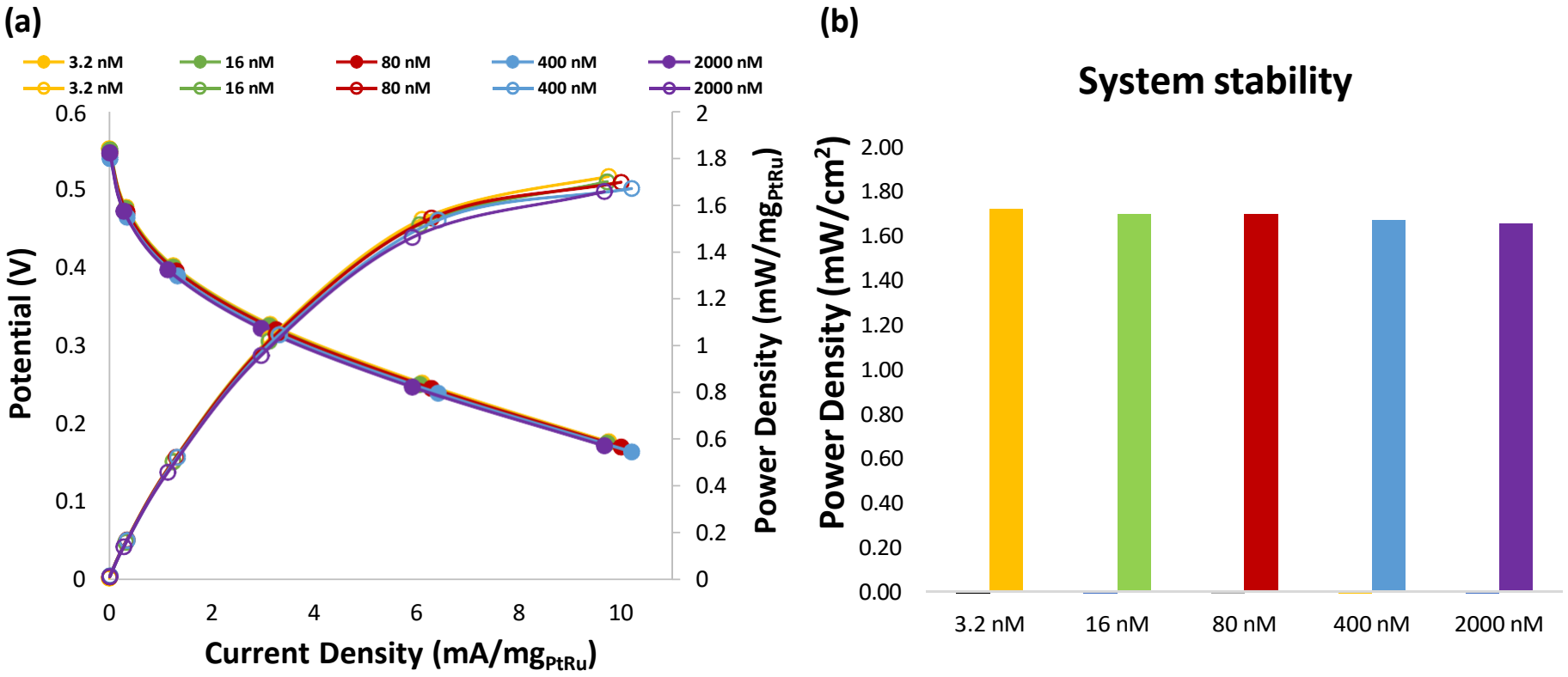

Figure 4.8 - Calibration data of the carbon support showing **(a)** typical polarization curves of the DMFC device with an unmodified anode (commercial) for sarcosine with increasing concentrations ranging from 3.2 to 2000 µM, in buffer, and **(b)** the normalized calibration curve obtained during calibration.

4.3.2.4. Calibration in serum

After optimization of the biosensor in the DMFC with standard solutions prepared in buffer, the selectivity of the biosensor was evaluated with standard solutions prepared in foetal bovine serum (FBS). FBS was used to mimic human samples and understand the effects of this fluid on the system. This FBS was diluted 1000-fold to reduce the presence of ions that could interfere with the Nafion® membrane in the DMFC.

The obtained results of a calibration in serum medium (**Figure 4.9**) show the changes in the performance of the cell with the increasing concentrations of sarcosine, with linearity from 3.2 to 2000 µM. The MIP reacts according to the previous calibrations with buffer (slope of 0.07, and correlation coefficient of 0.997), and the 1000-fold diluted serum has no significant interference in the cell, having a similar slope and correlation value of the calibration curve (slope of 0.0394, and correlation coefficient of 0.986). On the other hand, the NIP shows a random behavior with a decrease in response when using the highest concentration of sarcosine, which could be the adsorption of the molecules present in the FBS. These results suggest that the biosensor is selective for sarcosine in the presence of FBS.

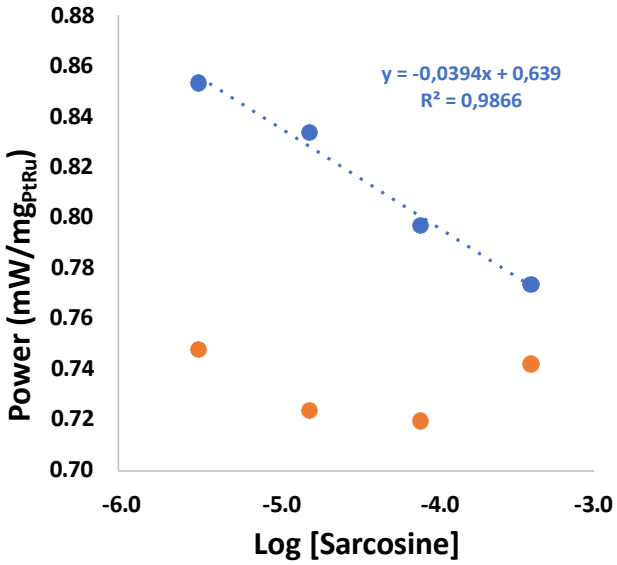

Figure 4.9 - Normalized calibration curves were obtained during the calibration of a DMFC-Biosensor device with a MIP modified anode (blue dots and line) and with a NIP modified anode (orange dots and line) in Foetal Bovine Serum.

4.3.3.Final assembly DMFC-EC/Biosensor

The final DMFC-EC/biosensor combines the DMFC device, the biosensor unit, and the electrochromic cell, which operates as a unique and fully autonomous device. Following a previous work by some of the authors [7], where color modulation at ±2 V was achieved, an optimization process was performed to reduce the electrical potential and power consumption of the device. For this purpose, the deposited volume of WO_3 nanoparticles in the WE was increased from 1.5 to 3 µL, achieving coloration at ±1.5 V and reducing the current density from 2.7 to 0.4 µA cm^2 (**Figure 4.10**). The hydrophilic paper encapsulated in the device, covering both WE and CE, served only to soak up the electrolyte during the time of use. Several hydrophilic papers were tested (data not shown). Due to its high porosity, the grade 4 Whatman paper proved capable of absorbing a large amount of electrolyte and allowing good contact with the nanoparticles, resulting in increased ionic charge.

Given the behavior of the EC, the DMFC biosensor should generate enough current to power the electrochromic device, which in this case required a voltage of 1.5 V. To achieve this voltage, a stack of DMFCs had to be used, since each one generates only about 0.5 V. It is important to note the fine line between the initial cell potential and the potential reached after incubation of the target molecule. While there are potential differences that can be observed during calibration (with a potentiostat), the sarcosine molecule is small, and the potential variation is not so large that a cell stack with a very high initial potential can drop off so that it does not trigger the EC. This means that a cell stack with an initial potential as close as possible (slightly higher) to 1.5 V is necessary to obtain the desired colour change after incubation of the target molecule.

Originally, a stack of 5 DMFCs was to be used, but it turned out that a stack of 4 was sufficient to trigger the EC. **Figure 4.11a** shows the EC in its initial state (white) and **Figure 4.11b-c** shows the colour change of the EC, when interconnected with 4 and 5 cells, proving that a stack of 4 cells was sufficient to promote the colour change from white to blue. The colour change was fast and took about 20 seconds to reach full stability. It was also very stable and reproducible when different cells were compared. The colour reversal can also be easily achieved by simply switching the polarity, and two reversals can be performed while maintaining the effectiveness of the system.

Figure 4.10 - Optimized electrochromic device operating at 1.5 V: Chronoamperometry coloration/discoloration cycle, cyclic voltammogram showing the obtained current density (0.4 µA.cm 2), and photographs of the device during coloration/discoloration.

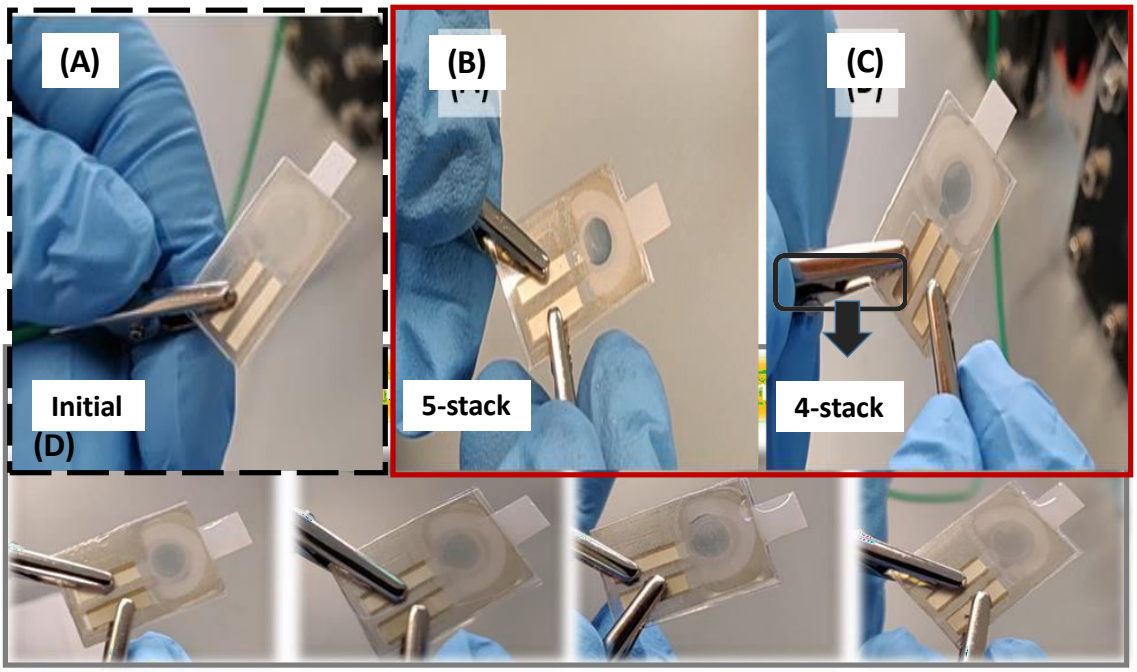

Figure 4.11 - Images of the electrochromic cell (EC) in operation: **(a)** in the initial state before coupling with the DMFC biosensor (white colour); **(b)** after coupling with a 5-stack DMFC; and **(c)** 4-stack DMFC that was able to trigger the EC from white to blue; **(d)** colour gradient obtained with a 4-stack DMFC biosensor from incubation in MES buffer (blank signal) to increasing sarcosine concentrations, showing the colour change from blue to very light blue.

After evaluating the electrical properties of EC, the stack of 4 DMFCs was incubated with MES buffer (during 30 min), as was done previously with the single DMFC. The influence of the buffer was small, as previously observed with the single cell, and the color produced by EC was the same as that of the empty MeOH solution before buffer incubation. Then, the sarcosine standard solutions were incubated at the lowest concentration and the color variation obtained is shown in **Figure 4.11d** compared to the color of the buffer. Analysis of the images shows that the color produced by the buffer was intense. After incubation of the sarcosine standards, the color loses intensity and almost disappears in the highest concentrated solution. Thus, as the sarcosine incubation concentration increased, the overall power of the 4-stack DMFC decreased and it was no longer able to generate 1.5 V, so the device EC did not receive any color. The EC in combination with the DMFC biosensor made it possible to obtain a self-powered and self-signaling system that does not require a potentiostat to enable quantification of the sarcosine target by a color change in the gradient that is perceptible to the naked eye.

4.4. Conclusion

Using a passive DMFC as a power supply, a MIP as a biosensor unit, and an EC as a signalling element, a self-powered and self-signalling biosensor was developed to determine sarcosine.

The self-powered approach was achieved by developing a MIP film on the catalyst material of the fuel cell operating under steady-state conditions. Calibrations in buffer and FBS confirmed the good selectivity and sensitivity of the combined device for sarcosine. The electrochemical performance of the DMFC-modified biosensor showed a linear trend with the log concentration of sarcosine ranging from 3.2 to 2000 µM in both buffer and FBS (compatible with the concentrations expected in real samples).

The self-signalling approach was achieved by coupling an EC to the DMFC-EC /biosensor. This EC showed an intense blue coloration at maximum cell power and this coloration decreased with decreasing power values. The DMFC-EC /biosensor showed a naked eye detectable colour change in the presence of sarcosine standards, proving that it is possible to obtain a self-sustaining and self-signalling system capable of detecting sarcosine within seconds.

Overall, this type of setup may prove to be a promising approach that has never been reported before to achieve sensitive analytical analysis using instrument-free methods. The final DMFC-EC /biosensor setup could be improved in a future work by miniaturizing the four stack DMFCs and using another EC with lower potential requirement, allowing the use of a single DMFC.

4.5. References

[1] P. Martinkova, A. Kostelnik, T. Valek, M. Pohanka, Main streams in the Construction of Biosensors and Their Applications, Int. J. Electrochem. Sci. 12 (2017) 7386–7403. https://doi.org/10.20964/2017.08.02.

[2] D.R. Thévenot, K. Toth, R.A. Durst, G.S. Wilson, Electrochemical biosensors: Recommended definitions and classification, Biosens. Bioelectron. 16 (2001) 121–131. https://doi.org/10.1016/S0956-5663(01)00115-4.

[3] W. Zhang, R. Wang, F. Luo, P. Wang, Z. Lin, Miniaturized electrochemical sensors and their point-of-care applications, Chinese Chem. Lett. 31 (2020) 589–600. https://doi.org/10.1016/j.cclet.2019.09.022.

[4] E.T.S.G. da Silva, D.E.P. Souto, J.T.C. Barragan, J. de F. Giarola, A.C.M. de Moraes, L.T. Kubota, Electrochemical Biosensors in Point-of-Care Devices: Recent Advances and Future Trends, ChemElectroChem. 4 (2017) 778–794. https://doi.org/10.1002/celc.201600758.

[5] Y.D. Han, H.J. Chun, H.C. Yoon, Low-cost Point-of-Care Biosensors Using Common Electronic Components as Transducers, Korean BioChip Soc. 14 (2020) 32–47. https://doi.org/10.1007/s13206-020-4104-8.

[6] J.V. and E.R. Dorothee Grieshaber, Robert MacKenzie, Electrochemical Biosensors - Sensor Principles and Architectures, Sensors. (2008) 1400–1458. https://doi.org/10.3390/s80314000.

[7] L.A.A.N.A. Truta, F.T.C. Moreira, M.G.F. Sales, A dye-sensitized solar cell acting as the electrical reading box of an immunosensor: Application to CEA determination, Biosens. Bioelectron. 107 (2018) 94–102. https://doi.org/10.1016/j.bios.2018.02.011.

[8] A.P.M. Tavares, L.A.A.N.A. Truta, F.T.C. Moreira, L.P.T. Carneiro, M.G.F. Sales, Self-powered and self-signalled autonomous electrochemical biosensor applied to cancinoembryonic antigen determination, Biosens. Bioelectron. 140 (2019) 111320. https://doi.org/10.1016/j.bios.2019.111320.

[9] A.P.M. Tavares, L.A.A.N.A. Truta, F.T.C. Moreira, G. Minas, M.G.F. Sales, Photovoltaics, plasmonics, plastic antibodies and electrochromism combined for a novel generation of self-powered and self-signalled electrochemical biomimetic sensors, Biosens. Bioelectron. 137 (2019) 72–81. https://doi.org/10.1016/j.bios.2019.04.055.

[10] F.T.C. Moreira, M.G.F. Sales, Autonomous biosensing device merged with photovoltaic technology for cancer biomarker detection, J. Electroanal. Chem. 855 (2019) 113611. https://doi.org/10.1016/j.jelechem.2019.113611.

[11] S. Hao, X. Sun, H. Zhang, J. Zhai, S. Dong, Recent development of biofuel cell based self-powered biosensors, J. Mater. Chem. B. 8 (2020) 3393–3407. https://doi.org/10.1039/c9tb02428j.

[12] F.T.C. Moreira, M.G.F. Sale, M. Di, Towards timely Alzheimer diagnosis : A self-powered amperometric biosensor for the neurotransmitter acetylcholine, Biosens. Bioelectron. 87 (2017) 607–614. https://doi.org/10.1016/j.bios.2016.08.104.

[13] M. Kim, M. Sik, M. Gadd, H. Joo, A novel biomonitoring system using microbial fuel cells, J. Environ. Monit. 9 (2007) 1323–1328. https://doi.org/10.1039/b713114c.

[14] Y. Han, J.M. Chabu, S. Hu, L. Deng, Y. Liu, S. Guo, Rational Tuning of the Electrocatalytic Nanobiointerface for a “ Turn-Off ” Biofuel-Cell-Based Self-Powered Biosensor for p53 Protein, Chem. Eur. J. 21 (2015) 13045–13051. https://doi.org/10.1002/chem.201502062.

[15] M.S. Alias, S.K. Kamarudin, A.M. Zainoodin, M.S. Masdar, Active direct methanol fuel cell: An overview, Int. J. Hydrogen Energy. 45 (2020) 19620–19641. https://doi.org/10.1016/j.ijhydene.2020.04.202.

[16] Z.A.C. Ramli, S.K. Kamarudin, Platinum-Based Catalysts on Various Carbon Supports and Conducting Polymers for Direct Methanol Fuel Cell Applications: a Review, Nanoscale Res. Lett. 13 (2018). https://doi.org/10.1186/s11671-018-2799-4.

[17] N. V. Raghvaiah, G.N. Srinivasulu, I.H. Prasad, Review of Challenges in Direct Methanol Fuel Cell and Contemporary Status, Res. Appl. Therm. Eng. 3 (2020) 1–8. https://doi.org/10.5281/zenodo.3989515.

[18] N. Sazali, W.N.W. Salleh, A.S. Jamaludin, M.N.M. Razali, New perspectives on fuel cell technology: A brief review, Membranes (Basel). 10 (2020). https://doi.org/10.3390/membranes10050099.

[19] M. Goor, S. Menkin, E. Peled, High power direct methanol fuel cell for mobility and portable applications, Int. J. Hydrogen Energy. 44 (2018) 3138–3143. https://doi.org/10.1016/j.ijhydene.2018.12.019.

[20] M.G.F. Sales, L. Brandão, Autonomous electrochemical biosensors: A new vision to direct methanol fuel cells, Biosens. Bioelectron. 98 (2017) 428–436. https://doi.org/10.1016/j.bios.2017.07.021.

[21] B.A. Berns, M.F. Torres, V.B. Oliveira, Performance of passive Direct Methanol Fuel Cell : modelling and experimental studies, U.Porto J. Eng. 1 (2015) 89–103. https://journalengineering.fe.up.pt/article/view/110/111.

[22] L.P.T. Carneiro, N.S. Ferreira, A.P.M. Tavares, A.M.F.R. Pinto, A. Mendes, M.G.F. Sales, A passive direct methanol fuel cell as transducer of an electrochemical sensor, applied to the detection of carcinoembryonic antigen, Biosens. Bioelectron. 175 (2021) 1–9. https://doi.org/10.1016/j.bios.2020.112877.

[23] L.P.T. Carneiro, A.M.F.R. Pinto, A. Mendes, M. Goreti, An all-in-one approach for self-powered sensing: A methanol fuel cell modified with a molecularly imprinted polymer for cancer biomarker detection, J. Electroanal. Chem. 906 (2022) 116009. https://doi.org/10.1016/j.jelechem.2022.116009.

[24] S. Khodabakhshi, P.F. Fulvio, E. Andreoli, Carbon black reborn: Structure and chemistry for renewable energy harnessing, Carbon N. Y. 162 (2020) 604–649. https://doi.org/10.1016/j.carbon.2020.02.058.

[25] M.F. Frasco, L.A.A.N.A. Truta, M.G.F. Sales, F.T.C. Moreira, Imprinting Technology in Electrochemical Biomimetic Sensors, Sensors. 17 (2017) 523. https://doi.org/10.3390/s17030523.

[26] J.J. Belbruno, Molecularly Imprinted Polymers, Chem. Rev. 119 (2019) 94–119. https://doi.org/10.1021/acs.chemrev.8b00171.

[27] L. Chen, X. Wang, W. Lu, X. Wu, J. Li, Molecular imprinting: Perspectives and applications, Chem. Soc. Rev. 45 (2016) 2137–2211. https://doi.org/10.1039/c6cs00061d.

[28] A. Marques, L. Santos, S. Pereira, U. Emanuele, S. Sinopoli, R. Igreja, G. Sales, R. Martins, E. Fortunato, A Planar Electrochromic Device using WO3 Nanoparticles and a Modified Paper-Based Electrolyte, Proceedings. 2 (2018) 1065. https://doi.org/10.3390/proceedings2131065.

[29] M. Ferro, C. Buonerba, D. Terracciano, G. Lucarelli, V. Cosimato, D. Bottero, V.M. Deliu, P. Ditonno, S. Perdonà, R. Autorino, I. Coman, S. De Placido, G. Di Lorenzo, O. De Cobelli, Biomarkers in localized prostate cancer, Futur. Oncol. 12 (2016) 399–411. https://doi.org/10.2217/fon.15.318.

[30] S. Koutros, T.E. Meyer, S.D. Fox, H.J. Issaq, T.D. Veenstra, W.Y. Huang, K. Yu, D. Albanes, L.W. Chu, G. Andriole, R.N. Hoover, A.W. Hsing, S.I. Berndt, Prospective evaluation of serum sarcosine and risk of prostate cancer in the prostate, lung, colorectal and ovarian cancer screening trial, Carcinogenesis. 34 (2013) 2281–2285. https://doi.org/10.1093/carcin/bgt176.

[31] A. Sreekumar, L.M. Poisson, T.M. Rajendiran, A.P. Khan, Q. Cao, J. Yu, B. Laxman, R. Mehra, R.J. Lonigro, Y. Li, M.K. Nyati, A. Ahsan, S. Kalyana-Sundaram, B. Han, X. Cao, J. Byun, G.S. Omenn, D. Ghosh, S. Pennathur, D.C. Alexander, A. Berger, J.R. Shuster, J.T. Wei, S. Varambally, C. Beecher, A.M. Chinnaiyan, Metabolomic profiles delineate potential role for sarcosine in prostate cancer progression, Nature. 457 (2009) 910–914. https://doi.org/10.1038/nature07762.

[32] V. Narwal, P. Kumar, P. Joon, C.S. Pundir, Fabrication of an amperometric sarcosine biosensor based on sarcosine oxidase/chitosan/CuNPs/c-MWCNT/Au electrode for detection of prostate cancer, Enzyme Microb. Technol. 113 (2018) 44–51. https://doi.org/10.1016/j.enzmictec.2018.02.010.

[33] P. Kumar, V. Narwal, R. Jaiwal, C.S. Pundir, Construction and application of amperometric sarcosine biosensor based on SOxNPs/AuE for determination of prostate cancer, Biosens. Bioelectron. 122 (2018) 140–146. https://doi.org/10.1016/j.bios.2018.09.003.

[34] C. Wang, Y. Wang, H. Zhang, H. Deng, X. Xiong, C. Li, W. Li, Molecularly imprinted photoelectrochemical sensor for carcinoembryonic antigen based on polymerized ionic liquid hydrogel and hollow gold nanoballs/MoSe2 nanosheets, Anal. Chim. Acta. 1090 (2019) 64–71. https://doi.org/10.1016/j.aca.2019.09.029.

[35] T. Rajarathinam, M. Kwon, D. Thirumalai, S. Kim, S. Lee, J.H. Yoon, H. jong Paik, S. Kim, J. Lee, H.K. Ha, S.C. Chang, Polymer-dispersed reduced graphene oxide nanosheets and Prussian blue modified biosensor for amperometric detection of sarcosine, Anal. Chim. Acta. 1175 (2021) 338749. https://doi.org/10.1016/j.aca.2021.338749.

[36] T.P. Nguy, T. Van Phi, D.T.N. Tram, K. Eersels, P. Wagner, T.T.N. Lien, Development of an impedimetric sensor for the label-free detection of the amino acid sarcosine with molecularly imprinted polymer receptors, Sensors Actuators, B Chem. 246 (2017) 461–470. https://doi.org/10.1016/j.snb.2017.02.101.

[37] P. Tang, Y. Wang, F. He, Electrochemical sensor based on super-magnetic metal–organic framework@molecularly imprinted polymer for Sarcosine detection in urine, J. Saudi Chem. Soc. 24 (2020) 620–630. https://doi.org/10.1016/j.jscs.2020.06.004.

[38] Z. Ramezani, M. Safdarian, A.A. Ghadiri, Metal-coded hydrogel magnetic molecularly imprinted polymer for preconcentration and cleanup of sarcosine: Determination in urine; coupled to on-column capillary electrophoresis, Talanta. 230 (2021) 122309. https://doi.org/10.1016/j.talanta.2021.122309.

[39] L. Santos, J.P. Neto, A. Crespo, D. Nunes, N. Costa, I.M. Fonseca, P. Barquinha, L. Pereira, J. Silva, R. Martins, E. Fortunato, WO3 nanoparticle-based conformable pH sensor, ACS Appl. Mater. Interfaces. 6 (2014) 12226–12234. https://doi.org/10.1021/am501724h.

[40] M. Claybourn, P. Colombel, J. Chalmers, Characterization of Carbon-Filled Polymers by Specular Reflectance, Appl. Spectrosc. 45 (1991) 279–286. https://doi.org/https://doi.org/10.1366/0003702914337669.

[41] J. Coates, Interpretation of Infrared Spectra, A Practical Approach, Encycl. Anal. Chem. (2006) 10815–10837. https://doi.org/10.1002/9780470027318.a5606.

[42] Y.F. Huang, P.J. Kooyman, M.T.M. Koper, Intermediate stages of electrochemical oxidation of single-crystalline platinum revealed by in situ Raman spectroscopy, Nat. Commun. 7 (2016) 1–7. https://doi.org/10.1038/ncomms12440.

[43] Y. Hyun, J.Y. Choi, H.K. Park, C.S. Lee, Synthesis and electrochemical performance of ruthenium oxide-coated carbon nanofibers as anode materials for lithium secondary batteries, Appl. Surf. Sci. 388 (2016) 274–280. https://doi.org/10.1016/j.apsusc.2016.01.095.

[44] M.S. Dresselhaus, A. Jorio, R. Saito, Characterizing Graphene, Graphite, and Carbon Nanotubes by Raman Spectroscopy, Annu. Rev. Condens. Matter Phys. 1 (2010) 89–108. https://doi.org/10.1146/annurev-conmatphys-070909-103919.

[45] A. Shrivastava, V. Gupta, Methods for the determination of limit of detection and limit of quantitation of the analytical methods, Chronicles Young Sci. 2 (2011) 21. https://doi.org/10.4103/2229-5186.79345.

[46] Q. Wang, C. Yang, Q. Yang, S. Yu, H. Yang, Platinum-loaded mesoporous nickel phosphonate and its electrochemical application for sarcosine detection, Anal. Chim. Acta. 1046 (2019) 93–98. https://doi.org/10.1016/j.aca.2018.09.027.

[47] J. Hu, W. Wei, S. Ke, X. Zeng, P. Lin, A novel and sensitive sarcosine biosensor based on organic electrochemical transistor, Electrochim. Acta. 307 (2019) 100–106. https://doi.org/10.1016/j.electacta.2019.03.180.

[48] H. Wang, Y. Qi, D. Wu, Q. Wei, A photoelectrochemical self-powered sensor for the detection of sarcosine based on NiO NSs/PbS/Au NPs as photocathodic material, J. Hazard. Mater. 416 (2021) 126201. https://doi.org/10.1016/j.jhazmat.2021.126201.

5. CONCLUSIONS AND FUTURE PERSPECTIVES

This thesis aimed to develop biosensors for cancer biomarker detection and integrate them into a modified DMFC to accommodate the biosensors and act as a potential power supply. Based on this, different biosensors were developed using different techniques: an immunosensor (described in detail in **Chapter 3**), and a MIP-based biosensor (described in detail in **Chapter 4**). This work was motivated by the increasing need for cancer detection and screening in a World with more and more mortality derived from this disease.

The work done during this thesis showed the possibility to develop different biosensors with analytical responses in the range of normal to high biomarker values in the Human body, with the possibility to be a self-powered device with biomarker quantification by color change. This kind of autonomous sensing device would be very useful as a diagnosis but also as a screening tool not only as a widespread and low-cost method, but also used in low-income countries and in case of a World crisis, pandemics, and Wars.

Although there is great potential for this research to be used in the future, there is still some need for improvement. This device is still a proof-of-concept and in the future, it is important to achieve full autonomy by developing a miniaturized stack involving all components. To accomplish that, it is necessary to adapt and optimize a stack of DMFCs with the integrated biosensor, and an electrochromic device that has a wide range of color changes to be sensitive to the shift in biomarker concentration.

One of the major problems encountered by these fuel cells is the reduction of cost without losing reasonable power density. Therefore, different optimizations on the final device can be made, such as the used catalysts, the fuel, and even the setup can be modified to achieve lower cost and the best performance of this biosensing device.

The normally used catalyst for the anode of the DMFC is a Pt/Ru alloy, and for the cathode Pt. both are described in the literature as the best-performing catalysts. However, the cost associated with the DMFC when using these catalysts is high, not only because of the metals themselves but also because of the high quantity of these that are needed for the synthesis (only a small percentage will be attached to the carbon

support). Therefore, the use of low-cost catalysts for methanol oxidation and oxygen reduction, without losing reasonable power density is an important step towards a device able to be produced for PoC diagnosis.

Methanol is known to be a toxic and dangerous alcohol. Although the methanol solution used in these works is in low concentration and can be used safely outside the laboratory, this fuel could be switched by some greener and safer options, such as ethanol or even glucose. Both kinds of fuel cells are already being researched and have promising results. However, the achieved power is far lower than the DMFC, and, in the case of the glucose fuel cell, the best performance is achieved in very alkaline media, which is not a good fit to integrate a biosensor. Thus, a fuel cell would need to be adapted to perform in a similar way as the DMFC. Also, miniaturization and fuel cell printing on a high scale needs to be achieved in the future to make this device market friendly and low-cost.

This work with further optimizations has a good perspective of being a viable and low-cost device that may be used in PoC evaluation of cancer biomarkers, and even can be modified to detect other substances of interest.